Cosmic Noise Absorption Pulsations

by

J. S. Reid

Submitted in fulfilment of the
requirements for the degree of

Doctor of Philosophy

University of Tasmania

Hobart.

November 1972.

To Rosie

Abstract

The fast cosmic noise absorption (c.n.a.) pulsations observed with fast response riometers at Macquarie Island in the southern auroral zone are discussed in relation to the parameters of the lower ionosphere. The pulsations which are similar to and associated with pulsations in auroral luminosity (at λ 4278Å), Pi2 micropulsations and fast bremmstrahlung X-ray pulsations are unique in that they exhibit a time asymmetry or relaxation time which is believed to be a consequence of the relatively slow rate of removal of secondary electrons in the ionosphere. The relaxation time, τ is defined as

$$\tau = -A/(\dot{a})_{max}$$

where A is the amplitude of the pulse above background and $(\dot{a})_{max}$ is the maximum (negative) slope of the relaxation part of the pulse. Measured values of τ varied between 1 and 30 seconds and scatter diagrams of τ versus A indicate a strong tendency for τ to increase with increasing pulse amplitude.

The properties and anomalies of the D-region of the ionosphere are discussed, as is the applicability of the Bates and Massey rate equations to fluctuations in electrons density in this region. A computer model was constructed in which the rate equations were numerically integrated using a variety of values of the parameters involved and for a variety of primary spectrum e-folding energies in an attempt to simulate the observed pulsations. Relaxation times as small as some of those observed were not obtained from the model. A new approximation formula for relaxation time as a function of height was derived.

The possibility that the observed positive relationship between relaxation time and pulse amplitude is due to the chemical dynamics of a situation in which electrons

recombine with positive ions of widely differing reaction rates is discussed and dismissed.

It is concluded that the observed c. n. a. pulsations are an E-region phenomenon associated with quasi mono-energetic peaks in the background primary flux with energies somewhere in the range of from 4 to 10 keV. The pulsations are believed to be due to fluctuations in the energy of this peak or to pulsations in primary particle flux on the high energy side of the peak.

Contents

Appendices

Forward

This work was commenced from the standpoint that the bulk of cosmic noise absorption occurs below 100 km in height, that is, in the D - region of the atmosphere. This was no doubt a natural assumption and one which is deeply embedded in the literature of riometry. The con - clusion of Section 5, that c. n. a. pulsations and the background absorption accompanying them are an E - region phenomenon did not become apparent to the author until the thesis was three - quarters written. Consequently much of the early material is concerned with D - region processes and the reader may perhaps gain an impression of inconsis- tency, as if the author " could not make up his mind."

It should be emphasised that such discussion of D - region processes is essential in order to eliminate this part of the atmosphere as the location of the puls- ations. Indeed the failure of the D - region model to adequately predict sufficiently short relaxation times forced the author to the conclusion which was finally reached. This thesis thus has a chronological as well as a lògical development and, one hopes, will lead the reader to the same conclusion.

The thesis is structured as a fairly short central argument accompanied by four appendices. The latter, taken together constitute almost half the wordage. The reasons for this format are twofold:

(i) It was originally intended to publish much of this material as a series of separate papers and then to combine these to form a thesis. Owing to lack of time this idea was abandoned and only Appendix I has received prior publication. Appendix II is ready to be submitted

for publication almost as it stands and it is intended that the body of the thesis be submitted for publication in an abridged form.

(ii) Written in this format it is possible for the reader to more readily perceive the main thread of the argument without being diverted by various digressions on the way.

INTRODUCTION

The riometer is an instrument devised by C.G.Little and N. Leinbach in 1958 to provide information about the electron content of the ionosphere by monitoring the ionospheric absorption of cosmic radio noise. It consists of a broad beam antenna, a low noise receiver at about 30 MHz and some sort of reference device such as a low noise diode which is often incorporated in a feedback loop with the receiver to give exceptional long term stability. Radiation from the Galaxy and from discrete radio sources is absorbed in the upper atmosphere by free electrons. The degree of absorption depends upon the density of the electrons and the rate at which they lose energy by collisions with heavier particles. Thus the degree of cosmic noise absorption (c.n.a.) displayed by the instrument provides a measure of the weighted mean of the electron density in the upper atmosphere within the beam of its antenna.

The resolution of the instrument is limited by the statistical nature of the cosmic radio noise detected and this in turn depends upon the bandwidth of the receiver. In order to improve the resolution while sacrificing such things as stability and freedom from man-made and solar interference, the bandwidth was widened from 20 KHz to 1.4 MHz thus increasing the time resolution by a factor of 70 for the same amplitude sensitivity.

This modified instrument, a "fast-response riometer" was first operated in the auroral zone in December 1966. Within the first few days of operation a new phenomenon was observed : fast cosmic noise absorption pulsations (Reid, 1967). These pulsations occurred in trains of from a few minutes to an hour or so in duration. They were generally sporadic although periodicities were also observed on occasion. The duration of an individual pulse was in

the range of from 2 to 30 seconds. Their amplitudes ranged from about 0.3 dB down to the .02 dB amplitude resolution of the instrument. Their most striking characteristic was a tendency to be asymmetric in time with rapid onsets (1 to 4 seconds) and slower decay times (up to 30 seconds). Some examples of fast c.n.a. pulsations can be seen in Figs. 4.1, 4.2, 4.3.

This thesis is concerned with these fast c.n.a. pulsations, their origin and their possible use as a diagnostic tool in investigating the ionosphere and the magnetosphere. The pulsations were observed from Macquarie Island (54.5°S, 158.9°E Geographic, Invariant Latitude 64.5°S) during the Summer months of 1967, 1968 and 1969. Appendix III provides a technical description of the fast response riometers used. The relationships observed at this time between fast c.n.a. pulsations and other pulsating phenomena has already been described in the literature (Reid & Phillips, 1971 - Appendix 1).

SECTION I

The D-region

1.1. The association of fast c.n.a. pulsations and fast bremmstrahlung x-ray pulsations (Appendix I) indicates that they are caused by pulses of electrons in the energy range of tens of KeV precipitating from the magnetosphere into the ionosphere. Such high energy, "primary", electrons will create many times their number of free low-energy "secondary" electrons and positive ions by collision with air molecules. It is these secondary electrons which are observed by the riometer. After the primary pulse has ceased, many secondary electrons will remain, being removed relatively slowly by mutual neutralization with positive ions and and by attachment to neutral molecules to form negative ions.

The slow decay of the fast c.n.a. pulsations is then an atmospheric process, dependant on the chemistry of the atmosphere at heights over which the absorption of cosmic noise is taking place. The height distribution of the free, absorbing secondary electrons will in turn be dependant upon the energy spectrum of the primaries which give rise to them. The atmospheric nature of the asymmetry of the pulsations is borne out by the fact that neither the fast bremmstrahlung x-ray pulsations nor the λ 4278 A^{o} auroral luminosity pulsations with which they have been observed show any asymmetry themselves.

It is the purpose of this work to examine in detail the relationship between the observed decay times of the pulsations and decay times deduced from various models of the atmosphere and primary particle spectra. If we can reliably relate the decay times to the characteristics of primary particle spectra, then the

fast response riometer becomes a powerful instrument for probing the magnetosphere since each pulsation would be effectively "tagged" with information about the primary pulse which created it. It might, for example, be possible using a series of riometers with narrow beam antennas, to obtain an energy or pitch angle cross section of a single pulse of precipitating electrons.

On the other hand if we have some idea of the characteristics of the primary particle spectrum and hence of the height distribution in ion pair production rate, it would be possible to verify or disprove some of the currently accepted values of the various parameters of ionospheric processes.

In order to fulfill this purpose it will be necessary to construct a mathematical model of the electrical behaviour of the lower ionosphere.

D-region Problems

1.2. The region of the atmosphere between 60 and 100 Km in which the bulk of cosmic noise absorption occurs during auroral zone activity, is perhaps the most complex region of the atmosphere. It is the region in which most of the ionizing radiation impinging upon the earth is absorbed. Despite the fact that a variety of techniques have been used for a number of years in probing this region, its behaviour both electrically and chemically is still by no means fully understood; a number of anomalies remain. Indeed the more information that becomes available the more complex the region appears to be.

Most of the problems hinge upon the chemical composition of the D-region atmosphere since this must determine its electrical behaviour; the rate at which free electrons are created and removed depends upon the chemical composition. The fluxes of

ionizing radiation which includes energetic particles, x-rays and hard and soft ultraviolet radiation from the sun, from stellar and galactic sources and from the environs of the earth itself can now be experimentally measured outside the atmosphere. Their effects on the atmosphere can be computed. Electron density profiles of the upper atmosphere can be obtained with a high degree of accuracy by means of rockets and in recent years the concentrations of the various positive and negative ion species present have been measured with rocket borne instruments.

The problems concern these observed electron densities and their relationship to the computed production and loss rates.

1.3. The Ionospheric Rate Equations

The ionospheric rate equations (Bates and Massey, 1946) describe the rates at which electrons and ions are produced and lost in an ionized gas. They are

$$\frac{dN}{dt} = q - \alpha N N^+ - \beta N + \delta N^- \qquad (1.1a)$$

and

$$\frac{dN^-}{dt} = \beta N - \delta N^- - \gamma N^- N^+ \qquad (1.1b)$$

where q is the ion pair production rate,

α is the electron - ion recombination coefficient,

β is the attachment rate of electrons to neutral molecules to form negative ions,

γ is the ion-ion recombination coefficient,

δ is the detachment coefficient for negative ions, and

N, N^- and N^+ and the number densities of electrons, negative ions and positive ions respectively.

Diffusion terms and thermodynamic terms have been omitted from (1.1). The omission of diffusion terms may not be justified in the vicinity of large height gradients such as those mentioned below. Nevertheless these equations describe the gross features of the ionosphere. Numerous complex chemical reaction schemes have been put forward to explain and predict the concentration of various ion species and neutral reactants. It should be noted that the form of (1.1i) is independant of such reaction schemes while the values of the parameters α , β , γ , δ depend on the ionic composition of the atmosphere at the given height and are weighted means of perhaps a number of reaction rates. For example

$$\alpha = \Sigma \alpha_i \, N_i^+ \, / \, N^+$$

where α_i is the reaction rate of electrons with the ith species of positive ion with number density N_i^+. The term "macroscopic" or "effective" is used to distinguish the mean parameters of equation (1.1) from the actual rate parameters of the individual reactions.

It is immediately obvious that the macroscopic parameters α , β , γ , δ are likely to be not only functions of height in the atmosphere but also of time; the atmosphere may well behave differently to sudden changes in ion pair production rate from the way in which it reacts to quasi-steady - state changes since the positive and negative ion composition may differ in the two cases. For the same reason the rate equation parameters may also depend on the production rate q and on the types of positive ions that are produced by the ionizing source.

There is a third equation , that required by electrical neutrality :

$$N^+ = N + N^- \qquad (1.2)$$

which yields the continuity equation for positive ions. Adding (1.1a) and (1.1b)

$$\frac{dN^+}{dt} = q - \alpha N N^+ - \gamma N^- N^+ \qquad (1.3)$$

For simplicity let us introduce a further variable

$$\lambda = N^- / N$$

Then

$$N^- = \lambda N$$

and

$$N^+ = (1 + \lambda) N$$

Then (1.1) becomes

$$\frac{dN}{dt} = \frac{q}{1 + \lambda} + (\alpha + \lambda\delta)N^2 - \frac{N}{1 + \lambda} \frac{d\lambda}{dt} \qquad (1.4)$$

The assumption is frequently made that

$$\frac{d\lambda}{dt} = 0$$

whence

$$\frac{dN}{dt} = \frac{q}{1 + \lambda} - (\alpha + \lambda\gamma) N^2 \qquad (1.5)$$

i.e.

$$\frac{dN}{dt} = \frac{q}{1 + \lambda} - \alpha_{eff} N^2 \qquad (1.6)$$

where

$\alpha_{eff} = \alpha + \lambda\gamma$ is called the "effective recombination coefficient" (see, for example, Whitten & Poppoff, 1965 page 143). The assumption (1.5) is not justified and will be discussed again in a later section. Equation (1.6) is not a valid approximation to equations (1.1).

For steady-state conditions, all the derivatives are zero and we have

$$q = (1 + \lambda) (\alpha + \lambda\gamma) N^2 \qquad (1.7)$$

i.e. $q = \psi N^2$

Where $\psi = (1 + \lambda)(\alpha + \lambda\gamma)$ is termed the electron loss rate. Its value determines the steady state electron density at any height in terms of the ion pair production rate. When

$$\lambda \ll 1. \text{ then } \psi = \alpha$$

From equation (1.1b) for steady-state conditions we have

$$N = (\beta - \lambda\delta)/\gamma\lambda(1 + \lambda) \qquad (1.8)$$

from (1.7) and (1.8)

$$q = \frac{(\beta - \lambda\delta)(\alpha + \lambda\gamma)}{\gamma^2 \lambda^2 (1 + \lambda)} \qquad (1.9)$$

from which

$$\lambda = \frac{\beta}{\sqrt{\phi \gamma q} + \delta} \qquad (1.10)$$

where $\phi = (1 + \lambda)/(\alpha/\gamma + \lambda)$ is a slowly varying function of λ lying between 1 and γ/α.

1.4. The Rate Equation Parameters

1.4.1. Attatchment Processes

One process is thought to predominate in the formation of negative ions from electrons:

$$O_2 + O_2 + e \rightarrow O^-_2 + O_2 \qquad (1.11)$$

There is little disagreement over the rate coefficient for this process. Laboratory measurements have consistently yielded a value of between 10^{-30} and 3×10^{-30} cm.^{6} sec.$^{-1}$ (Chanin et al, 1959; Pack and Phelps, 1966). We will use the value

$$K = 1.6 \times 10^{-30} \text{ cm}^6. \text{ sec.}^{-1}$$

Another possibility for electron attachment is

$$e + O_2 \rightarrow O_2^- + h\nu \qquad (1.12)$$

which has a reaction rate coefficient of 9×10^{-17} at 375^oK (Pack and Phelps, 1966). Assuming that neither rate coefficient is a strong function of temperature, the process (1.12) will predominate over (1.11) only for O_2 concentrations of less than 6×10^{13} cm.$^{-3}$ i.e. above 82 Km. At such heights λ is likely to be much less than unity, there are few negative ions and attachment - detatchment processes are of little importance. We can therefore neglect process (1.12) and write

$$\beta = 1.6 \times 10^{-30} \text{ m}^2$$

where m is the concentration of molecular oxygen.

1.4.2 Detachment Processes

That radio-wave absorption increases during the daytime has been known since the days of the first radio transmissions. A striking example of such daytime enhancement of absorption is demonstrated by riometer observations of polar cap absorption (PCA) events. During these events cosmic noise absorption at polar cap stations at 30MHz increases markedly for periods of up to two or three days due to the bombardment of the polar cap ionosphere by solar protons. The absorption is typically about 3 dB at night compared with 9 dB or so during the day.

Molecular oxygen ions, O_2^-, are readily dissociated into molecular oxygen and free electrons by the action of visible light and for many years this process was invoked to explain day-night differences in D-region absorption. The parameter δ was written

$$\delta = \not{\rho} + \gamma n \qquad (1.13)$$

Where ρ is the photodetatchment rate for molecular oxygen ions with a value of .3 to .4 sec^{-1} and γ is the collisional detatchment rate for these ions and was believed to have a value as small as 10^{-16} to 10^{-20} cm^3 sec^{-1} (Bailey, 1959; Phelps and Pack, 1961; Whitten et al., 1965). Here n is the number density of neutral species at the given height. In equation (1.10) λ will be strongly dependant on the value of ρ ; during the day ρ will be the dominant term while at night ρ falls to zero with a consequent increase in λ for similar values of q . This will result in an increase in ψ and decrease in N the electron density and hence in absorption. That is, photo detatchment of O_2^- during the day keeps the electron density high while at night electrons are removed by attachment.

The inadequacy of this picture was demonstrated by G. C. Reid (1961) who examined changes in c.n.a. occuring at dawn at Fort Churchill during a PCA event. A fairly sudden change would be expected as the visible light shadow of the earth crosses the absorbing region and photodissociation of O_2^- ions commences. Instead the observed change was slower and later than predicted (or earlier in the case of the sunset effect) indicating that the shadow of the ozone layer was the important factor not the visible light terminator. This implies that ultra-violet radiation rather than visible light is necessary to dissociate whatever negative ions are present.

More recent work has changed the simple photodetatchment model completely. Associative detatchment of negative ions in the presence of atomic oxygen has been found to be a fast process

by Fehsenfeld et al (1966,1967) and by Moruzzi and Phelps (1966). These experiments showed that the rate is so fast that with more than 10^{10} oxygen atoms per cm.^{3} above 40 Km during the daytime, the O_2^- destruction rate by associative detachment is ten times faster than by photodetachment. Various reaction schemes (Le.Levier and Branscomb, 1968; G.C.Reid 1970; Arnold and Krankowski,1971; Ferguson,1971) indicate that O_2^- is not the dominant negative ion but that it should react rapidly to form CO_3^-, NO_3^- and CO_4^- which are much more stable. Furthermore direct rocket measurements of negative ions densities have shown that ions as heavy as these do indeed make up the bulk of negative ions in the lower ionosphere (Narcisi et al, 1971; Arnold et al,1971).

The strong day night variation in absorption during PCA events now becomes explicable in terms of the day-night variation in molecular oxygen concentration. This is controlled by the photo-dissociation of O_2 and O_3 during the day and the reaction of atomic oxygen back to ozone at night.

Negative ions other than O^-, O_2^- and O_3^- are believed to be stable with regard to photodetachment and collisional and associative detachment and are removed only by mutual neutralization with positive ions. Therefore the removal rate of negative ions will depend largely on the concentrations of these three ions and on the concentration of atomic oxygen i.e.

$$\delta N^- = \sum_{i=1}^{3} (\rho_i + k_i \cdot [O]) \; O_i^- \qquad (1.14)$$

where ρ_i is the photodetachment rate and k_i the collisional or associative detachment rate of the species O_i^-. Thus

$$\delta = \sum_{i=1}^{3} \mu_i (\rho_i + k_i \cdot [O]) \qquad (1.15)$$

where

$$\mu_i = \left[O_i^- \right] / N^-$$

and δ is dependant on the proportion of negative ions which are O^-, O_2^-, and O_3^- and on the neutral molecular oxygen concentration.

1.4.3 Recombination Processes

The ion-ion recombination coefficient, γ, is generally assumed to have a value of about 10^{-7} cm^3.sec.$^{-1}$. The value chosen was found to have little effect on the behaviour of rate equations (1.1). The reasons for this are discussed by Le Levier and Branscomb (1968).

The electron-ion recombination coefficient on the other hand is perhaps the most important single parameter of the rate equations. It was believed that dissociative recombination

$$e + (MN)^+ \rightarrow M + N \qquad (1.16)$$

proceeded much faster than other electron-ion recombination processes and so it is frequently called the "dissociative recombination coefficient". Since the discovery that heavy positive ions predominate below 90 Km this term may prove to be a misnomer.

The recombination coefficient occurs in three forms in the literature, as α, in ψ and in α_{eff}. α_{eff} has been estimated from the time varying behaviour of the ionosphere and ψ from steady state conditions. Estimates of these parameters are summarised graphically by Mitra (1968) and by Jacobs et al (1969).

Estimates of α can be made by examining the high altitude trend of their figures. They vary over a range of two orders at magnitude; from 10^{-8} cm.^{3} sec.$^{-1}$ to 7×10^{-7} cm.^{3} sec.$^{-1}$.

More recent estimates have placed α at greater than 10^{-6} cm.^{3} sec.$^{-1}$ (Gunton and Shaw, 1965).

Thus the controlling parameter of the lower ionosphere is among those for which estimates are least reliable. Estimates of its value are intimately related to estimates of ion pair production rate and are discussed again in section 1.5.2.

1.5 Ion Pair Production

1.5.1. The Nitric Oxide Problem.

The direct sources of ionization in the daytime D-region are solar x-rays, solar ultraviolet radiation and, at higher latitudes, particles from the magnetosphere.

The bulk of the ultraviolet radiation from the sun is in the form of Lyman -α radiation (λ 1215.7 Å) from solar hydrogen. The flux contained in the Lyman -α line is comparable with the integrated flux of the remainder of the solar ultraviolet spectrum. The absorption cross section of N_2 in the u.v. region is very small and so O_2 is the main absorber of solar u.v. in the earth's atmosphere. By coincidence, O_2 has an exceptionally small cross section at almost exactly the frequency of Lyman -α forming a "window" which allows Lyman -α radiation to penetrate deep into the atmosphere i.e. down to 70 Km or so.

Nitric oxide is present in this region of the atmosphere and has a high ionization cross section at λ1215.7 Å. Thus trace quantities of this molecule can give rise to relatively large numbers of electrons and NO^+ ions. The altitude profile of NO between 70 and 80 Km and the flux of Lyman -α radiation are crucial in determining the ion pair production rate in this region of the mid-latitude daytime ionosphere.

Early estimates of NO concentration derived from hypothetical D-region reaction schemes using laboratory measurements of

rate coefficients implied concentrations of 10^5 to 10^6 cm^{-3} which in turn implied ion pair production rates of the order of .1 ion pair cm^{-3} sec^{-1} (Mitra, 1968). However rocket measurements at NO dayglow by Barth (1966) and Pearce (1969) gave much higher values ranging from 4×10^7 cm^{-3} to 1.7×10^8 cm^{-3} which should give rise to ion pair production rates, q, of the order of 10 cm^{-3} sec^{-1}.

These more recent estimates of q place a further strain on α . If attachment processes are neglected, α is required to be as high as 5×10^{-5} $cm.^3$ sec^{-1} in order to explain the observed electron density profiles (G. C. Reid, 1970). Even if these more recent values of NO concentration prove to be in error, our estimates of the ion-pair production rate profile would be unlikely to be restored to its old value. It has recently been shown (Hunten and McElroy, 1968) that excited O_2 in the $^1\Delta g$ state can be ionized by Lyman-α . Measured concentrations of O_2 ($^1\Delta g$) indicate that the production rate of electrons from this source alone is of the same order as that derived from the higher NO concentrations.

1.5.2. The 90 Km. Ledge and Water Cluster Ions

G. C. Reid (1970) has pointed out the frequent occurrence, in rocket electron density profiles, of a "ledge" between 80 and 90 Km in altitude. The ledge consists of an increase in electron density by about an order of magnitude with changes in height of one or two kilometres. Such a sharp gradient is difficult to explain in terms of ionizing electromagnetic radiation since the production rate profile must fall off with decreasing height at a rate determined solely by the scale heights of the ionizing and absorbing species. Molecular and eddy diffusion seem to preclude such large gradients.

In the same height interval Narcisi and Bailey using rocket borne mass spectrometers found a similar ledge in the positive ion composition of the ionosphere. Significant in their findings was the unexpected predominance of positive ions of high molecular weight below the ledge believed to be water cluster ions, $H.(H_2O)_n^+$. G. C. Reid (1970) explains the existence of the electron density ledge and of the anomolously low electron concentrations below the ledge in terms of an enhanced ability of the more complex water cluster ions to recombine with electrons. Consequently α will be higher than previously supposed at these levels. Reid uses the empirical rocket data for electron density and an ion pair production rate profile computed from the high NO figures of Barth to compute an height profile for . He finds α to be 5×10^{-7} above 87 Km and about 5×10^{-5} $cm^3 sec^{-1}$ below this height. He excludes the possibility of attatchment processes contributing significantly to electron loss near 80 Km. this assumption is based on a negative ion reaction model derived from that of LeLevier and Branscomb (1968) in which O_2^- is the dominant negative ion at this height and is destroyed by associative detatchment with O almost as soon as it is formed. He does not seek to explain the abrupt change in positive ion composition at the ledge.

Hunt (1971) has constructed a model based on the reaction scheme of Ferguson and Fehsenfeld (1969) which predicts height variations in H_3O^+ and $H_5O_2^+$ similar to those observed by Narcisi and Bailey. He does not take diffusion into account. On the other hand Hesstvedt (1968) and Bowman et al (1970) using H_2O and O_2 reaction schemes (they ignore ions and NO completely) have shown that ledges in neutral constituent concentration profiles predicted by multiple reaction schemes are altered but not smoothed out by molecular and eddy diffusion processes.

1.5.3 Ionization by Particle Precipitation

There is a growing body of evidence that electrons precipitated from the magnetosphere provide a significant source of ionization in the quiet mid-latitude D-region (O'Brien, 1962, 1964; O'Brien and Laughlin, 1963; Hultquist, 1964; O'Brien et al., 1965; Paulikas et al, 1966; Tulinov 1967; Fritz, 1968; Tulinov et al, 1969; Potemra and Zmuda, 1970; Manson and Merry, 1970). Figures are available for total particle fluxes at energies above 40 KeV and upper limits can be placed on the ionization rates from this source from N_2^+ night airglow measurements.

However the spectra of the precipitating electrons are more uncertain. Manson and Merry (1970) consider a spectrum with e-folding energy of 15 KeV and particle fluxes of the order of 5×10^3 cm^{-2} sec^{-1} (for $E \geq 40$ KeV). Such a spectrum would create a peak in the ionization rate near 90 Km and a ledge near 80 Km. Potemra and Zmuda on the other hand consider power law spectra with exponents around 3.3. Such particles would penetrate deep into the D-region, down to 60 Km, without creating any ledges in the production rate profile.

Precipitating electrons with spectra slightly softer than that used by Manson and Merry, i.e. with about 5 to 10 KeV e-folding energy, would be capable of giving rise to a ledge in ion pair production rate at similar heights to the one discussed above.

1.6 Relevance to High Latitudes

It may be asked : what is the relevance of the discussion in this section of mid latitude phenomena when high latitude phenomena are the subject of this work? The answer lies in the

fact that nearly all that is known about the D-region is known only for mid and low latitudes and must be extrapolated to higher latitudes; many of the processes must be the same. Of greater significance is the possibility that the sudden decrease in cluster ion concentration at 88Km may be brought about by an increase in precipitating electron flux above this altitude and by the increased proportion of N_2^+ ions which would be produced. The reactions which lead from the formation of simple positive ions such as O_2^+ and NO^+ to water cluster ions are not fully understood and the possibility exists that such reactions might be suppressed or inhibited in the presence of higher free electron densities or higher N_2^+ densities. If this is so it suggests that the water cluster ion-high α profile discussed above may not be appropriate to auroral zone phenomena which are controlled by particle precipitation to a greater extent.

SECTION 2.

A D-region Model

2.1 Small Perturbations

Hitherto there seems to have been little discussion in the literature of the response of the ionosphere to small, rapid perturbations in q, the ion pair production rate. The various proposed negative ion reaction schemes have usually been dealt with under steady-state or quasi steady-state conditions and time rates of change of ion densities have been nearly always equated to zero.

The discovery of c.n.a. pulsations exhibiting a time asymmetry adds a new dimension, a new parameter to our empirical knowledge of the D-region. Here we have small perturbations in cosmic noise absorption for which a relaxation time can be read directly from a pen recorder chart. The c.n.a. pulsations observed with fast response riometers are fast; their rise times vary from 1 to 5 seconds. They are also small, their measured amplitudes are less than .4dB. Superimposed on backgrounds of greater than .5 dB. of absorption.

To what extent are observed c.n.a. pulsations consistent with know D-region processes? Can they be utilised as a diagnostic tool to glean additional information about this most complex region of the atmosphere? It is the purpose of this thesis to attempt to answer these questions.

The obvious way to go about this is to construct a mathematical model of the relevant part of the atmosphere and to compare the sort of pulsation predicted by the model with those observed experimentally. Values of parameters used in the model

which give rise to unrealistic results can then be eliminated and some of the uncertainties in our estimates of D-region parameters and processes can perhaps be reduced.

2.2 Complete Reaction Schemes

Any complete reaction scheme would involve one differential equation for each species of positive or negative ion present. Many of these d.e.s. would be non-linear (even for small perturbations) and would need to be solved numerically. The number of parameters needing to be varied in order to gain an insight into the dependence of the output pulse on them is likely to be large.

For this reason it seems more reasonable to use a simplified model which includes fewer parameters. A model was constructed based on the Bates and Massey equations (1.1), as discussed in the previous section. These equations were solved numerically for N as a function of time for a number of discrete heights in the atmosphere using a suitable driving function $q = q(h,t)$.

The resulting absorption pulse was then computed from N(t) using the Sen-Wyller(1960) formula for non-deviative absorption.

The question now arises: to what extent can the pulsations in q and N be regarded as small perturbations in that the rate parameters, $\alpha, \beta, \gamma, \delta$ can be regarded as constant during the course of a pulsation ? The attachment rate coefficient β is a property of the atmosphere and predicted absorption pulses are almost completely independant of the value of γ used in the model. The electron-ion recombination coefficient and the electron detachment coefficient remains to be discussed.

2.3 Negative Ion Reaction Schemes

2.3.1 The Charge Transfer Matrix

Consider equation (14) of Le Levier and Branscomb(1968).

$$\Gamma_1\lambda_1 - K_b O_3 = 0$$

$$\Gamma_2\lambda_2 - K_3O\lambda_3 - K_5O\lambda_5 - K_a(O_2)^2 = 0$$

$$\Gamma_3\lambda_3 - (m_1O_3 + [O_2]^2)\lambda_1 - m_2O_3\lambda_2 = 0$$

.....

etc. (2.1)

where λ_i is the ratio N_i/N where N_i is the number density of the ith species and Γ_i is the loss rate for this species. Multiplying each equation by N, the electron density, we have

$$\Gamma_1N_1 - K_bO_3N = 0$$

$$\Gamma_2N_2 - K_3O\,N_3 - K_5ON_5 - K_a(O_2)^2N = 0$$

.....

etc. (2.2)

These equations describe the quasi-steady-state situation. The dynamic situation is arrived at by simply replacing the zeros on the right hand sides by $-dN_i/dt$. Thus

$$\frac{dN_1}{dt} = K_bO_3N - \Gamma_1N_1$$

$$\frac{dN_2}{dt} = K_a(O_2)^2N + K_3ON_3 + K_5ON_5 - \Gamma_2N_2$$

.....

etc. (2.3)

A complete model representing the behaviour of the ionosphere in the presence of pulses in q would incorporate the differential equations appropriate to each ion species, together with the d.e. for electrons (similar to (1.1a)) the change

neutrality condition, and a similar set of d.e.s. for positive ions.

Since the Γ_i include a recombination term, $\gamma_i N^+$, the equations (2.3) are nonlinear and, in general, would have to be solved numerically. They can however be written as a matrix equation.

$$\frac{d\{N\}}{dt} = \{Q\} + \{B\}.\{N\} \qquad (2.4)$$

where

$$\{N\} = \begin{Bmatrix} N_1 \\ N_2 \\ \cdot \\ \cdot \\ \cdot \\ N_n \end{Bmatrix}$$

$$\{Q\} = \begin{Bmatrix} q(t) \\ 0 \\ 0 \\ \cdot \\ \cdot \\ \cdot \\ 0 \end{Bmatrix}$$

and

$$\{B\} = \begin{Bmatrix} -\Gamma_1 & \beta_{12} & \beta_{13} & \cdots & \beta_{1n} \\ \beta_{21} & -\Gamma_2 & \beta_{23} & \cdots & \beta_{2n} \\ \beta_{31} & \cdots & & & \\ \cdot & & & & \\ \cdot & & & & \\ \cdot & & & & \\ \beta_{n1} & \cdots & & & -\Gamma_n \end{Bmatrix}$$

where N_1 is here the number density of electrons, N_i $(1 < i \leqslant m)$ is the number density of the i th negative ion species and β_{ij} is the loss rate of the i th species in the reaction $N_i^- + X \rightarrow N_j^- + Y$ (2.5)

i.e.

$$\beta_{ij} = K \cdot [X]$$

where K is the reaction rate of (2.5).

For small pulses where changes in N^+ can be ignored all the elements of $\{B\}$ are constant and B is a property of the atmosphere at any height. Equation (6) can then be solved for $\{N\}$.

The solution is

$$\{N(t)\} = e^{\{B\}t}\{N_o\} + e^{\{B\}t} \int_o^t e^{-\{B\}t} \{Q\}\, dt$$

Here the matrix e^{Bt} can be given a precise definition and it can be shown that its elements can be written in the form

$$\sum_{K=1}^{n} b_k e^{\lambda_k t}$$

where the λ_k are the eigen-values of the matrix $\{B\}$ (see Apostol (1969), Chapter 7.)

Thus ultimately the negative-ion dynamic behaviour of the ionosphere depends on the eigen-values of the charge trnasfer matrix $\{B\}$.

In practice it is scarcely worthwhile computing the eigen-values of $\{B\}$ since all of the elements of $\{B\}$ are not known with any degree of certainty and most are, of course, strongly dependant on height.

2.3.2 Detachment Coefficient Variability

As mentioned in 1.4.2. only O^-, O_2 and O_3^- ions are likely to suffer collisional detachment or photo detachment at a rate expressed by equation (1.14). The reaction schemes of Le Levier

and Branscomb (1969) and of G. C. Reid (1970) indicate that

$$[O_2^-] \gg [O^-]$$

and $$[O_2^-] > > [O_3^-] \quad .$$

at all heights for both day and night equilibrium conditions.

Following LeLevier and Branscomb, in (1.15) -

$k_1 = 2 \times 10^{-10}$ cm^3 sec^{-1} $\rho_1 = 1.4$ sec.$^{-1}$

$k_2 = 3.3 \times 10^{-10}$ cm^3 sec.$^{-1}$ $\rho_2 = 0.4$ sec.$^{-1}$

$k_3 = 10^{-10}$ cm^3 sec^{-1} $\rho_3 = 0.01$ sec.$^{-1}$

Hence $K_2 [O] [O_2^-]$ is easily the dominant term in the expression for δN^- (1.14).

Hence

$$\delta = K_2 [O] \frac{[O_2^-]}{N^-} \qquad (2.7)$$

Since the factor $K_2 . [O]$ is a property of the atmosphere, the way in which δ varies with time and with q is entirely dependant on how the ratio $[O_2^-] / N^-$ varies. This in turn is dependant on the detail of all of the reactions involving negative ions expressed by equation (2.4) above.

In order to get a rough idea of the behaviour of this ratio with changes in q let us consider an abbreviated version of the negative ion reaction scheme of LeLevier and Branscomb (1968). Negative ions in this scheme fall into three classes, -

viz :

i) Attatchment - detatchment species, 0^- and 0_2^-. These ions are the only ones likely to be formed by direct attatchment of electrons to neutral molecules and the major ones to experience direct detatchment of electrons by collisions with atomic oxygen. Let their number density be N_a ;

ii) Storage species, 0_3^-, $C0_3^-$ and $C0_4^-$, which are formed directly from 0^- and 0_2^- and can be converted back into 0^- and 0_2^-. Let their number density be N_s;

iii) terminal species, $N0_2^-$ and $N0_3^-$. These are highly stable ions which are only removed by mutual neutralization. Let their number density be N_t.

Let us assume that loss by neutralization is only significant compared with change interchange processes in the case of electrons and terminal ions.

The system is described by the four differential equations

$$\frac{dN}{dt} = q - \alpha N N^+ - \beta N + \delta' N_a \qquad (2.8)$$

$$\frac{dN_a}{dt} = \beta N - \delta' N_a - \psi N_a + \theta N_s \qquad (2.9)$$

$$\frac{dN_s}{dt} = \psi N_a - \theta N_s - \xi N_s \qquad (2.10)$$

$$\frac{dN_t}{dt} = \xi N_s - \gamma_t N_t N^+$$

in matrix form

$$\frac{d\{N\}}{dt} = \{Q\} - \{B\}\{N\}$$

where $\{B\} =$

$$\begin{Bmatrix} -(\beta + \alpha N^+) & \delta' & 0 & 0 \\ \beta & -\delta' + \psi & 0 & 0 \\ 0 & \psi & -(\theta + \xi) & 0 \\ 0 & 0 & \xi & -\gamma_t N^+ \end{Bmatrix} \qquad (2.12)$$

We have assumed that direct conversion of attachment to terminal ions is small compared with other processes.

Equating the derivatives (2.8) through (2.11) to zero for steady state conditions we find

$$N_t/N_s = \xi / \gamma_t N^+ \qquad (2.13)$$

$$N_s/N_a = \psi/ \theta \qquad (2.14)$$

$$N_a/N = \beta / \delta' \qquad (2.15)$$

$$q = \alpha N N^+ \qquad (2.16)$$

Thus $N_a/N^- = N_a/(N_a + N_s + N_t)$

$$= 1/(1 + \frac{\psi}{\theta} \quad (1 + \frac{\xi}{\gamma_t N^+} \quad)) \qquad (2.17)$$

The variation of the ration in (2.13), (2.14), (2.15) with height in the quiet mid-latitude daytime ionosphere can be seen in figures (6) and (8) of G. C. Reid's (1970) paper. For small values of

$$\xi /\gamma_t N \quad , \text{ i.e. for } N_t/N_s << 1$$

$$\frac{N_a}{N^-} = \frac{1}{1 + \psi/\theta}$$

Below about 80 Km Nt/Ns > 1 and $/\theta >> 1$ and we have

$$\frac{N_a}{N^-} \simeq \frac{\theta \gamma_t N^+}{\psi}$$

Substituting (2.13) through (2.16) into the neutrality equation

$$N^+ = N + N_a + N_s + N_t$$

we have

$$N^+ = \frac{q}{\alpha N^+} + \left[\left(1 + \frac{\beta}{\delta} + \frac{\beta\psi}{\delta\theta} \right) + \frac{\beta\psi}{\delta\theta\xi\alpha_t N^+} \right]$$

i.e.

$$N^{+3} = \frac{q}{\alpha} \quad (AN^+ + B)$$

where A and B are independant of q. Thus N^+ varies either as the square root or cube root of q. the detatchment coefficient S is given by

$$\delta = \delta' \frac{N_a}{N^-}$$

$$= \frac{\delta' \theta \gamma_t \quad N^+}{\psi}$$

Thus δ will not be a strong function of q for small quasi equilibrium variations in q.

For the non-steady-state case, where there is a pulse in q the time behaviour of N, N_a, N_s and N_t is dependant on the eigen values of the matrix $\{B\}$ in equation (2.12). It can be shown that these are real and negative implying that the behaviour of the pulse as it passes from one ion species to another is "diffusive" i.e. the pulse will be smaller and more spread out as it passes from species to species. Thus the time variation of the ratio N_a/N^- is likely to be even less dependant on q for a short pulse than for a quasi steady state variation.

2.4 Recombination Coefficient Variation

The macroscopic electron-ion recombination coefficient, α, is a function of the positive ion composition of the atmosphere and is a weighted mean of the individual recombination coefficients of each positive ion species. A large coefficient for recombination of electrons with water cluster ions has been postulated in order to account for the anomolously low electron content of the day time, mid-latitude D-region (see 1.5.2.). The question now arises as to how strongly dependant is the proportion of water cluster ions, and hence α, on the ion pair production rate q and on rapid variations in q.

The rate of formation of cluster ions would be expected to be proportional to the ambient positive ion density at any height. Let KN^+ be the rate of formation of cluster ions with number density C^+ from such ions as NO^+, O_2^+, N_2^+ with concentration N^+. Let α_c and α_D be the electron-ion recombination coefficients of the cluster ions and of the more slowly reacting ions respectively. The parameters K, α_c and α_D are perhaps weighted means of various reaction rates but this does not greatly affect what follows. The following equations describe the steady state balance of electrons, cluster ions and slowly recombining ions.

positive ions balance:

$$0 = q - KN^+ - \alpha_D NN^+ \qquad (2.21)$$

cluster ion balance:

$$0 = KN^+ - \alpha_c C^+N \qquad (2.22)$$

electrons:

$$0 = q - \alpha_D NN^+ - \alpha_c NC^+ \qquad (2.23)$$

where q is the ion pair production rate and $N(= N^+ + C^+)$ is the electron density. Attachment processes are ignored for simplicity. Equation (2.23) can be written:

$$0 = q - \alpha N^2$$

$$\text{where } \alpha = (\alpha_D N^+ + \alpha_c C^+)/N \qquad (2.24)$$

is the effective recombination coefficient. From (2.22) we have

$$0 = K(N-C^+) - \alpha_c C^+ N$$
$$= KN - (K + \alpha_c N) C^+$$

Thus

$$C^+ = KN/(K + \alpha_c N) \qquad (2.25)$$

and C^+ has a maximum value of K/α_c however large the electron density may be. For small electron densities i.e. for $N \ll K/\alpha_c$ $C^+ \simeq N$ i.e. nearly all the positive ions will be in the form of water cluster ions.

Substituting (2.25) in (2.24)

$$\alpha = \alpha_D (1 - C^+/N) + \alpha_c C^+/N$$

i.e.
$$\alpha = \alpha_c \cdot \left\{ \frac{K + \alpha_D N}{K + \alpha_c N} \right\} \qquad (2.26)$$

thus when $N > K/\alpha_D$, $\alpha \simeq \alpha_D$

and when $N < K/\alpha_c$, $\alpha \simeq \alpha_c$

Equation (2.25) can be rewritten

$$\frac{K}{\alpha_c} = \frac{N C^+}{N^+} = \frac{N(N - N^+)}{N^+} \qquad (2.27)$$

hence we can estimate K/α_c by examination of the ion species density profiles obtained by Narcisi and Bailey (1965). At 85 Km the only known slowly recombining species is NO^+ which makes up about ten per cent of the total positive ion content of 6×10 cm^{-3}. If we assume that all the other species are rapidly recombining we have at 85 km

$$\frac{K}{\alpha_c} = 5 \times 10^4 \text{ cm.}^{-3}$$

Similarly at 70 Km $K/\alpha_c = 1.6 \times 10^4$ com^{-3}. Electron densities of this order at these heights could give rise to c.n.a. of about 1 dB, i.e. in the range of the observed absorption background for c.n.a. pulsation events. That is for real events the condition

$$K/\alpha_D > N > K/\alpha_c \quad \text{is likely to}$$

apply, in which case according to equation (2.26), α will be strongly dependant on N and therefore on q.

In a non-steady-state situation (2.21), (2.22) and (2.23) become

$$\frac{dN^+}{dt} = q - S - \alpha_D N N^+ \qquad (2.28)$$

$$\frac{dC^+}{dt} = S - \alpha_c C^+ N \qquad (2.29)$$

$$\frac{dN}{dt} = q - \alpha_D N N^+ - \alpha_c N C^+ \qquad (2.30)$$

where $S = S(t)$ is the rate at which cluster ions are formed from other positive ions. $S = KN^+$ only for the quasi equilibrium

situation since cluster ions are likely to be formed from NO^+, N_2^+ and O_2^+ by a series of three or four reactions involving such intermediate species as O_4^+ and $O_2 \cdot (H_2O)^+$ (Ferguson, 1971). To a large extent the production of cluster ions in the course of a pulse will be decoupled from the pulse in N^+. For fast pulses S will be almost constant and an increase in N will result in a negative value of dC^+/dt, a decrease in C^+ and hence a decrease in α. If G. C. Reid's high α cluster ion theory is correct α is likely to be not only strongly q dependant but also time dependant.

For the moment however in order to develop the simple model based on the Bates and Massey rate equations (1.1) we will assume that α can be regarded as constant at any height in the atmosphere. We will return to this topic in discussing the experimental results in section 4.

2.5 The Ion Pair Production Rate

2.5.1. The Primary Spectrum

The absorption of cosmic noise by free electrons in the ionosphere is dependant on the collision frequency, the rate at which electrons lose energy by collisions with neutral molecules. The collision frequency is strongly dependant on height. Above 60 Km the absorption of cosmic noise at 32 MHz for a given electron density falls off by 1/e for each $6\frac{1}{2}$ Km increase in height. Thus in computing the absorption as seen from the ground brought about by a pulse of ionizing radiation entering the top of the atmosphere, the height at which the absorbing electrons are created is of crucial importance.

Equations (1.1) are non-linear which implies that the shape of a pulse in N will, in general, depend on the background value

of N itself. Furthermore at least one of the parameters of (1.1), β is strongly dependent on the height. These features indicate that the size and shape of a pulse in absorption computed from a pulse in q will be strongly dependent on the height distribution of the pulse in q and on the height distribution of the background ionization profile on which the pulse in q is superimposed.

The association of c.n.a. pulsations with fast bremmstrahling X-ray pulsations and with luminosity pulsations in the IBC 1-2 range (Appendix I) indicates that electrons precipitated from the magnetosphere over quite large regions (Appendix II) are responsible for pulsations in ion pair production rate, $q(h,t)$, which in turn yield the observed absorption pulsations. The height distribution of $q(h,t)$ will be a function of the energy spectrum and angular distribution of these dumped electrons.

Observation of precipitating electrons during both active and quiet auroras by means of rocket borne electrostatic analyzers (Chase, 1970) indicate that their spectrum consists of two parts which are almost unrelated viz. (i) a region from 1KeV to 10 or 20 KeV which is flat during a quiet aurora and develops a strong peak when the aurora becomes active and (ii) an exponental tail above 20 KeV with an e-folding energy of from 3 to 5 KeV which is relatively unchanged during large changes in the flux in the low energy component.

Since c.n.a. pulsations or associated phenomena were not reported during this particular experiment these spectra can in no way be taken as representative of the electrons responsible for c.n.a. pulsations. Since c.n.a. pulsations are observed largely in the mid-morning hours when the spectra of precipitating particles appears to harden (Ansari, 1964;

Bewersdorff et al,1967) their e-folding energies may be much larger than this. Nevertheless we will adopt the concept of a two component spectrum i.e. one that is flat from 1 to 10 KeV with an exponential tail above 10 KeV. The e-folding energy of this tail and the total flux of electrons will be the only variables associated with the spectra used in the model. The precipitating patricles are assumed to be isotropic over the downward hemisphere.

2.5.2 Bremmstrahlung Ionization

A number of workers have investigated the transport and energy deposition of electrons in the atmosphere (e.g. Chamberlain,1961; Rees,1963,1964; Kamiyama,1967; Walt et al, 1967; Berger et al,1970; Catchpoole,1970). Their orientation has been largely towards the computation of auroral luminosity profiles and intensity ratios. At the time of commencing this project only Rees (1964), and Kamiyama (1967) had paid much attention to ion-pair production below 80 Km where photo-ionization of air by the bremmstrahlung x-rays created by the precipitating electrons becomes predominant. Both of these authors computed ionization profiles for an exponential spectrum of primary electrons with e-folding energy of 5 KeV and their results should be directly comparable (i.e. compare Fig.5(b) of Rees (1964) and Fig. 4 of Kamiyama (1967). Unfortunately their profiles for bremmstrahlung ionization are quite different. Kamiyama's profile has a peak at 90 Km while that of Rees peaks at 50 Km. This may be explicable in that Rees uses a spectrum of the form

$$f(\mathcal{E}_o)\, d\mathcal{E}_o \sim \mathcal{E}_o \exp(-\mathcal{E}_o/\alpha)\, d\mathcal{E}_o$$

while Kamiyama's has the form

$$f(\mathcal{E}_o)\, d\mathcal{E}_o \sim \exp(-\mathcal{E}_o/\alpha)\, d\mathcal{E}_o$$

resulting in a much larger flux of primaries below 5 KeV.

Despite this, the two spectra should yield similar bremmstrahlung ionization rates deep in the atmosphere whence only the higher energy x-rays can penetrate because of the high photoelectric absorption cross-section of air below 10 KeV. At a height of 50 Km Rees predicts an ionization rate three orders of magnitude less than the peak rate due to impact ionization while Kamiyama predicts a bremmstrahlung ionization rate at this height which is six orders of magnitude less than his impact ionization peak.

This discrepancy in estimates of bremmstrahlung ion pair production rates at 50 Km is of some significance. For a given electron density, N, the absorption of cosmic noise at 32 MHz is about three orders of magnitude greater at 50 Km than at 105 Km where the impact ionization maxima lie. Thus if the electron density were to be proportional to ion pair production rate the situation described by Rees would imply a degree of cosmic noise absorption at 50 Km greater than that at 105 Km due to impact ionization, while Kamiyama's curves imply a degree of c. n. a. due to bremmstrahlung which is negligably small. For steady state conditions the electron density is certainly not proportional to the ion pair production rate since we have

$$q = \psi N^2$$

and ψ is likely to be so large at 50 Km that N can be neglected whichever value of q is correct. However we are concerned here with pulses. The equations (1. 1) imply that for sufficiently short pulses in with amplitude Δq, the corresponding increase in electron density ΔN may be approximated by

$$\Delta N \simeq \int_0^{\Delta t} \Delta q \, dt \simeq \Delta q . \Delta t \qquad (2.31)$$

Thus for transient phenomena there is a degree of proportionality holding between N and q which makes the discrepancy between the bremmstrahlung ion-pair production rates of Rees and of Kamiyama of utmost importance. If the former is correct the bulk of cosmic noise absorption occurring during a pulse of 5 KeV primaries takes place at a height of about 50 Km, while if the latter's profile is correct, for the same conditions the bulk of the pulse absorption will occur at over 100 Km in height.

Neither Rees nor Kamiyama take multiple compton scattering into account and both treat the compton scattering cross-section as if it were a simple absorption cross-section.

For these reasons the ionization rate profiles produced by a variety of precipitating electron spectra were calculated afresh taking multiple compton scattered bremmstrahlung into account. The computor program for doing this is described in Appendix IV. The resulting 5 KeV profile resembles Kamiyama's profile much more closely than that of Rees at lower heights.

The impact ionization part of the profiles were computed in a similar manner to those of Rees (1963). The height distribution of ion-pair production rate produced by spectra with e-folding energies of 5, 10, 20, 40 and 80 KeV are shown in Fig. 2.1.

The discrepancy between the profiles of Kamiyama and Rees can be attributed to the latter's incorrect use of the differential cross-section for bremmstrahlung production in equations (5) and (6) of his 1964 paper. His equation (5) was written

$$P_h^D(k) = \int_{\varepsilon_{o\,min}}^{\varepsilon_{o\,max}} \phi(\varepsilon_o, k)\psi^D(\varepsilon_o)\, g(\varepsilon_o, h)\, d\varepsilon_o$$

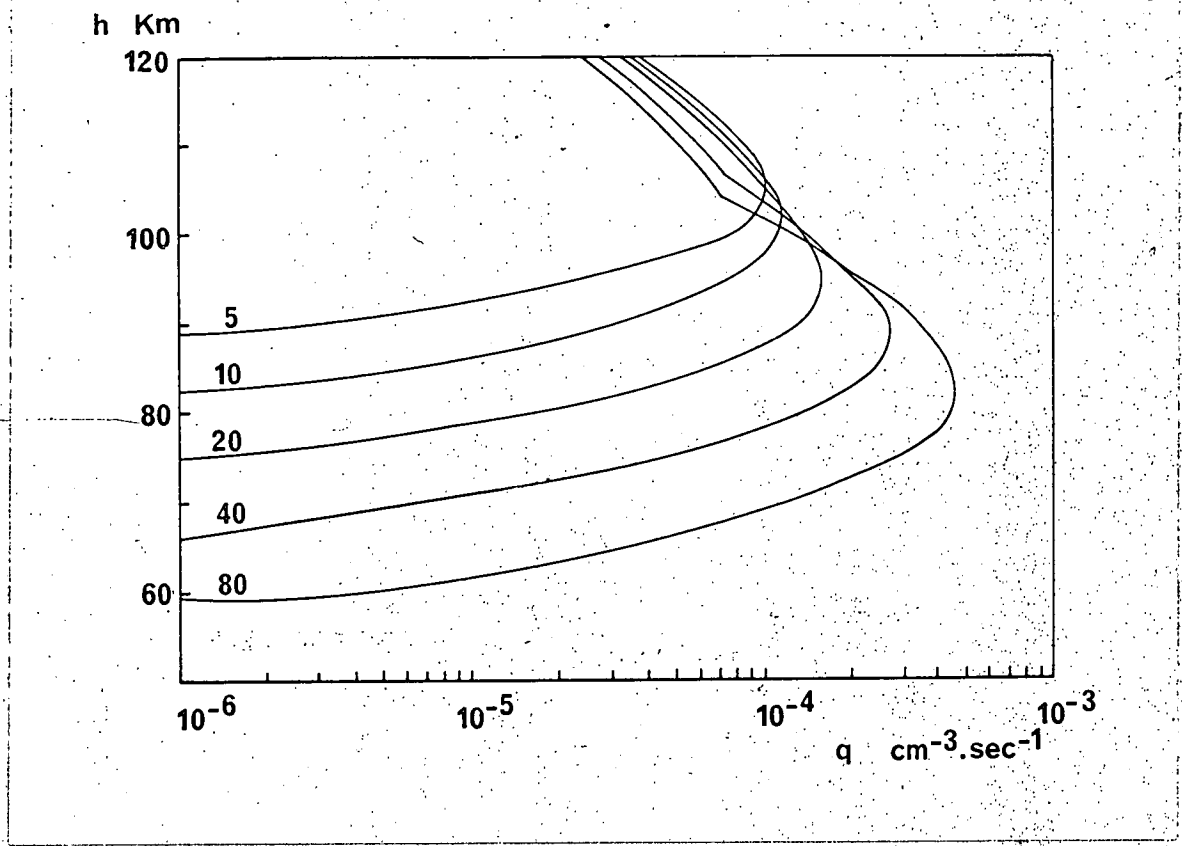

Fig. 2.1.

Ion - pair production rates calculated for unit fluxes of electrons in the energy range 1 keV to 510.8keV incident on the top of the atmosphere. Each flux was taken as isotropic over the downward hemisphere and as having a differential energy spectrum flat from 1 to 10 keV and falling off exponentially with increasing energy for energies greater than 10 keV. Each curve is labelled with the e - folding energy in keV. of this high energy tail.

and should have been written

$$P_h^D(k)\,dk = \int_{\mathcal{E}_{o\min}}^{\mathcal{E}_{o\max}} \frac{(\mathcal{E}_o,k)}{k}\,\psi^D(\mathcal{E}_o)\,g(\mathcal{E}_o,h)\,d\mathcal{E}_o\,dk$$

since the cross-sections $(\mathcal{E}_o,k)$ is given in Table 1 of the paper and computed from the empirical formulae of Kirkpatrick and Weidmann(1945) must be differential energy cross-sections not number cross-sections which diverge at zero. The bremmstrahlung flux computed using the energy cross-section incorrectly in this way will be spuriously high at higher energies yielding a much greater degree of ionization much lower down in the atmosphere than would otherwise be the case.

2.5.3 Some Reservations

The assumptions made about the nature of the precipitating particle spectra and pitch angle distributions should not perhaps, be taken too seriously. The complexity and wide variability of spectra and pitch angle distributions observed in actual precipitation events have been demonstrated by O'Brien and Reasoner (1971). Discrepancies between predicted and observed ion pair production rates, as measured with rocket borne instruments, have been observed by Ulwick et al (1967) and attributed by them to the effects of auroral electric fields on the range of precipitating particles. Catchpoole (1970) has demonstrated that quite small electric fields parallel to $\underline{B}$ can have a significant effect on depths of penetration, particularly for the lower energy particles. Nevertheless some assumptions must be made; the e-folding energies associated with the rate profiles of Fig. 2.1 can, at worst, be regarded merely as numbers characterizing the individual members of a group of profiles.

2.6 The Computor Model

A computor program was written in Elliot 503 Algol to solve equations (1.1) numerically for N, for a pulse in q at various heights in the atmosphere from 50 to 160 Km for an assortment of values at the parameters α, β, γ and δ, and then to evaluate the resulting riometer absorption as a function of time. Since the equations are non-linear and the observed pulses are superimposed on a relatively steady background of absorption, some sort of steady background must be incorporated into the model. The ionization rate profile $q(h,t)$ was taken as

$$q(h,t) = q_o(h) + \Delta q(h)\, p(t)$$

$$= q_r(h) + F_b q(h, E_{ob}) + F_p q(h, E_{op}) p(t) \qquad (2.32)$$

where h is the height in the ionosphere in Km.,

t is the time in seconds,

q_r is the rate of background ionization, due to electromagnetic radiation and to cosmic rays,

F_b is the flux at the top of the atmosphere the steady background of primary electrons with e-folding energy E_{ob},

$q(h, E_{ob}0$ in the ion pair production rate at height h, due to incident electron flux at the top of the atmosphere with e-folding energy E_{ob},

F_p is the peak top-of-the-atmosphere flux of the pulse of primary electrons with e-folding energy E_{op},

$q(h, E_{op})$ is similar to $q(h, E_{ob})$ but is the rate profile appropriate to the e-folding energy E_{op} of the pulse component of the primary flux, and

p(t) is a function which describes the time variation of the pulse in primary electron precipitation and, provided it is symmetric and almost zero outside a certain range of t its shape is fairly arbitrary. For computing reasons, the following function was used:

$$p(t) = \frac{1.111111}{1 + w^2t^2} - 0.111111 \quad \text{when } |t| < 3/w$$

and $$p(t) = 0 \quad \text{when } |t| \geq 3/w \qquad (2.33)$$

where 1/w approximates the half width at half maximum of the pulse in seconds.

The q_r profile of Ogawa and Tohmatsu (1966) to represent night conditions and the (low NO) profile of Mitra (1968) to represent daytime conditions at intermediate heights. The daytime profile of Watanabe and Hinteregger (1962) was used above 110 Km and Webber's (1961) cosmic ray ionization profile was used below 70 Km. For some runs the (high NO) profile of G. C. Reid (1970) was used at intermediate heights. It turns out that for even moderate absorption events i. e. for quite small values of F_b, the q_r profile has very little effect on the predicted pulse shapes and amplitudes.

Programming q in the form (2. 32) made it possible to examine the situation where pulses of precipitating electrons with one spectrum were superimposed on a steady background with an entirely different spectrum since q_o (h) and Δq (h) can represent different ionization rate profiles. In practice the magnitude of the background flux F_b was adjusted so that its contribution to

the steady-state cosmic noise absorption after subtraction of the q_r component was equal to a predetermined level. This level of background c. n. a. was intended to typify that of the SVIA events during which c. n. a. pulsations are observed. It was usually chosen to be either .5 dB or 2.0 dB of absorption.

For each run a q_o (h) profile corresponding to particular values of E_{ob}, F_b and q_r (h) was specified together with values of α, β, γ and δ. The parameter β was taken as $1.6 \times 10^{-30} [O_2]^2$ cm.$^{-3}$sec.$^{-1}$ throughout. The parameters α and δ, usually height independant were, for some runs made functions of height utilizing an Algol edit facility to insert suitable procedures. The parameter F_p was varied for each successive integration across three or four orders of magnitude so as to adequately span the range in which realistic absorption pulse amplitudes resulted. This was done for values of E_{op} corresponding to each of the five profiles shown in Fig. 2.2. (These profiles were also used to determine q (h, E_{ob}), of course).

Equations (1.1) were integrated over a 10 second interval using a fourth order Runge-Kutta process which has the advantage of either converging satisfactorily or diverging rapidly when it does diverge. A step length of 0.1 sec. was usually sufficiently small. The integration was carried out for heights between 50 and 160 Km, the height being incremented in 2 Km steps. The variation in behaviour of equations (1.1) between one value of h and the next was sufficiently small for the integration at one height to serve as a check on its neighbours against divergence and round-off errors.

At each height the absorption resulting from the computed electron density was calculated at 0.1 sec intervals using the expression for longitudinal propogation of Sen and Wyller (1960). Benson's (1964) curves indicate that the error arising from

using this expression for propagation paths which are not parallel to the magnetic field will be less than four per cent for three of the four antenna orientations used at Macquarie Island in 1969. Since the cosmic noise is randomly polarized and since the gyrofrequency is small compared with the operating frequency of 32MHz we may also safely ignore the gyrofrequency term in the Sen-Wyller expression. Thus the absorption in dB, $a(h,t)$ at f MHz which takes place in a 2 Km slab in which the electron density is $N(h,t)cm^{-3}$, and the collision frequency $\nu(h)sec.^{-1}$ will be given by

$$a(h,t) = 2 \times \frac{.1153 \times 10^6}{\nu(h)} C_{\frac{5}{2}}\left(\frac{2\pi f}{\nu(h)}\right) \times N(h,t) \quad (2.34)$$

The function

$$C_{5/2}(x) = \Gamma(7/2)^{-1} \int_o^\alpha E^{5/2}(E^2 + x^2)^{-1} e^{-E} dE \quad (2.35)$$

is tabulated by Dingle, Arndt and Roy(1957). The collision frequency was taken as

$$\nu(h) = 10^8 \exp\ (50-h)/6.47 \quad (2.36)$$

which fits reasonably well the observations of Kane(1960) and Phelps and Pack(1959).

The absorption values computed for each value of h and t in this way were summed over the entire height range and the background absorption subtracted to yield the absorption pulse, a(t), which would be observed by a fast response riometer.

Curves of "specific absorption" i.e. of the function

$$\mu(h) = \frac{.1153 \times 10^6}{\nu(h)} C_{5/2}\ (dBKm^{-1}/(elect.cm^{-3}))$$

are given by Lerfald et al (1964) and quoted by Hargreaves (1969).

The background absorption, A_o, is given by

$$A_o = \int_o^\alpha N_o(h)\, \mu(h)\, dh \qquad (2.38)$$

where N_o is the steady background of electron density. Equation (1.9) was solved for λ which was substituted in (1.8) to obtain $N_o(h)$. The value of q used in (1.9) was given by the term in parenthesis in (2.32).

The computed absorption pulse a(t) was thus an approximation to the function $a'(t)$ where

$$a'(t) = \int_o^\alpha N(h,t)\, \mu(h)\, dh - A_o \qquad (2.39)$$

where N(h,t) is the solution of (1.1) at height h km.

SECTION 3

C. N. A. Pulsations - Model Predictions

3.1 The A-τ Diagram

3.1.1 Rationale

The integration of equations (1.1) was carried out in the manner described in the previous section. There are a considerable number of possible combinations of parameters which were used, leading to an almost unmanageable number of predicted absorption pulsations. Some of these are shown in Fig. 4.4 for comparison with observed c.n.a. pulsations. It can be seen that the pulsations obtained from different combinations of parameters are quite similar in appearance; the only features which vary to any extent and the amplitude of the pulsation and the slope of the relaxation part of the pulsation. The characteristics of the pulsations obtained by integrating (1.1) can, then, be summarised and displayed in terms of two quantities.

If the equations (1.1) were linear the shape of the absorption pulse would be independant of its magnitude. Larger pulses would have proportionately steeper slopes. Where the pulse in q is short compared with the decay time, the shape of the relaxation part of the absorption pulse would be exponential and a time constant could be calculated by merely dividing the relative absorption a(t) at time t by the negative slope at that time -$\dot{a}$(t) i. e.

$$\tau = -a(t) \; / \; \dot{a}\,(t) \qquad (3.1)$$

In practice the observed pulses are usually too noisy to make detailed measurements worthwhile and it is simpler to define a "relaxation time", τ , as

$$\tau = -\,A \; /(\dot{a})_{max} \qquad (3.2)$$

i.e. the amplitude of the pulse above background, A, divided by the maximum slope. τ has the advantage of being a quantity which is independant of system sensitivity.

Owing to the non-linear terms αNN^+ and $\gamma N^- N^+$ in (1.1), τ will only be constant with pulse amplitude for small perturbations in N and will decrease with increases in N and hence in A. The most convenient way of summarising the characteristics of both the predicted and observed c.n.a. pulsations is to plot relaxation time, τ, versus pulse amplitude, A. Of particular interest in the theoretical case are the graphs of τ vs. A for

(i) Pulse precipitation spectra of constant e-folding energy and varying top-of-the-atmosphere flux(i.e. constant E_{op} and varying F_p in (2.31).)

and (ii) pulse precipitation spectra of constant flux and varying precipitation energy (i.e.constant F_p and varying E_{op} in (2.31)).

3.1.2 General Features

Fig. 31 shows such an A-τ diagram. The solid lines represent situation (i) above and are labelled with their respective values of E_o in KeV. The filled circles represent the situation (ii) above corresponding to a primary top-of-the-atmosphere flux of 10^8 electrons cm^{-2} sec^{-1} (integrated over the downward hemisphere and over energies of from 1 KeV to 510 KeV.)

The following features are of interest

(i) as we would expect, τ is almost constant for small values of A and decreases with increasing A.

(ii) for small values of τ, the slope decreases as τ becomes comparable with the width of the pulse in q

iii) in the region of interest i. e. between .04 and .04 dB τ is almost independant of A i. e. the equations can in fact be regarded as linear,

iv) for constant flux, pulse absorption A increases with increasing e-folding energy, as the more energetic spectra create more secondaries and create them lower down in the atmosphere where the collision frequency is higher.

v) for constant flux, τ increases and then decreases with increasing e-folding energy. As the primaries become more penetrating they achieve atmospheric depths of increasingly longer relaxation time until a turnover point is reached and relaxation time decreases with decreasing height. This subject will be discussed further in section 3.2,

3.1.3 Effect of Background

Comparison of Figs. 3.1, 3.2 and 3.3 reveals the effect of absorption background on the A -τ curves. The 80 Kev curve is almost unaffected while the effect of background variation on the softer spectrum curves is quite large.

τ is reduced by a factor of about 5 as the background increased from zero to 0.5 dB and by a factor of about 2.5 as it increases from 0.5 to 2.0 dB. Most of the observed c. n. a. pulsation are superimposed on backgrounds which lie in the latter range.

Only the relaxation time is affected; A/F_p, the absorption-flux sensitivity is almost independant of background for all of the spectra. This is true throughout - a given flux of primaries with a given spectrum always yields roughly the same absorption pulse amplitude. The only parameters which greatly

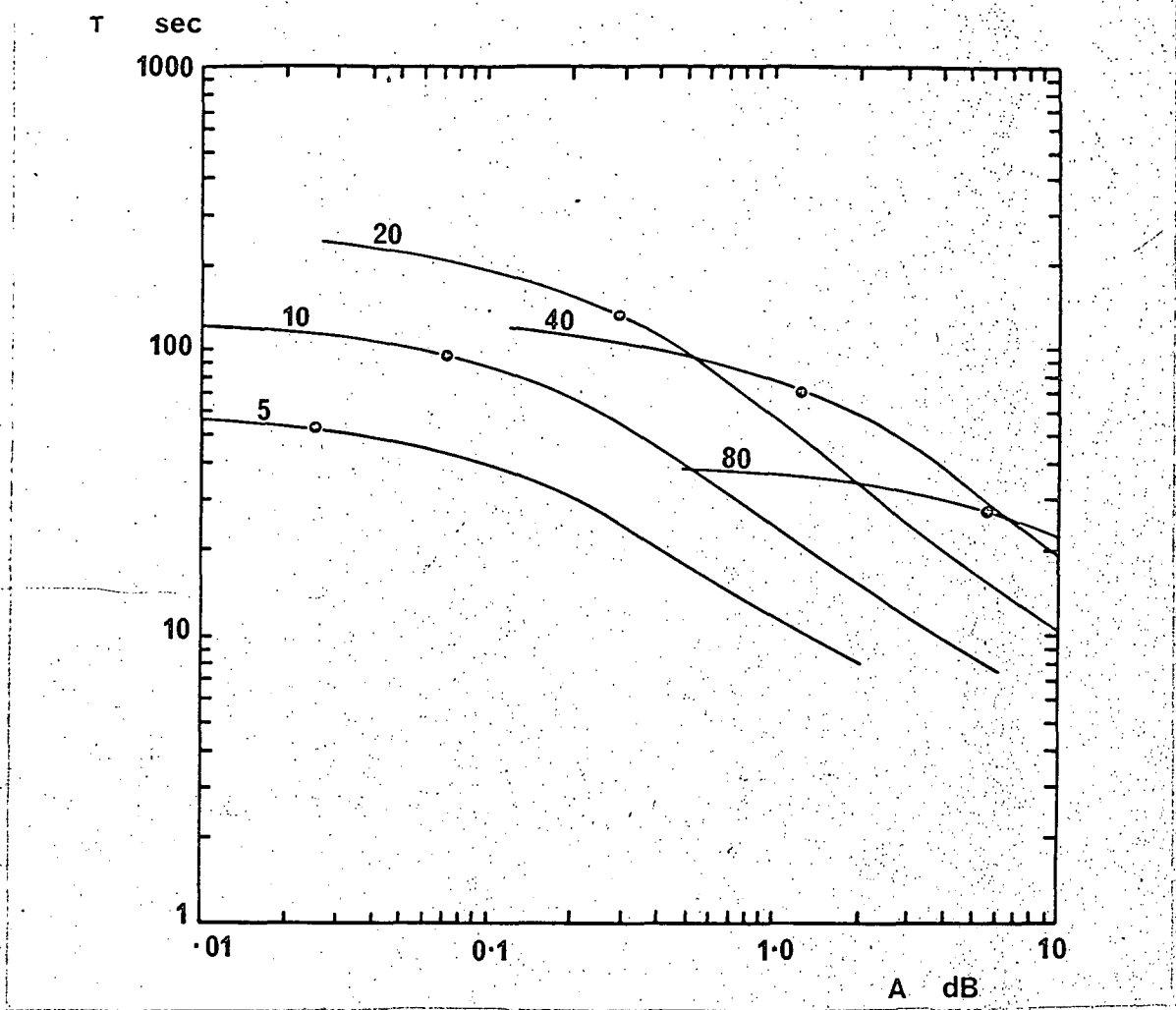

Fig. 3.1.

A-τ diagram for c.n.a. pulsations computed using the following parameters:

recombination coefficient, $\alpha = 2 \times 10^{-7} cm^3.sec^{-1}$.,

attachment coefficient, $\beta = 1.6 \times 10^{-3} m^2 sec^{-1}$.,

ion-ion recombination coeff. $\gamma = 10^{-7} cm^3.sec^{-1}$.,

detachment coefficient $\delta = 0.4\ sec^{-1}$.,

e-folding energy of background $E_{ob} = 5$ keV.,

event background absorption $A_o = 0$ dB.

The curves are labelled with the e-folding energy of the pulse spectrum, E_{op}. The filled circles indicate the locus of a constant flux F_{op} of 10^{-8} electrons $cm^{-2} sec^{-1}$ at the top of the atmosphere.

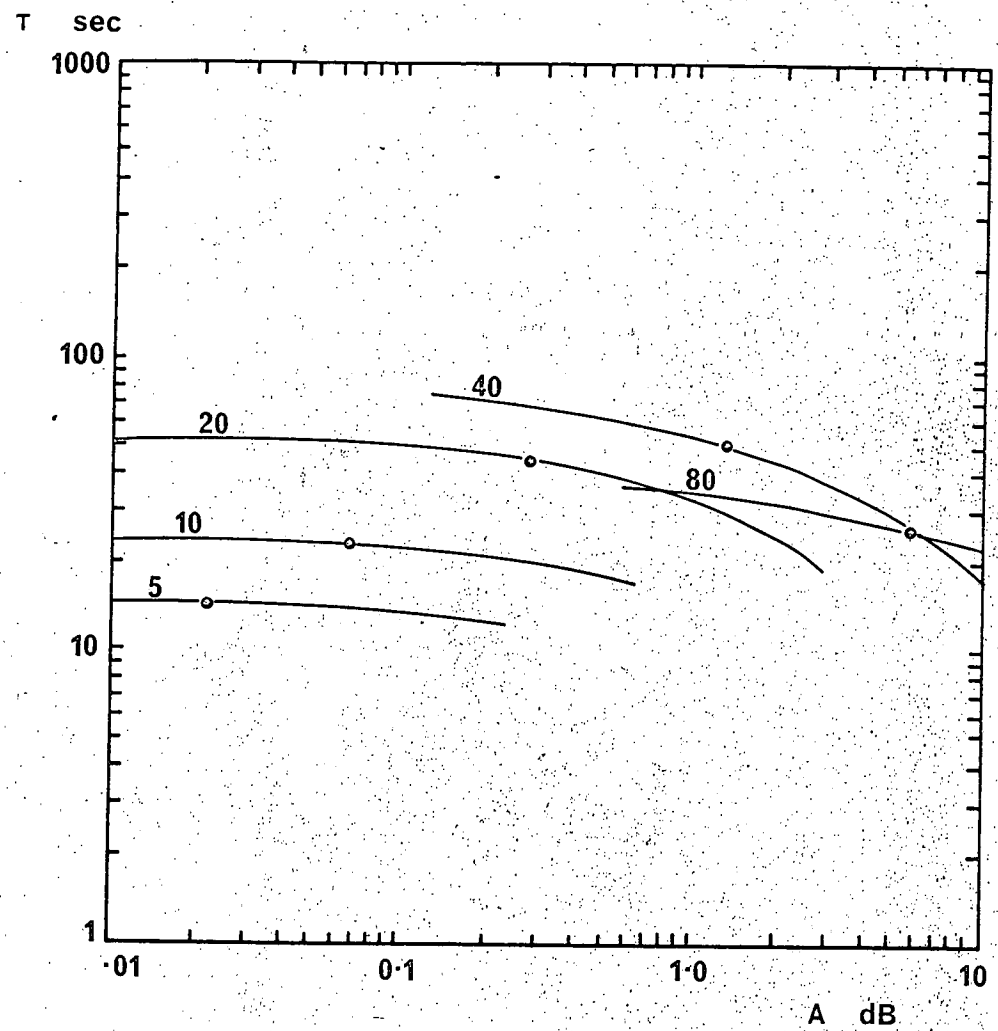

Fig. 3.2.

As for figure 3.1 but with event absorption background, A_o = 0.5dB that is

$\alpha = 2 \times 10^{-7}$

$\beta = 1.6 \times 10^{-30}$ m^2

$\gamma = 10^{-7}$

$\delta = 0.4$

$E_{ob} = 5$ keV

$A_0 = 0.5$ dB

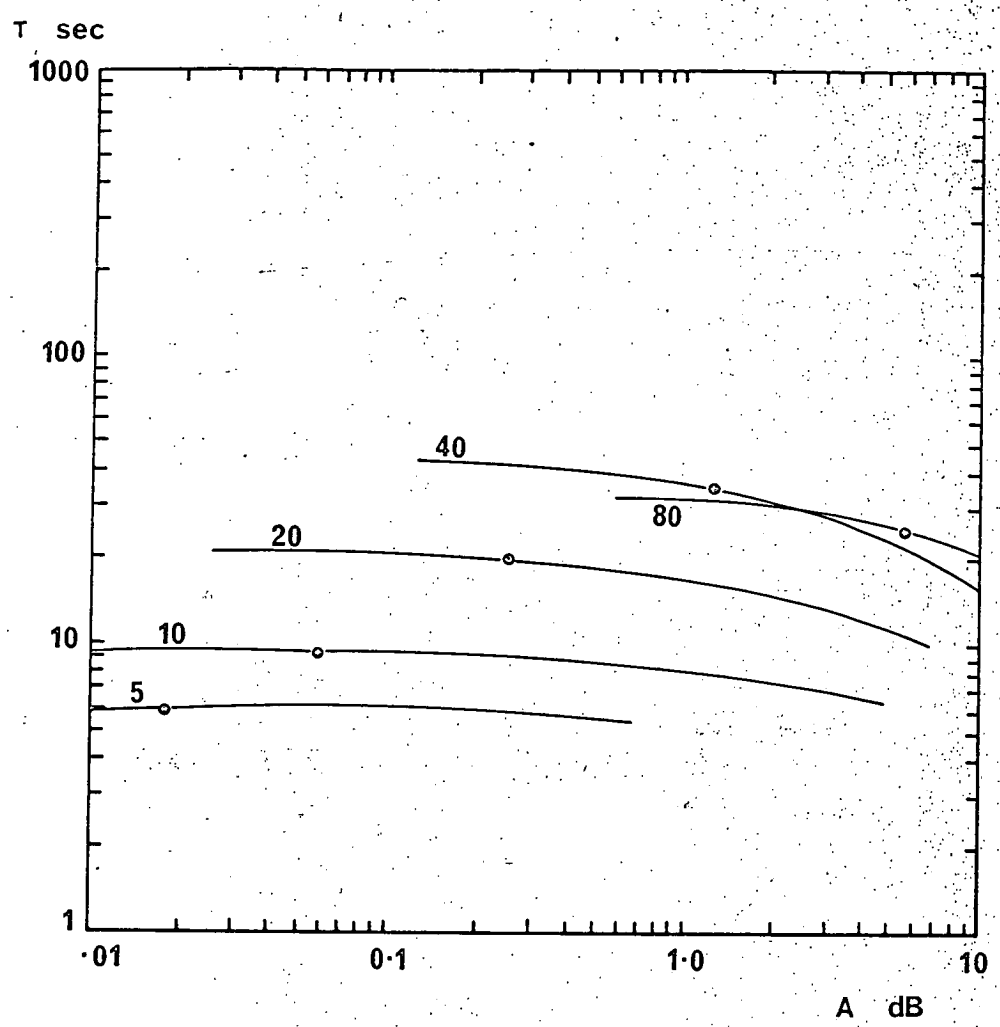

Fig. 3.3

As for figure 3.2 but with event background absorption, A_o = 2.0 dB

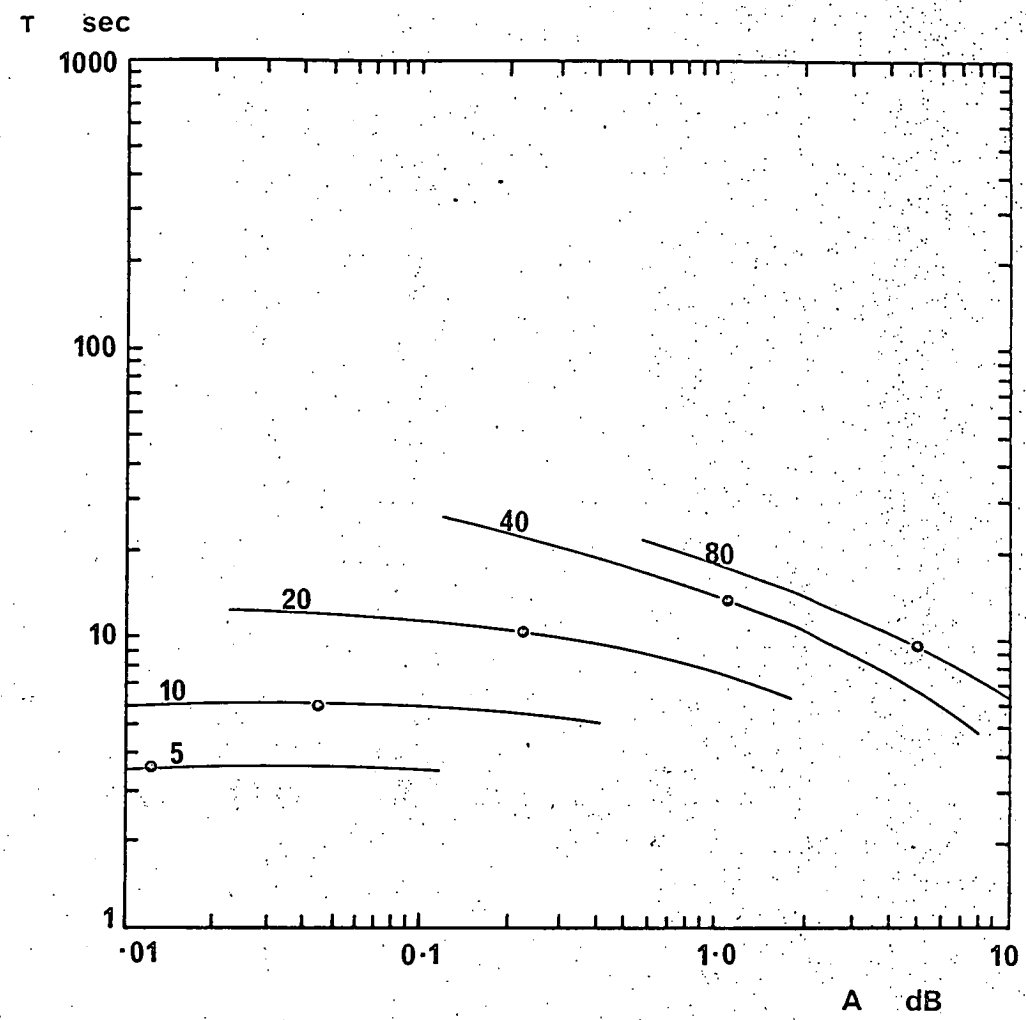

Fig. 3.4

Computed A - τ diagram, showing effect of α.
Parameters are the same as for Fig. 3.2 but with $\alpha = 2 \times 10^{-6}$.

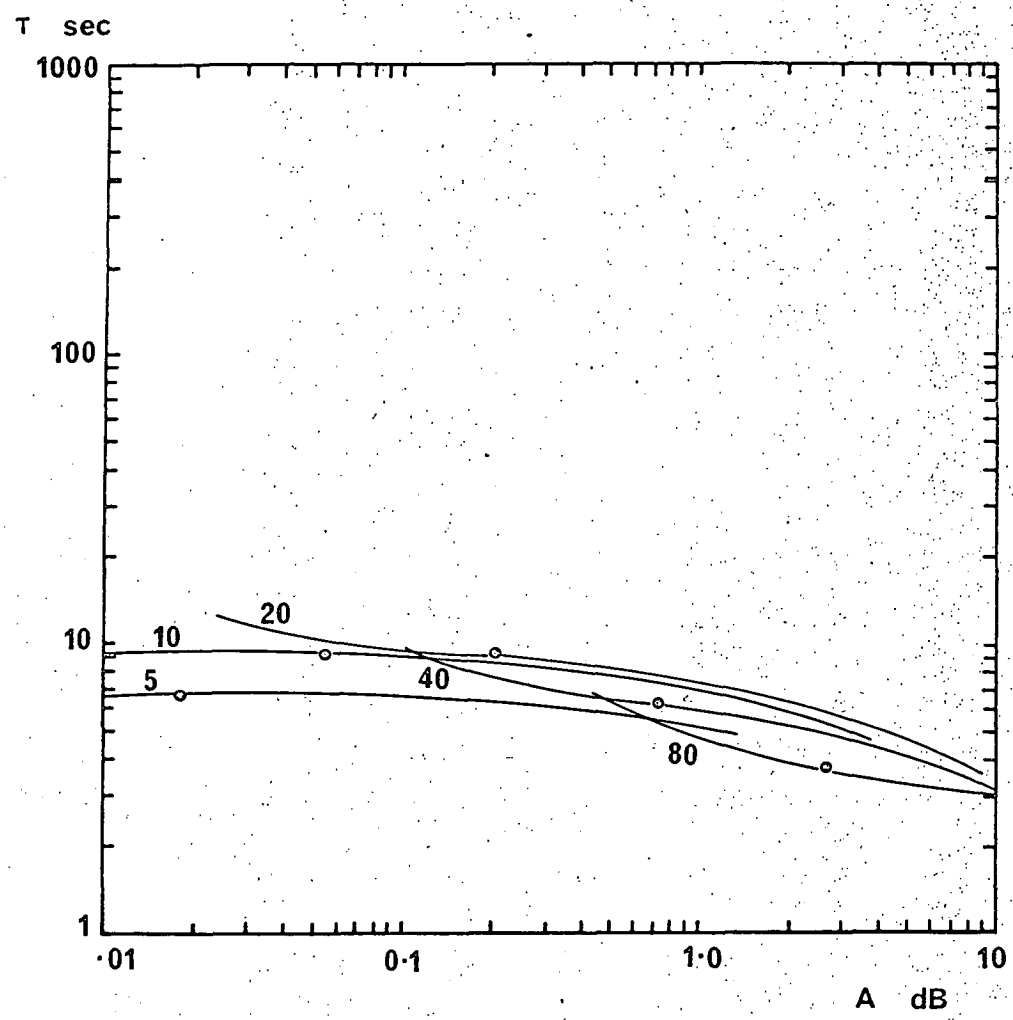

Fig. 3.5.

Computed A - τ diagram showing the effect of a height dependant α, i.e.

$\alpha = 5 \times 10^{-7}$ for $h > 87$ km.

$\alpha = 5 \times 10^{-5}$ for $h < 87$ km.

The other parameters are the same as for Fig. 3.2.

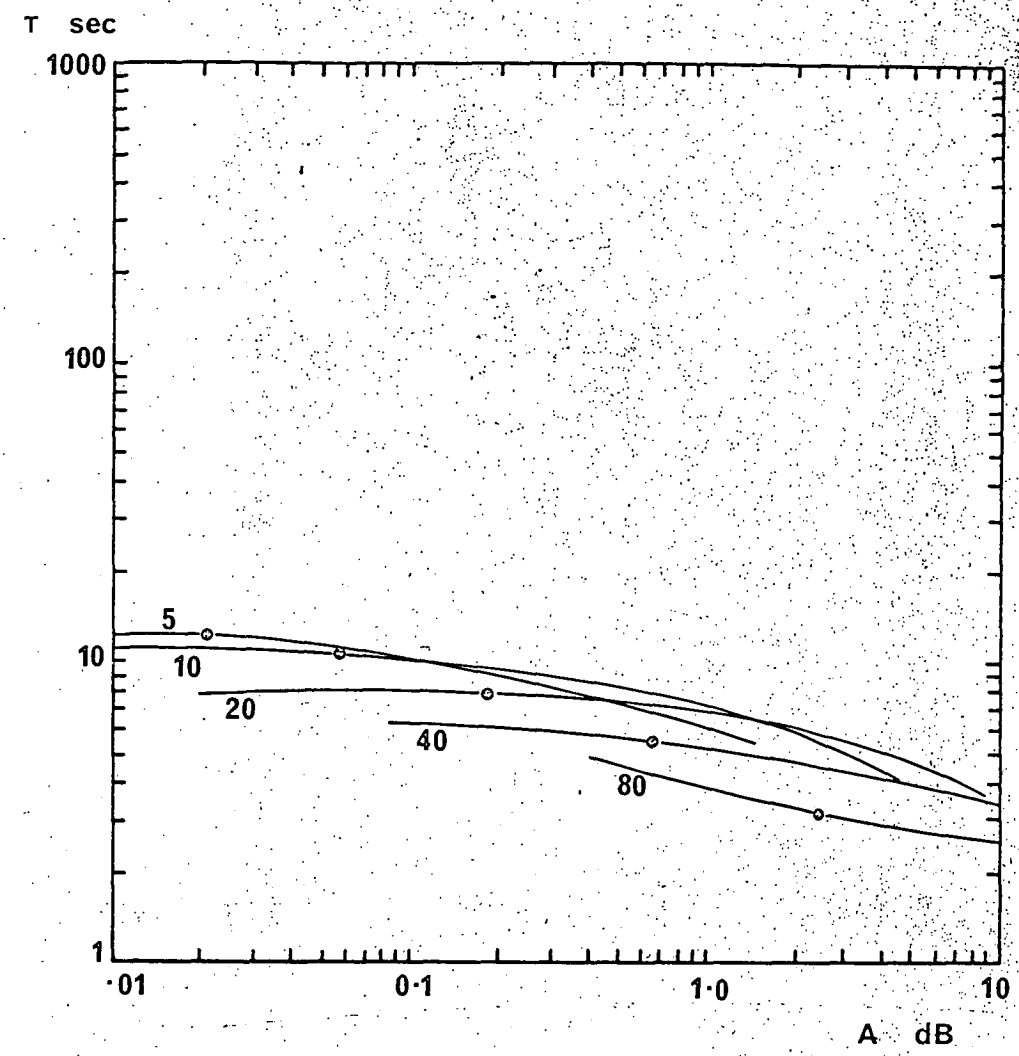

Fig. 3.6

Computed A-τ diagram showing the effect of a harder background spectrum (E_{ob} = 20 keV) and a dissociation coefficient, δ, which is a function of height. Parameters are

$\alpha = 5 \times 10^{-7}$ above 87 Km

$\alpha = 5 \times 10^{-5}$ below 87 Km

$\beta = 1.6 \times 10^{-30}$ m^2

$\gamma = 10^{-7}$

$\delta = 10 \left[O_2^- \right] / \left[N^- \right]$

where $\left[O_2^-\right]$ and $\left[N^-\right]$ are the concentration of O_2^- ions and of all negative ion respectively and are taken from G. C. Reid 1970. E_{ob} = 20 keV.

A_o = 0.5 dB.

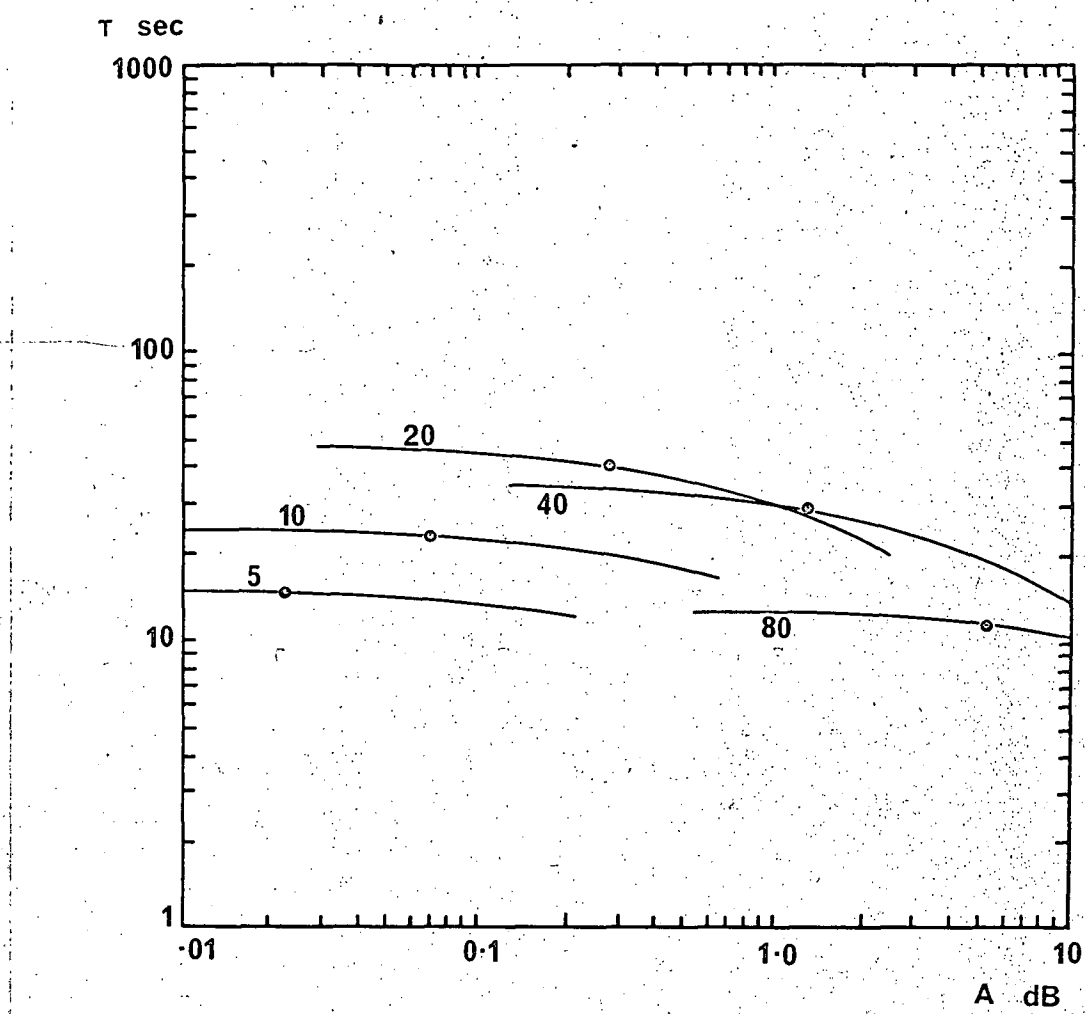

Fig. 3.7

As for figure 3.2 but with $\delta = 0$ corresponding to night- time conditions.

affect the absorption-flux sensitivity are the e-folding energy of the spectrum (i.e. the shape of the q (h) profile) and the half width of the pulse.

3.1.4 Effect of changes in α and δ

Figures 3.2, 3.4 and 3.5 show the effect that variations in α have on the A - τ curves. Increasing α by an order of magnitude decreases τ by a factor of 3 or 4 for soft parent spectra but does not greatly affect the curves for harder parent spectra. If α is made a function of height in a manner which approximates Reids (1970) profile of α, then the resulting curves are quite complicated (Fig. 3.5). Note that there is a considerable reduction in the spread in τ which now only varies between about 7 and 14 seconds for a wide spread in parent spectral hardness. Fig. 36 shows what happens when the background spectrum e-folding energy is increased from 5 KeV to 20 KeV and the detatchment coefficient is made a function of height in accordance with a collisional detatchment model of the atmosphere. The relaxation time has become a decreasing function of spectral hardness and the spread in τ is still small.

An A - τ diagram for nighttime conditions when collisonal and photodetatchment are almost inoperative is shown in Fig. 3.7 for which δ was taken as zero. Comparison with Fig. 3.2 reveals that, this time, the soft parent spectra curves are unaffected but the harder spectra curves have been lowered. τ has been reduced by a factor of 3 for the "80 KeV" curve.

3.1.5 Effect of other Parameters

Two other elements which may be thought likely to affect the integrated pulse relaxation times are the value of the ion-ion recombination co-efficient γ and the radiative background of ion-pair

production rate, i.e. whether a high or low nitric oxide profile is used. It was found that an order of magnitude increase in γ from 10^{-7} to 10^{-6} $cm^3 sec^{-1}$ caused at most a five per cent increase in τ, while changing the background radiative ionization component, q (h), from a low to a high nitric oxide profile had no discernible effect on the relaxation times of pulses superimposed on a .5 dB background.

Before we can discuss these features of the A - τ diagrams further we need to devise an approximation formula for the relaxation time.

3.2 An Approximation Formula for τ

3.2.1. Existing Formulas

The numerical integration of equation 1.1 for small short pulses in q makes it possible to check the validity of the various approximation formulae for τ which have appeared in the literature.

Appleton (1953) derived the expression

$$\Delta t \simeq 1/2\alpha N \qquad (3.3)$$

where Δt is the lag between the pulse in electron density N and the pulse in ion pair production rate q. The formula which is usually used to estimate τ is

$$\tau = \frac{1}{2\,\alpha_{eff}\,N}$$

or

$$\tau = \frac{1}{\alpha_{eff}\,N}$$

where α_{eff} is the "effective recombination coefficient" -

$$\alpha_{eff} = \alpha + \lambda\,\gamma$$

Relaxation time as a function of height for a small pulse in q can be obtained directly from the computor program used to compute the a - τ diagrams of Figures 3.1 to 3.7. In practice the background conditions and parameter values pertaining to Fig. 3.2 were used and the q- pulse used was that corresponding to a peak flux of 10^7 electrons cm^{-2} sec^{-1} at the top of the atmosphere with spectral e-folding energy of 80 KeV. The relaxation time at any height was taken as

$$\tau(h) = -\Delta N(t_o) \; / \left(\frac{dN}{dt}\right)_{t_o} \qquad (3.6)$$

by analogy with equation (3.1). Here ΔN is the variable component of the pulse in N and t_o was taken as the time at which $-\frac{dN}{dt}$ was a maximum.

Fig. 3.8 shows the profile of $\tau(h)$ obtained in this way (circles) compared with the profile of τ using equation (3.5). Values of background electron density, N_o, and negative ion-electron ratio λ used to derive the latter are also shown.

3.2.2 Unwarranted Approximation

It is obvious that the expression in 3.5 for τ is quite inadequate. The maximum value occurs 20 Km too low and is more than an order of magnitude too large.

The reason for this inadequacy is the inaccuracy of an approximation often used in connection with the rate equations (1.1). The substitution $\lambda = N^-/N$ is made and the equations become

$$\frac{dN}{dt} = \frac{q}{1+\lambda} - (\alpha + \lambda\gamma) N^2 - \frac{N}{1+\lambda} \frac{d\lambda}{dt}$$

and

$$\frac{1}{1+\lambda} \frac{d\lambda}{dt} = \beta m - \lambda \left[\delta + N(\gamma - \alpha) + \frac{q}{N(1+\lambda)}\right]$$

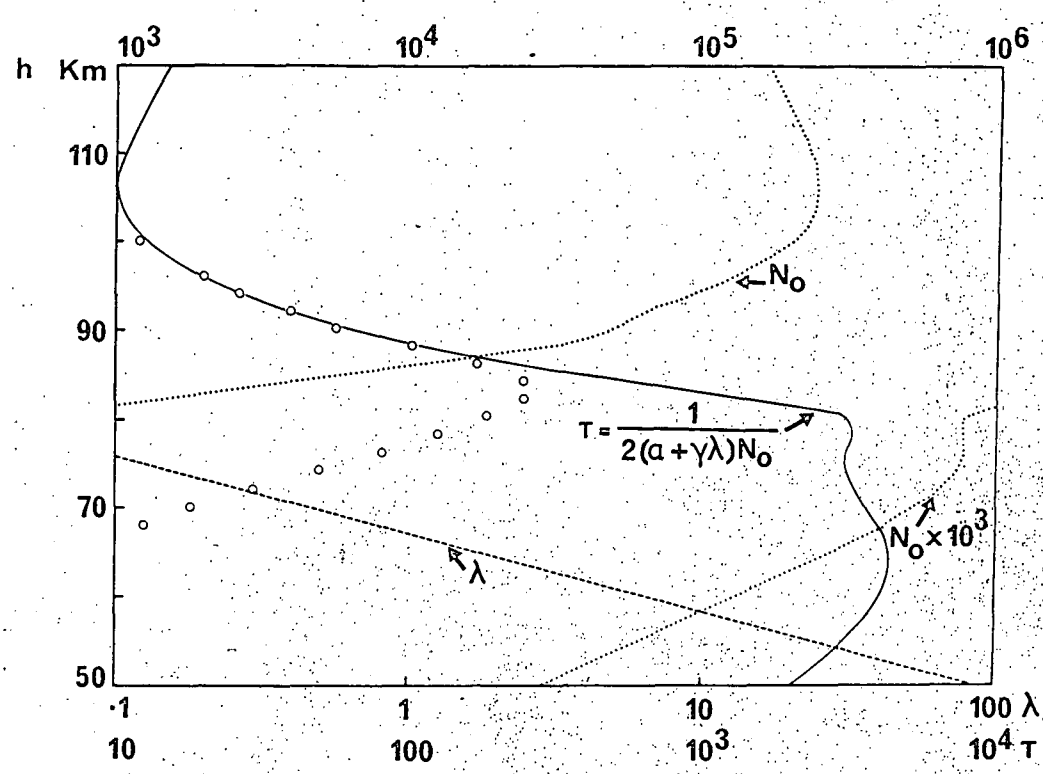

Fig. 3.8

A comparison of pulse relaxation time, τ, a function of height derived during the integration of the rate equations (1.1) (circles) and that calculated from the currently accepted approximation formula

$$\tau = 1/2\ \alpha_{eff}\ N \quad \text{(continuous line)}$$

The dotted and dashed lines show the values of background electron density N_o and negative ion-electron ratio λ respectively. The parameters have the values given for Fig.3.2. The τ profiles are those for a pulse peak flux of $10^7 cm^{-2} sec^{-1}$ with an e-folding energy of 80 keV.

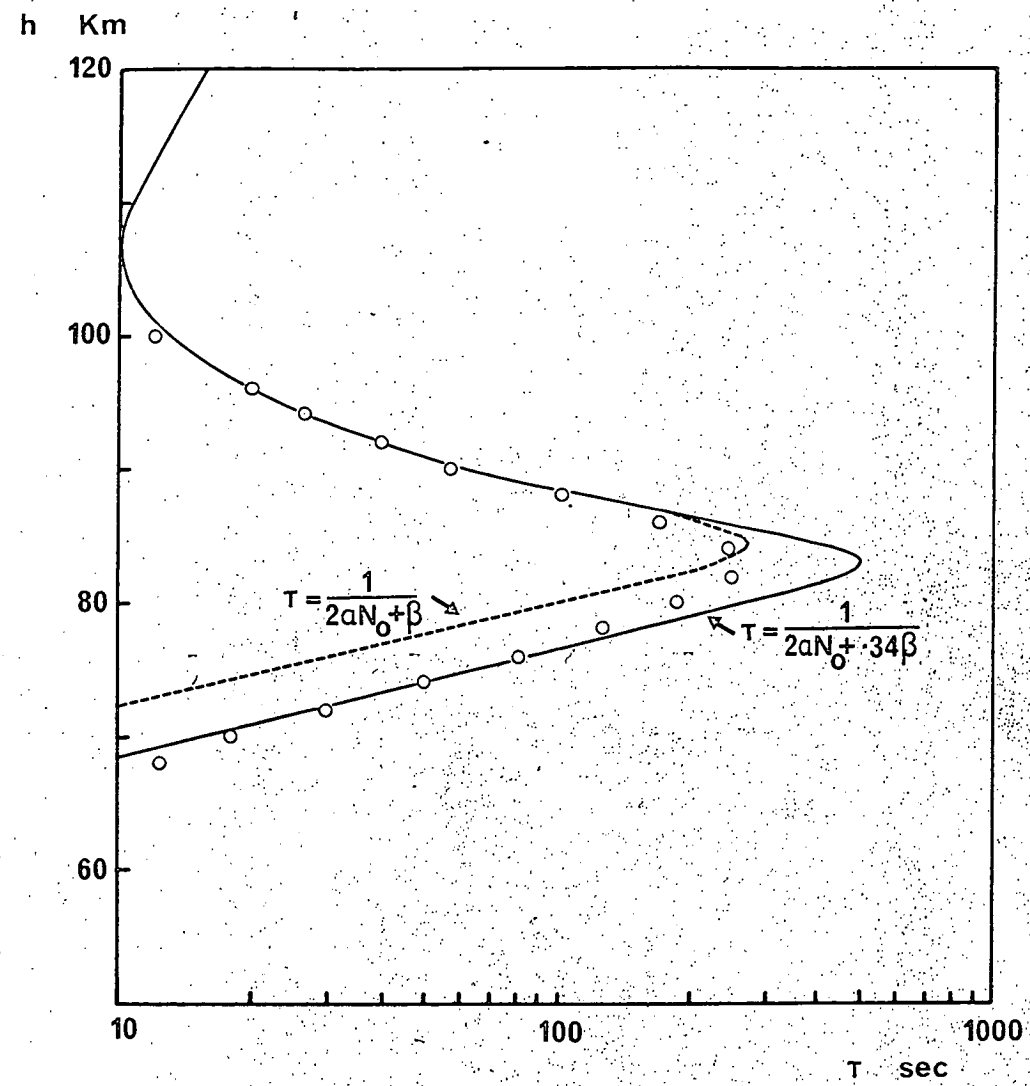

Fig. 3.9

As for Fig. 3.8 but using the improved formula for τ, viz:

$$\tau = 1/\ \alpha(N^+ + N^+_o) + \beta e^{-\delta t_e} \qquad (3.16)$$

$$\simeq 1/\ (2\ \alpha\ N_o + .34\beta)$$

where t_e = 2.7 sec. was chosen so as to give the best fit of the approximation formula to the points derived by integration of (1.1).

The approximation is then made

$$\frac{d\lambda}{dt} \simeq 0$$

and the last term is dropped from the equation for dN/dt. For small pulses where N is almost constant, the coefficient of N, $(\alpha + \lambda\gamma)$ N, will determine the time constant.

However numerical integration of a pulse under the conditions outlined above reveals that $d\lambda/dt$ has a value at 70 Km which varies between $-.14\ \text{sec}^{-1}$ and $+.077\ \text{sec}^{-1}$ during the course of the pulse. Since the background values of N and q at this height are $540\ \text{cm}^{-3}$ and $.127\ \text{cm}^{-3}\ \text{sec}^{-1}$ respectively the term $N(d\lambda/dt)$ is certainly not small compared with q, and the approximation is by no means valid.

3.2.3 A Height Profile of Relaxation Time

In order to arrive at a better formula for τ let us consider what happens after the cessation of a pulse when q has resumed its background value of q_o. Let N_o, N_o^- N_o^+ be the background (steady state) values of electron, negative ion and positive ion density respectively. Consider the "relative slope", ω, the reciprocal of τ, at time t_o when $q \simeq q_o$

$$\omega(h) = 1/\tau = -\frac{dN}{dt} / \Delta N \qquad (3.7)$$

$$= (\alpha N N^+ \beta N - \delta N^- - q_o) / \Delta N$$

$$= \left\{(\alpha N N^+ + \beta N - \delta N^-) - (\alpha N_o N_o^+ + \beta N_o - \delta N_o^-)\right\} / \Delta N$$

$$= \frac{\alpha(NN^+ - N_o N_o^+)}{\Delta N} + \beta - \frac{\delta \Delta N^-}{\Delta N} \qquad (3.8)$$

At heights where attatchment is negligable and the first term is dominant $N = N^+$ and $N_o = N_o^+$.

Hence

$$\omega = \alpha(N^+ + N_o^+) + \beta - \delta \Delta N^- / \Delta N \qquad (3.9)$$

$$\simeq 2 \alpha N_o^+ + \beta - \delta \Delta N^- / \Delta N$$

for small pulses in N^+.

At heights where attatchment in the dominant process we have

$$\frac{dN^-}{dt} = \beta N - \delta N^- \qquad (3.10)$$

since the term $-\gamma N^- N^+$ will be small compared with $-\delta N^-$

The solution of (3.10) is

$$N^- = N_o^- e^{-\delta t_o} + e^{-\delta t} \int_o^{t_o} \beta N e^{\delta t'} dt' \qquad (3.11)$$

Let $N(t) = \Delta N(t) + N_o$

then

$$N^- = N_o^- e^{-\delta t_o} \int_o^{t_o} \beta \Delta N e^{\delta t'} dt' + \frac{\beta N_o}{\delta} e^{-\delta t_o}(e^{\delta t_o} - 1)$$

$$= N_o^- + e^{-\delta t_o} \int_o^{t_o} \beta \Delta N e^{\delta t'} dt'$$

since $N_o^- = \beta N_o / \delta$

The pulse is assumed to commence at the instant $t = 0$

Hence $$\Delta N^- = e^{-\delta t} \int_o^{t_o} \beta \Delta N(t') e^{\delta t'} dt' \qquad (3.12)$$

$\Delta N(t)$ rises from zero at $t=0$ passes through a maximum and falls slightly to its value $\Delta N(t_o)$ at which dN/dt is a maximum. The numerically integrated pulses are similar in shape and show little variation in the value of t_o which occurs close to the maximum in ΔN. Let us define an"effective pulse time, t_e, such that

$$\int_{t_o-t_e}^{t_o} \Delta N(t_o)\, e^{\delta t}\, dt = \int_{o}^{t_o} \Delta N(t)\, e^{\delta t}\, dt \qquad (3.13)$$

Then we have

$$\Delta N^- = \frac{\beta}{\delta}\, \Delta N(t_o)\, e^{-\delta t_o} \left(e^{\delta t_o} - e^{\delta(t_o - t_e)}\right)$$

$$= \frac{\beta}{\delta}\, \Delta N (1 - e^{-\delta t_e})$$

$$w(h) = \alpha(N^+ + N_o^+) + \beta - \frac{\delta \cdot \beta}{\delta}\,(1 - e^{-\delta t_e})$$

$$= \alpha(N^+ + N_o^+) + \beta\, e^{-\delta t_e} \qquad (3.15)$$

$$\text{and } \tau(h) = \frac{1}{\alpha(N^+ + N_o^+) + \beta e^{-\delta t_e}} \qquad (3.16)$$

$$\simeq 1/(2\alpha N_o + \beta\, e^{-\delta t_e})$$

The approximation $2N_o = N^+ + N_o^+$ can be made because the pulse is a small proportion of the background and because this term only predominates at heights for which λ is small i.e. where the electron density is equal to the positive ion density.

The parameter t_e can be found empirically by examining numerically integrated pulses. It will presumably depend on the half width of the pulse in q and on the shape of the pulse. The half width of the pulses in q used in the program was .904 sec. A value of t_e equal to three times this was chosen, which gives

$$e^{-\delta t_e} = .34 \text{ for } \delta = 0.4 \text{ sec.}^{-1}$$

A profile of τ using this expression is shown in Fig. 3.9, together with the"empirical" relaxation times from Fig. 3.8. The good fit below this maximum indicates that t_e is remarkably constant for a wide variation in t.

The dotted curve is the profile of τ for an infinitely short pulse. Even this profile fits considerably better than the profile of Fig. 3.8.

3.2.4 Absorption Pulse Relaxation Time

To derive the relaxation time for the absorption pulse itself from the height profile of relaxation times consider the absorption pulse amplitude A.

Differentiating (2.39)

$$\dot{a} = \int_o^\alpha \dot{N}\, \mu d\, h \tag{3.17}$$

Let us assume that the maximum in $\dot{N}$ occurs at a time which is independant of height. Then

$$(\dot{a})_{max} = \int_o^\alpha (\dot{N})_{max}\, \mu\, d\, h \tag{3.18}$$

$$= - \int_o^\alpha w\,(h)\, \Delta\, N(h)\, \mu\, d\, h$$

$$= - \int_o^\alpha w\,(h)\, A\,(h)\, d\, h \tag{3.19}$$

For the absorption pulse

$$\bar{w} = 1/\tau = - \dot{a}_{max}/A = \frac{\int_o^\alpha w(h)\, A\, d\, h}{\int_o^\alpha A\, d\, h}$$

$$\text{i.e. } \frac{A}{\tau} = \int_o^\alpha \frac{A(h)}{\tau(h)}\, dh \tag{3.20}$$

Thus $\bar{w}$ is the mean of the height profile in w(h) wighted with respect to the pulse absorption profile. Since τ for the absorption pulse is an harmonic mean of the height profile $\tau(h)$ the peak in $\tau(h)$ will tend to be lost in the averaging process and the mean value of $\tau(h)$ will be, in general, much smaller than the peak value of the profile.

The pulse absorption as a function of height A(h) in (3.20) can be estimated using the approximation of (2.31), i.e.

$$A(h) = \Delta N \mu \simeq \Delta q \Delta t \mu$$

For frequencies above 30 MHz and heights above 50 Km we have

$$\mu \propto \nu$$

and (3.20) becomes

$$\bar{w} = 1/\tau \simeq \frac{\int_o^\alpha w(h) \Delta q \nu \, dh}{\int_o^\alpha \Delta q \nu \, dh} \qquad (3.21)$$

i.e. the relaxation time of the absorption pulse is weighted by the profile in the pulse in ion pair production rate and the collision frequency.

3.3 Interpretation

An appreciation of the various features of the $A - \tau$ diagrams of figures 3.1 to 3.7 now become possible in terms of the approximation formulas developed above.

The maximum of τ as a function of e-folding energy is explicable in terms of the maximum in $\tau(h)$ inherent in the formula (3.16). The sensitivity of the soft spectra $A-\tau$ curves to changes in α and in background (i.e. in N_o) and of the hard spectra $A-\tau$ curves to changes in δ can also be understood.

In the expression for $\tau(h)$ (3.16), both terms in the denominator are strong functions of height. For most background spectra the electron density decreases rapidly below the maximum while β increases rapidly with

decreasing height. The maximum in $\tau(h)$ occurs near where the two denominator terms are equal elsewhere either one or the other predominates. Hence that region of the curve, $\tau(h)$, above the maximum in Fig. 3.9 is controlled by the $\alpha(N_o+N)$ term, while that below is controlled by $\beta e^{-\delta te}$, the second term. Thus absorption pulsations brought about by less penetrating particles, i.e. softer spectra, are controlled by $2\alpha N_o$ and are independant of β and δ while for harder spectra the reverse is the case.

The small spread and low values of τ of Figures 3.5 and 3.6 become understandable when we examine the corresponding height profiles $\tau(h)$ shown in Figures 3.10 and 3.11. The discontinuity at 87 Km in these profiles is, of course, due to the discontinuity introduced into $\alpha(h)$ at this height. As the e-folding energy of the primary spectra increases an increasingly large fraction of the $\Delta q(h)$ profile lies below this ledge and so τ decreases with increasing spectral hardness in Fig 3.6, in contrast to the single peaked τ profiles of the simpler models of Figs. 3.1 to 3.4. The spread in τ as a function of spectral hardness has been reduced because the spread in $\tau(h)$ itself has been reduced and averaging with respect to $A(h)$ reduces this spread even further. Conversion from $\tau(h)$ to $\tau(E_o)$ where E_o is the parent spectrum e-folding energy involves convolution of $w(h)$ with the $q(h, E_o)$ curves of Figure 2.2 according to equation (3.21). Convolution is a smoothing process and as such reduces the range of a

function. The degree to which this happens depends upon the "width" of the convoluting functions. If the height thickness of the q profiles of Fig. 2.1 were to be reduced, the range in $\tau(E_o)$ would correspondingly increase.

All that remains is to compare the behaviour of the c.n.a. pulsations predicted by this model with that observed experimentally.

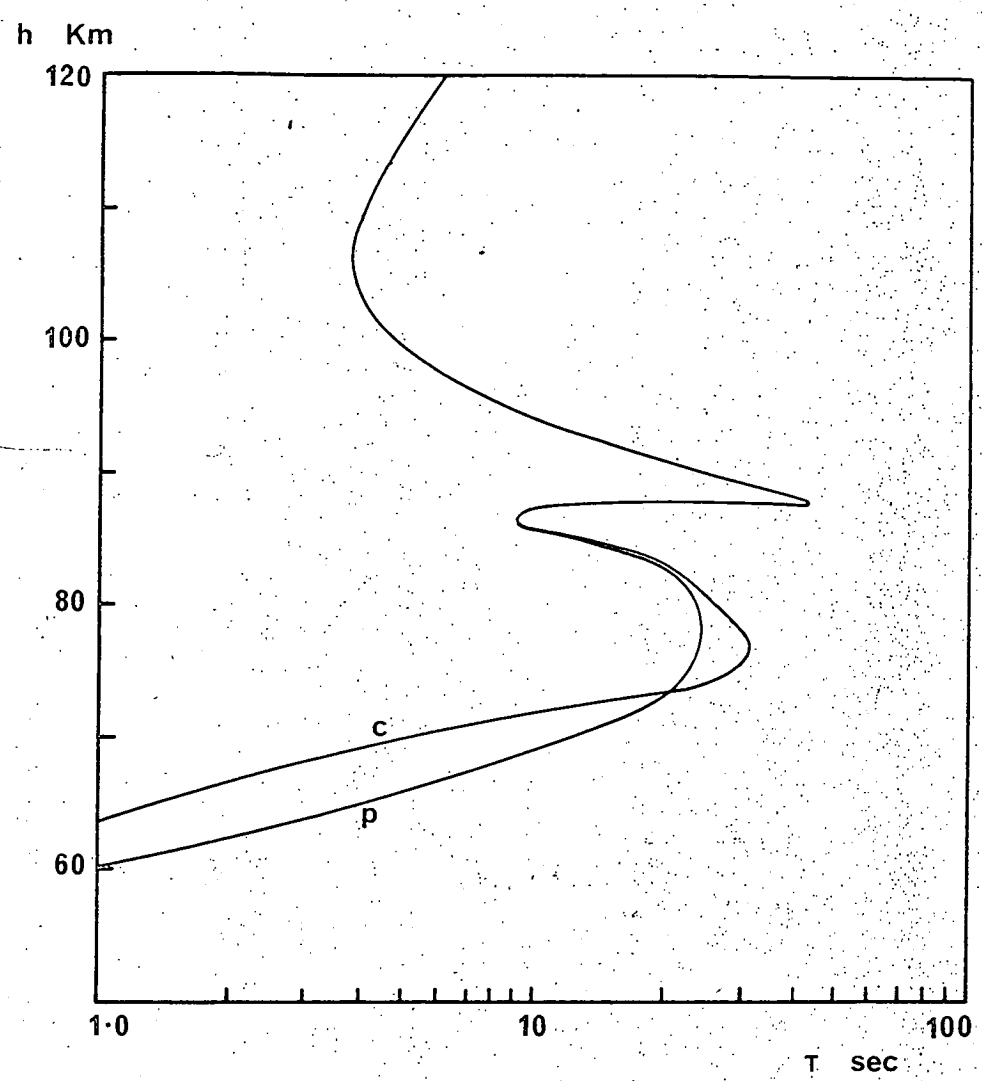

Fig. 3.10

Height profiles of τ calculated using equation (3.16) with α as a function of height.

(i) Curve "p" - τ profile for a photodetachment model in which $\delta = 0.4$ sec. The paramenters are the same as those quoted for Fig. 3.5.

(ii) Curve "c" - τ profile for a collisional detachment model in which

$$\delta = 10. \ [O_2^-]/[N^-]$$

The other paramenters are the same as for curve "p".

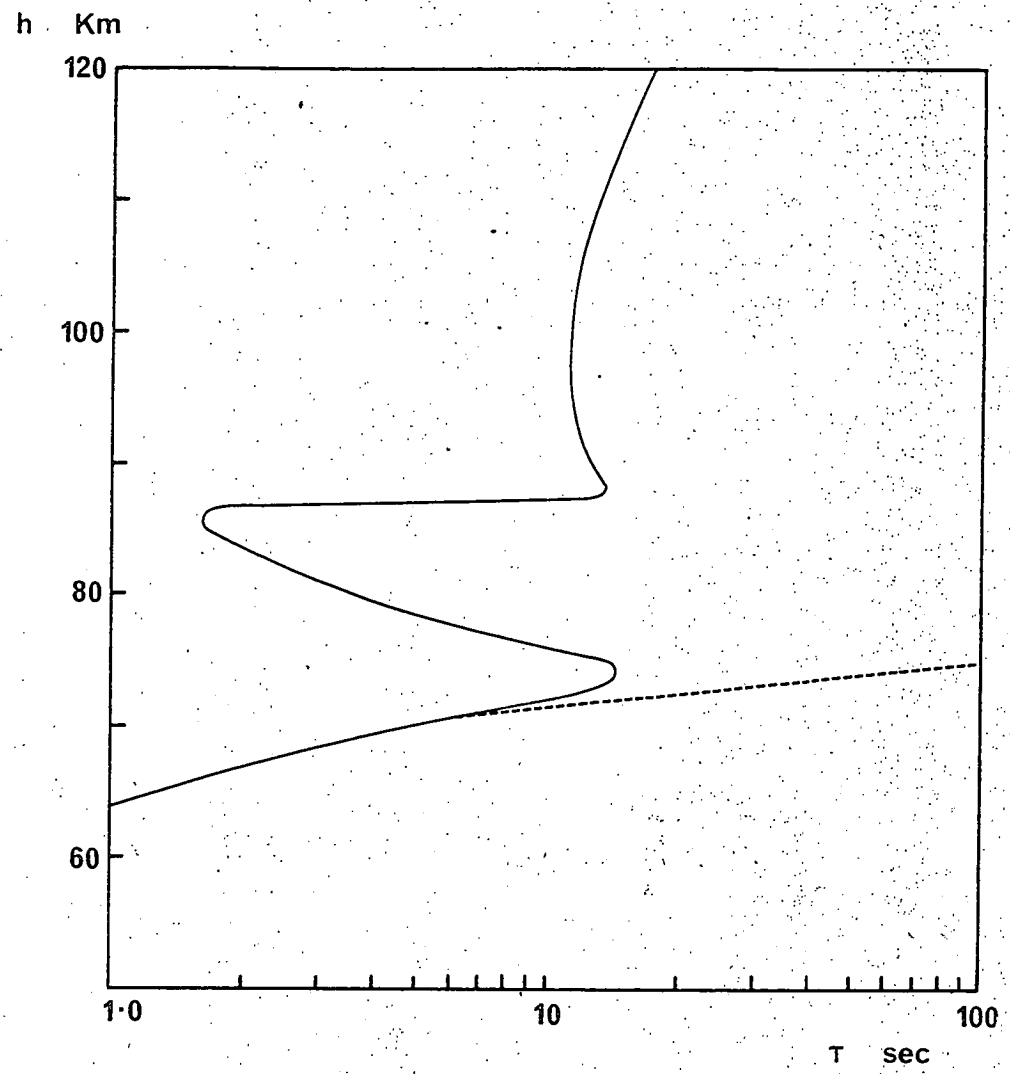

Fig. 3.11

Height profiles of τ using (3.16). The parameters are those quoted for Fig. 3.6. The dotted curve represents the attachment - detachment part of the formula for τ viz: the function $1/\beta \exp(-\delta t_e)$. It can be seen that this part of the expression for τ has little effect above 75 Km.

SECTION 4

C. N. A. Pulsations - Experimental Observations.

4.1 Observed Pulsations

Examples of chart recordings of c.n.a. pulsations can be seen in Figs. 4.1, 4.2 and 4.3. In Fig.4.1(a) quasi-periodic pulsations were detected in the west and south antenna beams simultaneously with the occurrence of more sporadic and longer relaxation time pulsations in the north and east beams. Both types of activity are common, although their simultaneous occurrence within the range of the four antennae is not.

Fig. 4.1(b) illustrates an example of a much more confused type of activity in which pulsations appear to be superimposed one on top of another. Fig. 4.2 shows a much simpler and more readily scalable type of pulsation activity in which discrete pulsations are superimposed on a relativately steady background of absorption.

Fig. 4.3 shows in greater detail some c.n.a. pulsations taken from the same event as those in Fig. 4.2. Pulsations predicted by the model are shown in Fig.4.4 for comparison. The predicted and observed pulsations are similar in shape although the observed pulsations appear to have more linear leading edges than those predicted. The small periodic "pulsations" of about .4 sec. period are not real but are due to tape recorder "wow".

The times of occurrence of c.n.a. pulsation events observed during the summer months of 1969 are summarized in Fig. 4.5. The ordinate represents the number of one hour time intervals during which c.n.a. pulsations were observed. The dotted histogram shows the number of intervals which contained pulsations of scalable quantity. The pulsations were always superimposed on a background of absorption which varied between 0.5dB and 4.0dB in magnitude and which was usually less than 2.0dB. These events observed with a

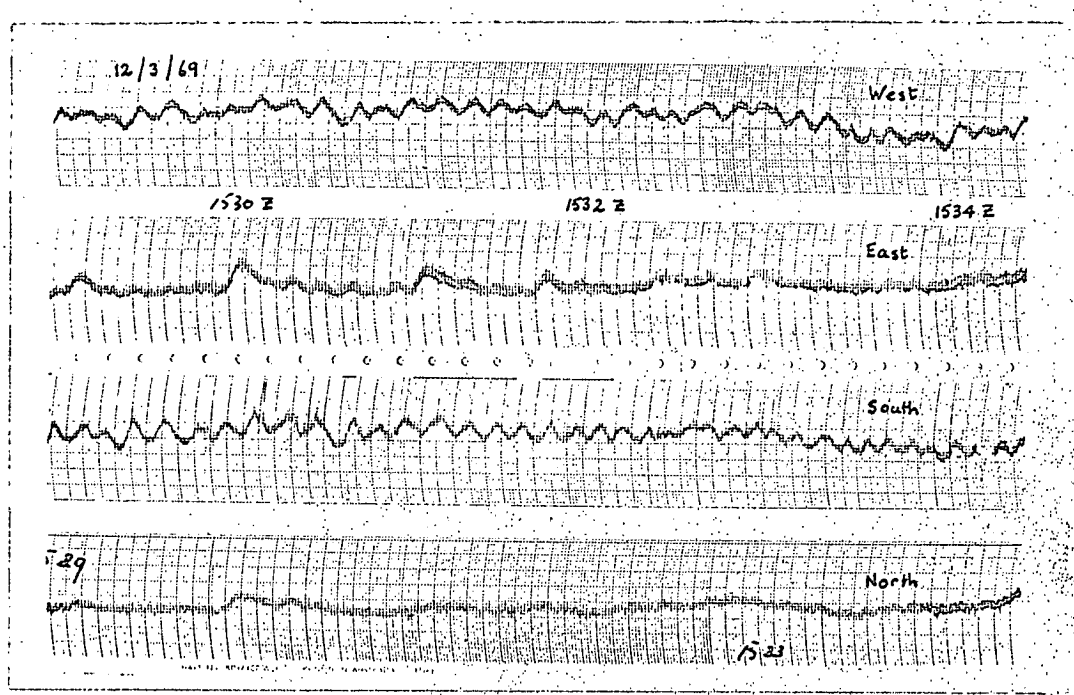

Fig. 4.1.

Chart records of five minutes of c. n. a. pulsation activity

(a) one of the events of 12th March, 1969 showing different types of activity in different parts of the sky.

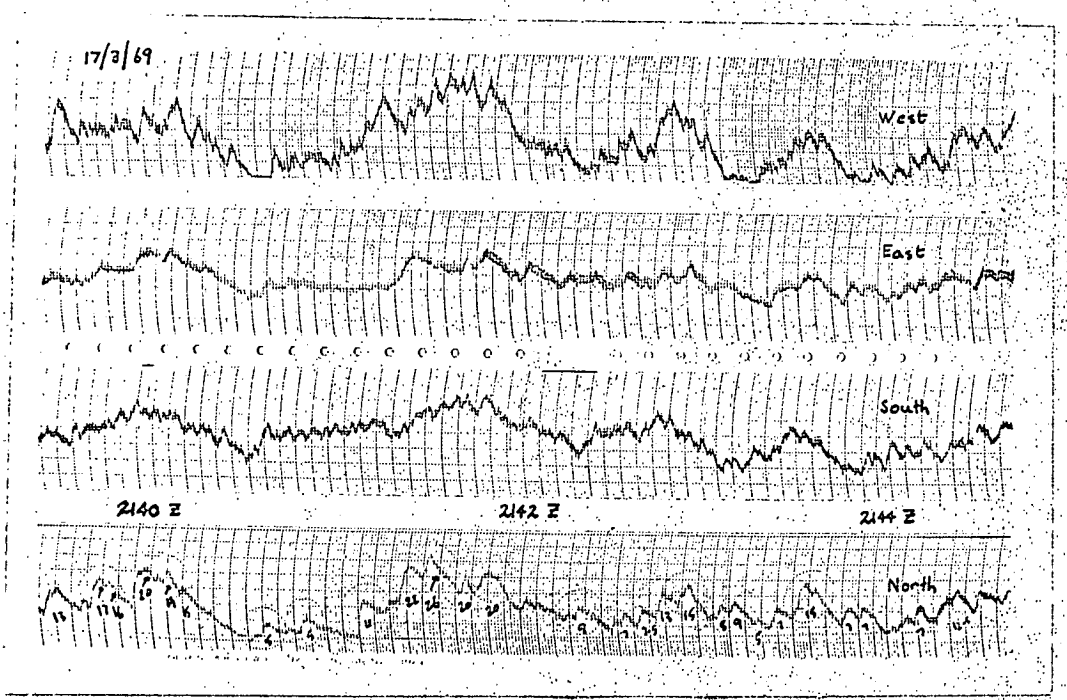

Fig. 4.1

(b) an extremely complex event which occurred on 7th March, 1969.

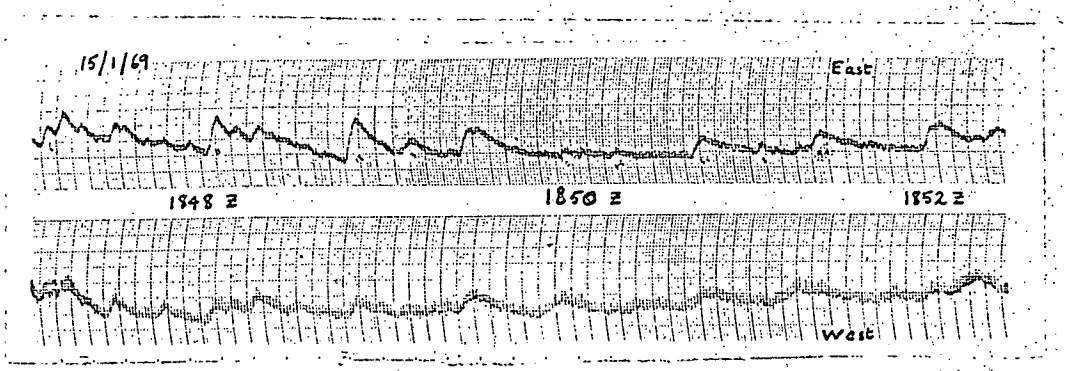

Fig.4.2

(a) Part of the "simple" event of 15th January 1969 showing big discrete "scalable" pulsations.

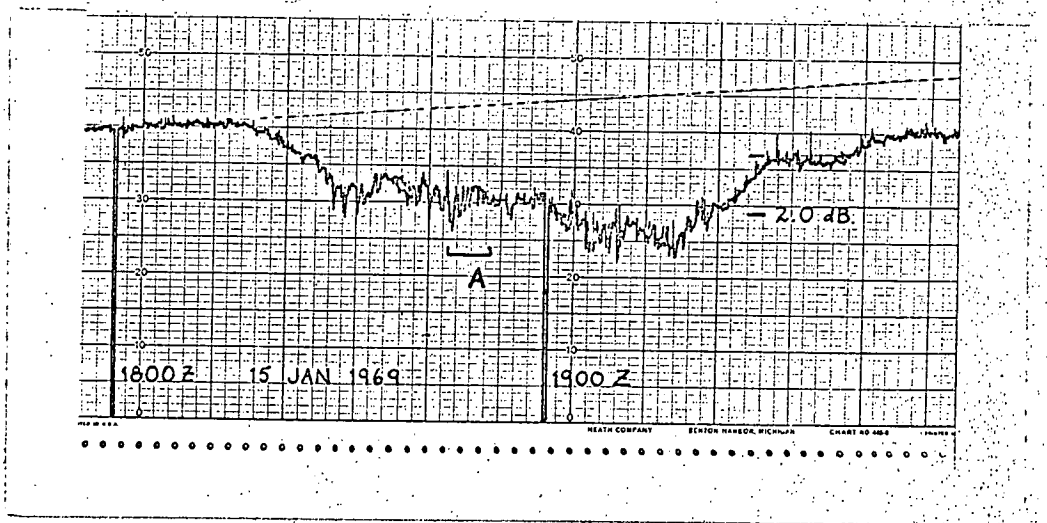

(b) Conventional riometer record of the event of which (a) is a part. Some of the larger pulsations can be seen on this slow riometer record. This S.V.I.A. event is typical of events during which c.n.a. pulsation activity occurs.

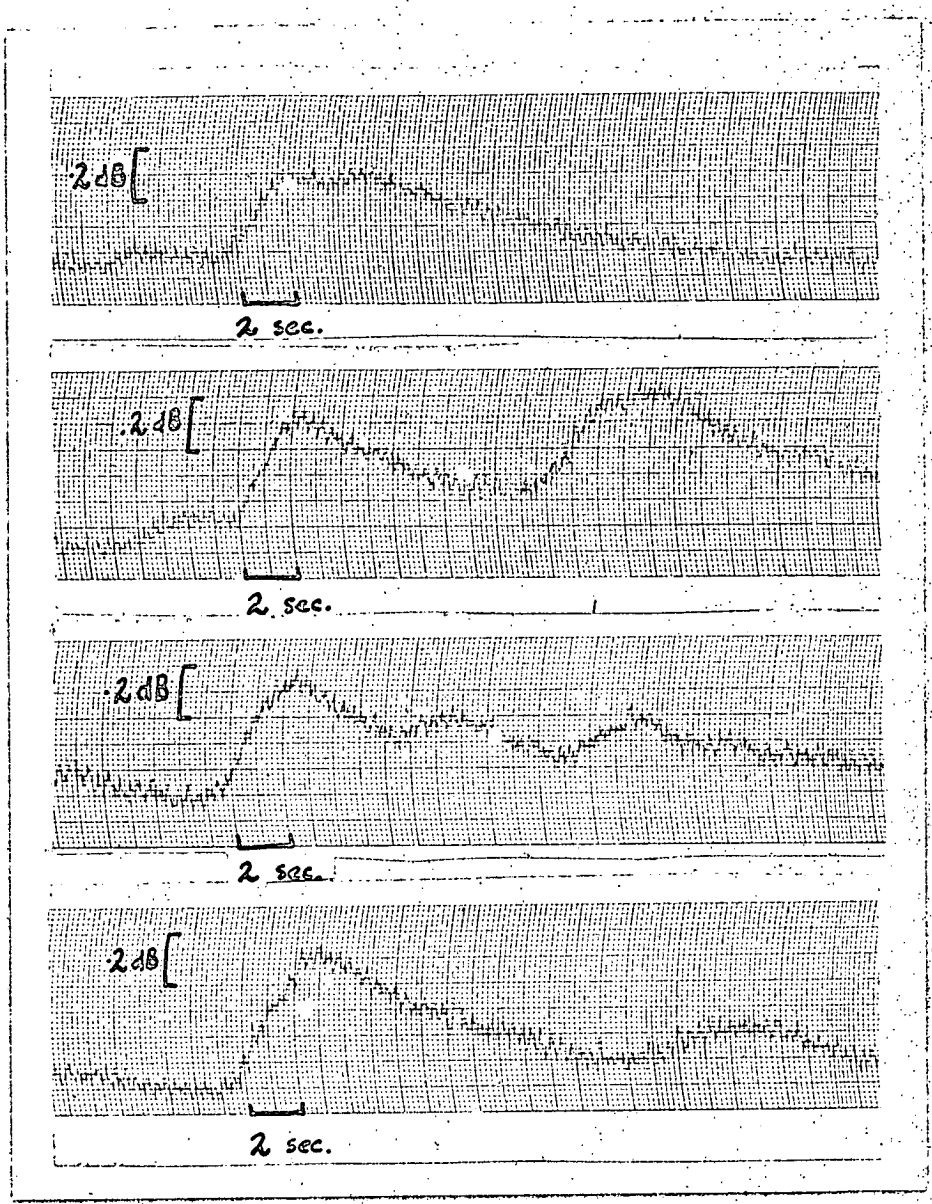

Fig. 4.3.

(a) Some larger c.n.a. pulsations shown on an expanded time scale.

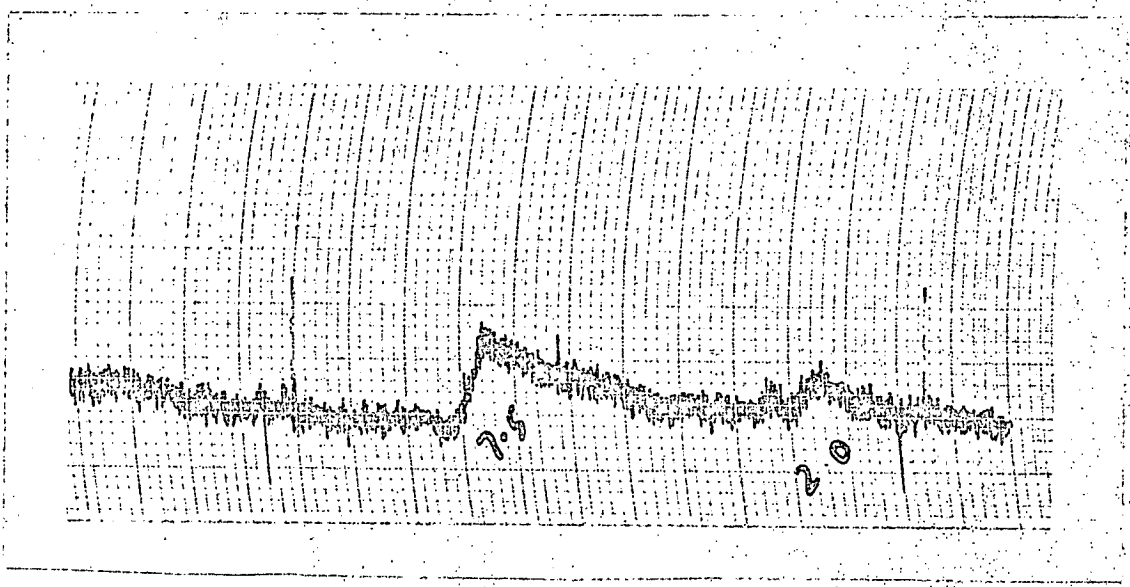

Fig. 4.3

(b) A group of observed c.n.a. pulsations which show very clearly the tendency of smaller pulsations to have faster decay times.

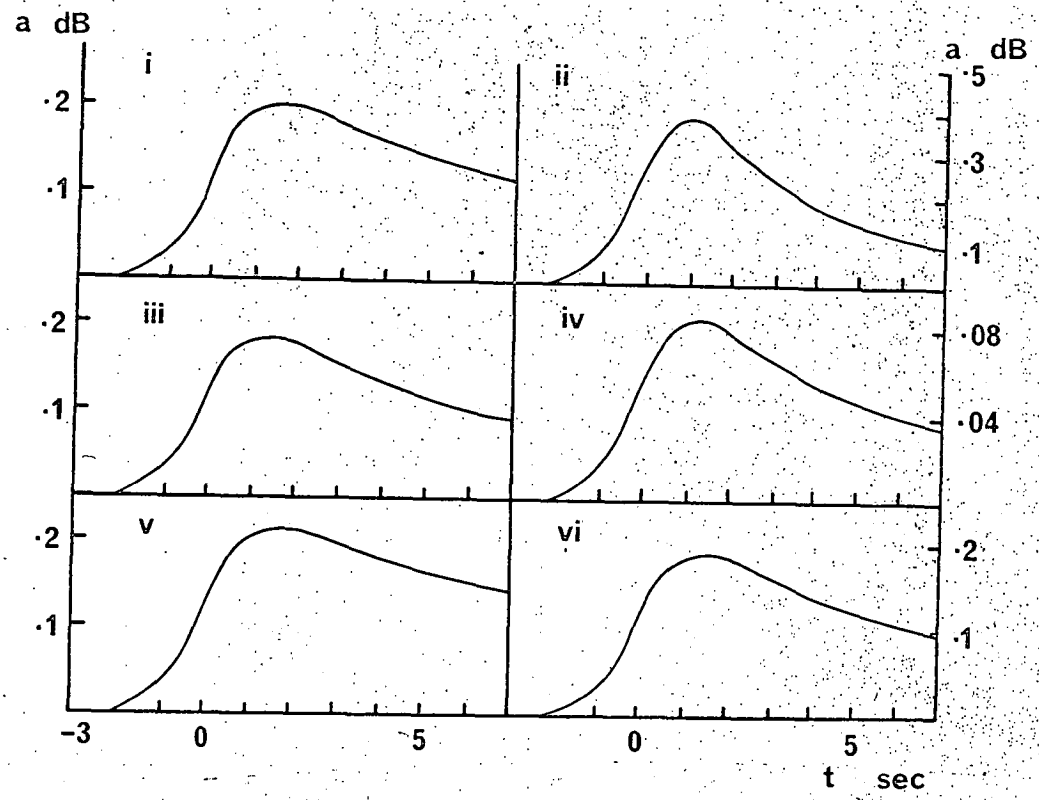

Fig.4.4

Theoretical c.n.a. pulsations predicted by the model. The combination of model parameters leading to each pulsation are shown together with the relaxation times as defined by (3.2)

Table 4.1.

	α	δ	A_o	E_{ob}	E_{op}	F_{op}	τ
(i)	$\alpha(h)$	$\delta(h)$	.5dB	20KeV	5KeV	$10^9 cm^{-2} sec^{-1}$	9.04sec
(ii)	"	"	"	" "	20 "	10^7 " "	4.64 "
(iii)	"	"	"	" "	80 "	10^8 " "	7.69 "
(iv)	"	"	"	" "	40 "	10^7 " "	6.33 "
(v)	2×10^{-7}	0.4	"	5 "	5 "	10^9 " "	12.44 "
(vi)	10^{-6}	10.0	"	20 "	5 "	10^9 " "	7.89 "

where $\alpha(h) = 5 \times 10^{-7}$ for $h > 87$ km.

$\alpha(h) = 5 \times 10^{-5}$ for $h < 87$ km.

and $\delta(h) = 10 [O_2^-] / [N^-]$.

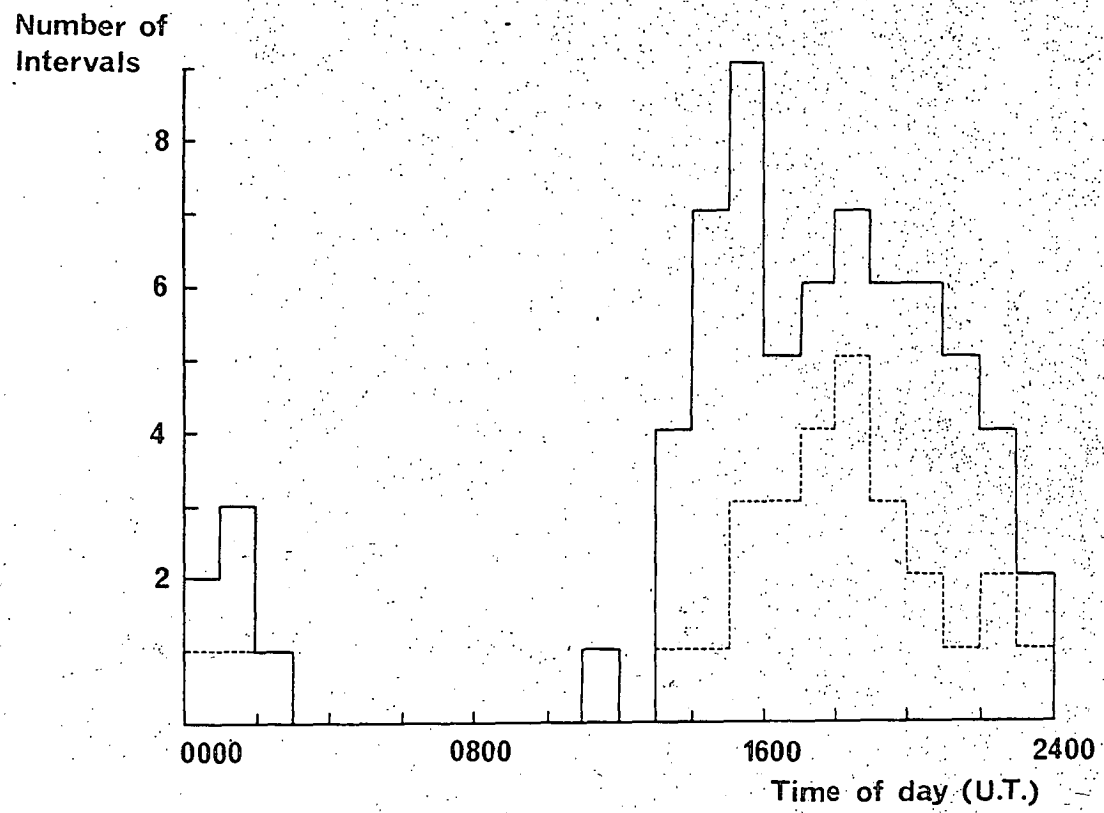

Fig. 4.5

Histogram summarizing the times of occurrence of c.n.a. pulsations observed at Macquarie Island in the first three months of 1969. The ordinate represents the number of occasions that c.n.a. pulsations were observed in each one hour interval of the day.

Solid line - all pulsations

Dashed line - pulsations of scalable quantity

Invariant midnight at Macquarie occurs at about 1200 U.T.

conventional riometer would be classified as S. V. I. A. events.

4. 2 A - τ Diagrams for Observed Pulsations.

Scatter diagrams of pulse amplitude versus relaxation time were plotted for c. n. a. pulsation events for comparison with the predicted A - τ curves of the previous section. The amplitude, A, of the pulsations was measured as the height of the leading edge of the pulsation and the maximum slope of the decay tail was determined by means of a graticule. The amplitude, A, could be measured to within about .02 dB and the slope, $(\dot{a})_{max}$, to within $\pm$ 20%. Thus the error in τ for a .1 dB pulse will be about thirty percent. τ is defined as above as $-A/(\dot{a})_{max}$ and is independent of the amplitude sensitivity of the riometer. On the other hand, A is dependent on the sensitivity of the system and this becomes important when we consider the case where the region of precipitation giving rise to the pulse does not completely cover the antenna. The observed amplitude will then be less than the "true" value, ie, that observed with a theoretical antenna of infinitely narrow beam. Fortunately, the region of impulsive precipitation is likely to be larger than the region covered by an antenna (Appendix II) and so the maximum value of A observed over a number of pulsations is likely to be close to the "true" value ie; the largest pulsations are likely to be those which correspond to a complete coverage of the sensitive part of the antenna beam by the pulse of primary electrons. Thus in an A - τ diagram of a number of observed pulsations, the relationship between pulse absorption per unit area and τ is depicted by the high A edge of the scatter diagram since antenna geometry effects can only reduce the observed value of A and do not affect τ in any systematic way.

4. 3 Proportionality of A and τ.

An A - τ diagram plotted for the event of 17/3/69 was plotted and is shown in Fig. 4. 6 - each point represents the relaxation time and amplitude of one pulsation. The most striking feature of this scatter diagram is the obvious positive correlation between A snd τ; larger pulsations have longer relaxation times. This is in direct contradiction to the simple assumption about the ionospheric time constant viz.

$$\tau = \frac{1}{2 \alpha N}$$

which implies that τ should decrease with increasing N and hence with increasing A.

The event scaled to produce the scatter diagram of Fig. 4. 6 was quite a complex one (see Fig. 4.1b). The pulsations are superimposed one on top of another and it is possible that the positive correlation of Fig. 4. 6 may, in fact, be a spurious effect introduced by the scaling process. In order to avoid such problems the five "best" events of Jan to March 1969 were chosen and scaled. The term "best" is used in the sense that many of the pulsations were discrete from one another and were superimposed on a steady background (e.g.Fig. 4.2). Pulses superimposed on the decay tails of preceding pulses were not scaled.

The resulting A - τ scatter diagrams are shown in Figs. 4. 7 through 4. 11. A positive correlation between A and τ is apparent in all five cases. The high-A edge has a positive slope as well, excepting in Figs. 4. 8 and 4. 9 which show interesting maxima.

Of the six events whose pulses are plotted in Figs. 4. 6 through 4. 11 only one occumed when the ionosphere was in darkness, the event of 26/1/69 (Fig. 4. 9). All of the other events discussed here occurred after ground level sunrise. The scatter diagram of Fig. 4. 9 does not differ radically from the

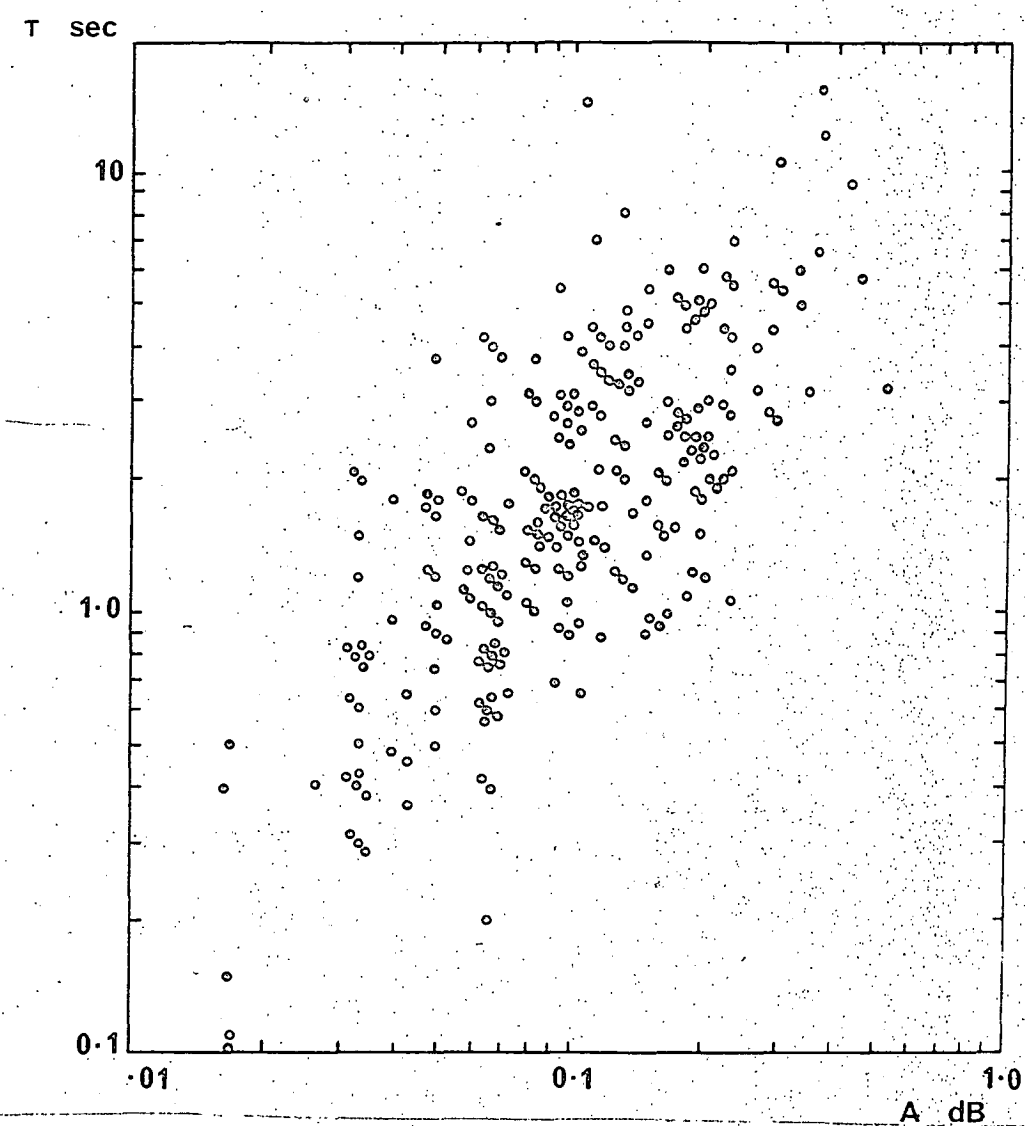

Fig. 4.6

Experimental A-τ diagram plotted for the event of 17th March 1969, a section of which is displayed in Fig. 4.1 (b). The ordinate of each point represents the relaxation time of a pulse, τ, as defined by (3.2) while the abscissa represents the amplitude of the same pulse, A. In practice, A was measured as the height of the leading edge of the pulse.

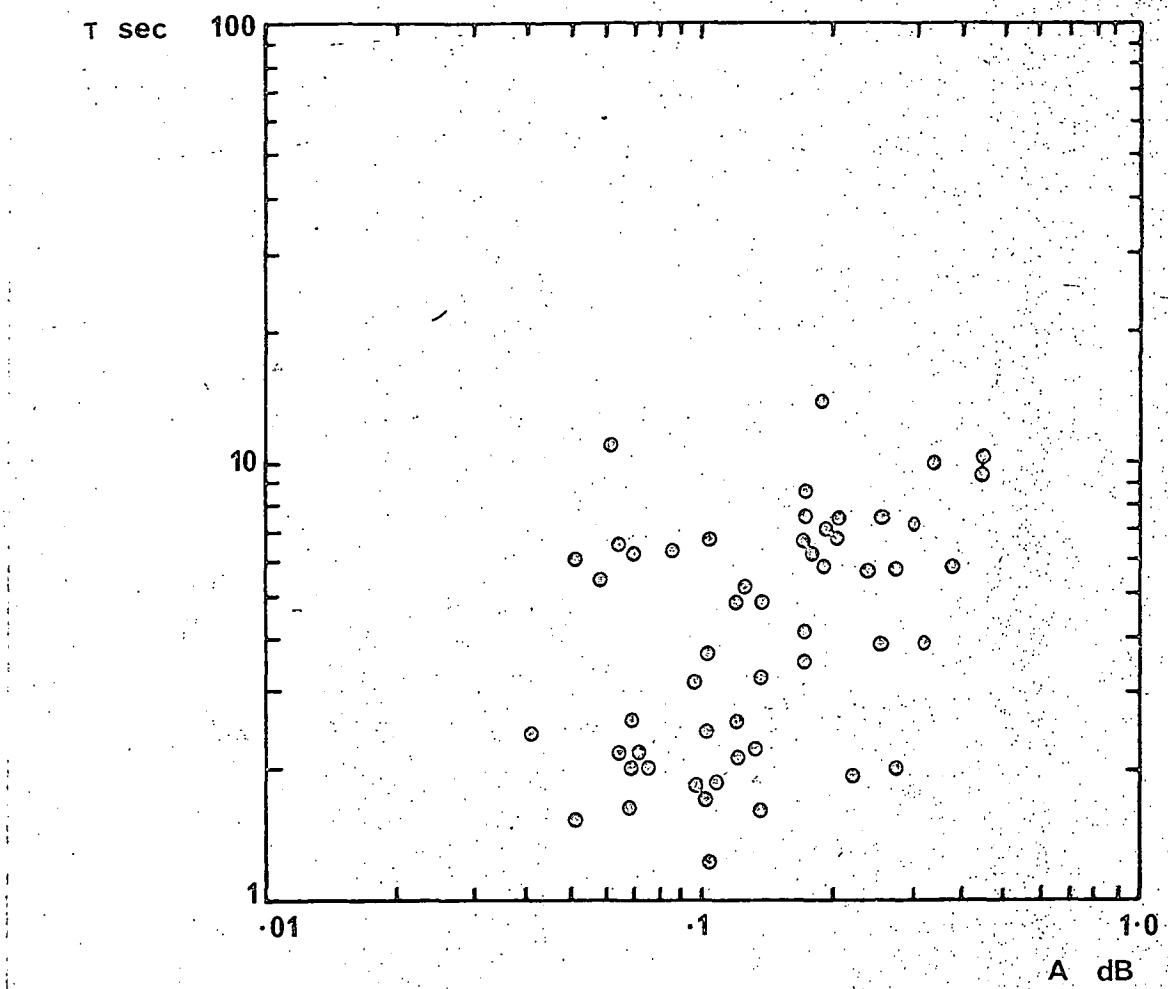

Fig. 4.7

Experimental A - τ diagram for the event of 15th January 1969, the event shown in Fig. 4.2.

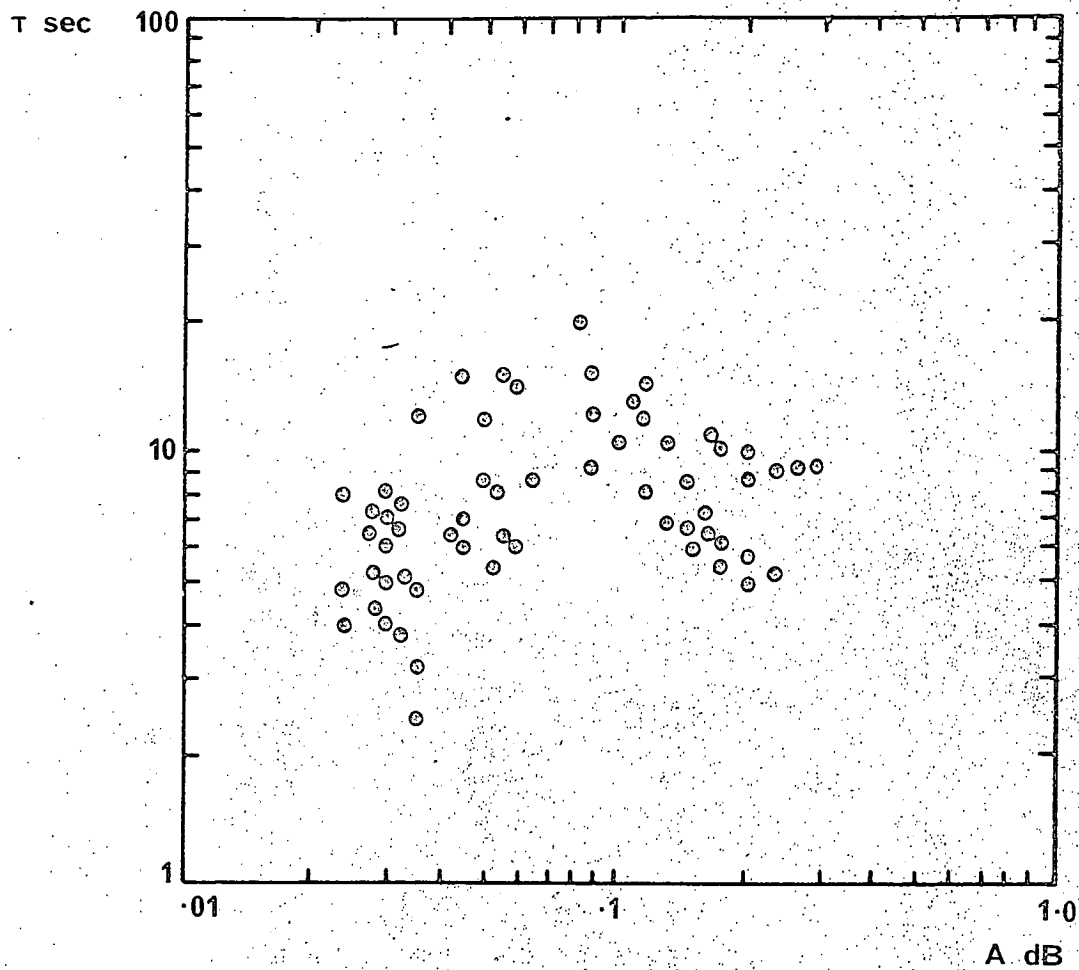

Fig. 4.8

A - τ diagram for the event of 18th January, 1969.

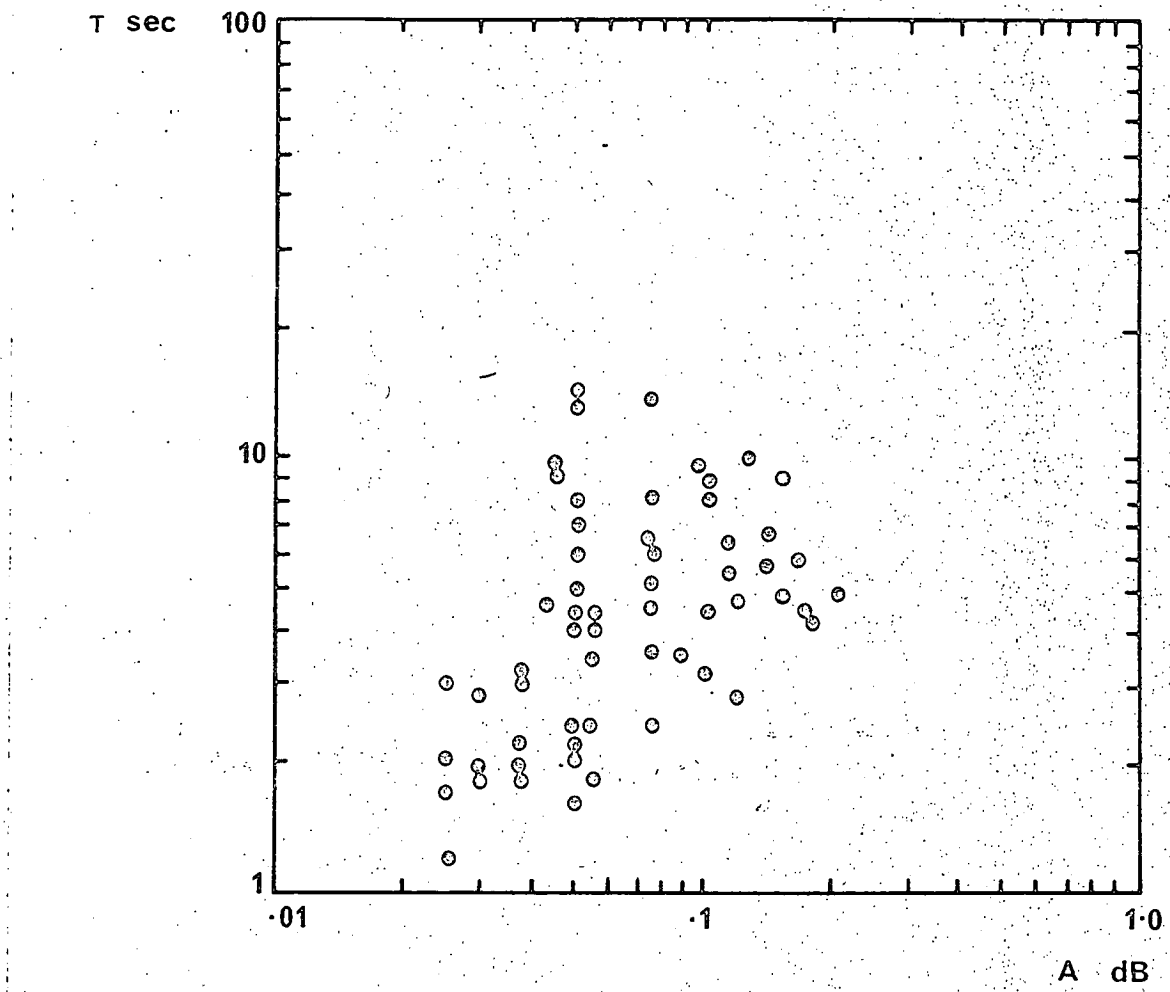

Fig. 4.9

A - τ diagram for the event of 26th January, 1969. This event occurred at night.

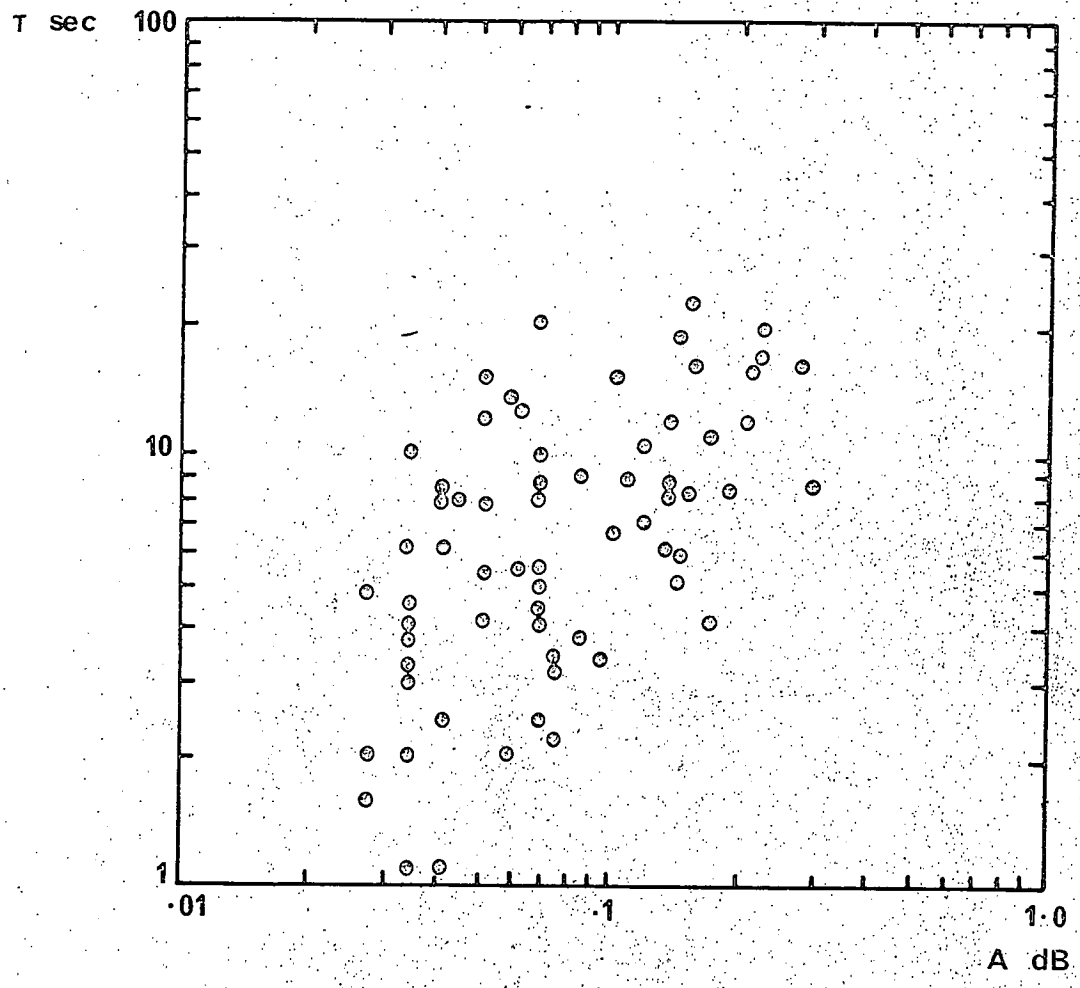

Fig. 4.10

A - τ diagram for the event of 13th February, 1969.

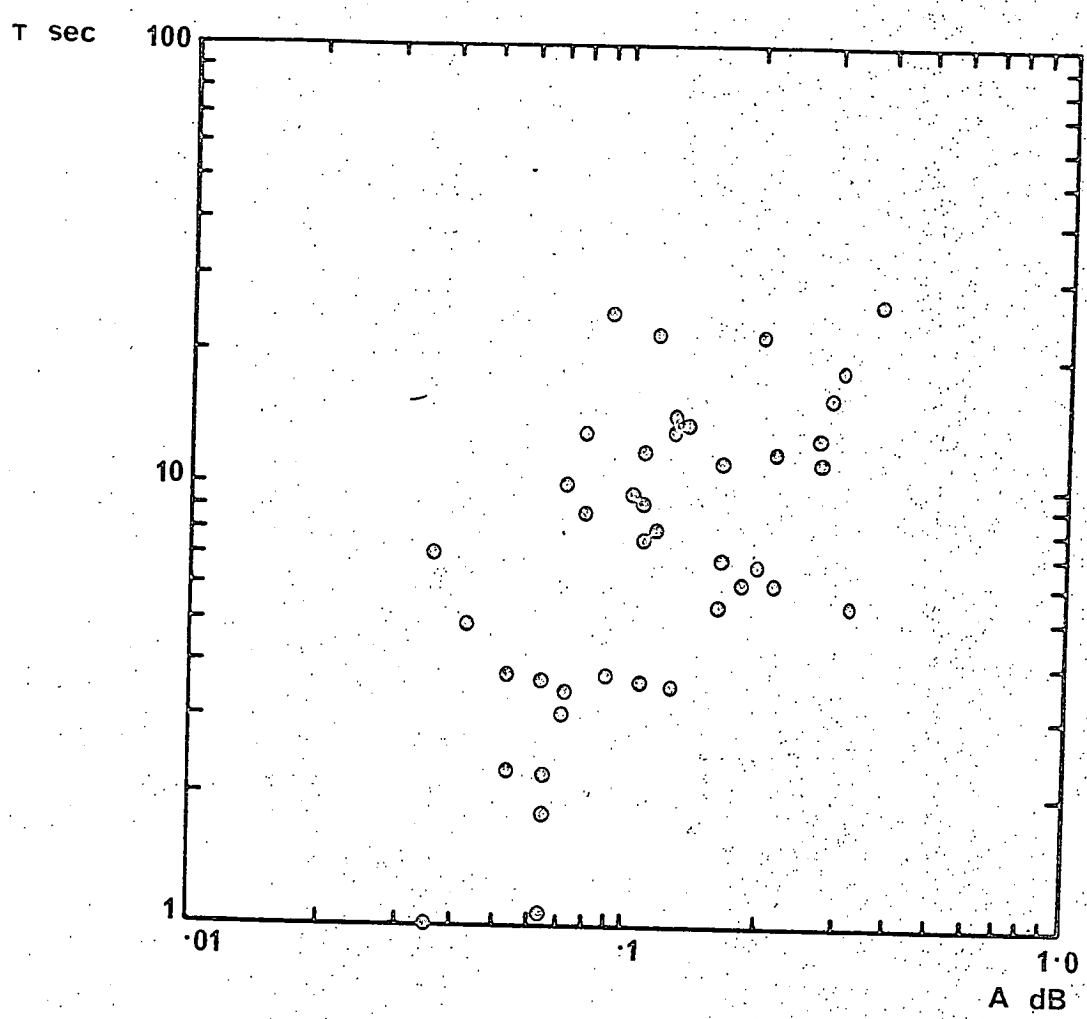

Fig. 4.11

A - τ diagram for the event of 14th March, 1969.

others suggesting that attachment - detachment processes are of little importance.

The range of values taken by the relaxation times is of great importance; they range from less than two seconds to almost 30 seconds. No pulses with relaxation times exceeding 30 seconds were observed in any of the records obtained during the three successive summers in which fast response riometers were operated at Macquarie Island.

4. 4 Interpretation.

There are two possible explanations of the major feature of the experimental data; ie. of the tendency for relaxation time to be in direct proportion to pulse amplitude. They are

(a) an interpretation in terms of a mixture of positive ion species with widely differing recombination rates, and (b) an interpretation in terms of differing depths of primary particle penetration from pulse to pulse.

4. 4. 1 A Two - Ion Theory.

Consider equations (2. 28), (2. 29) and (2. 30). It is intuitively obvious that over a range of values of N and C the time constant for N will be controlled by the quantity $1/\alpha_c C$ since we are assuming that $\alpha_c \gg \alpha_D$. It is also apparent that, if the decoupling hypothesis holds and s $\simeq$ constant, increases in N will bring about decreases in C and hence increases in the time constant for N.

Putting this in another way: the number density of rapidly reacting cluster ions will control the rate at which electrons are removed from the atmosphere while the cluster ion density in turn depends on the electron density. Larger pulses in q and hence in N will cause a depletion of cluster ions - fewer cluster ions lead to a slower removal rate for electrons. Thus larger pulses would have longer time constants.

Equations (2. 28) and (2. 29) were integrated numerically with $\alpha_D = 5 \times 10^{-} \text{ cm}^3 \text{ sec.}^{-1}$ and $\alpha_c = 5 \times 10^{-5} \text{cm.}^3 \text{sec.}^{-1}$ and

$$q = q_o' + \Delta q' . p(t) .$$

where $q_o' = 1000\ cm^{-3}sec^{-1}$.

Values of K/α_c ranging from .1 to 10 cm^{-3} and of $\Delta q'$ of from 10 to 10^5 $cm^{-3}sec^{-1}$ were used. Unlike in the previous model, no height integration was performed and attachment effects were neglected. The equations were intended to typify conditions at about 80 km during a moderate absorption event with a similar proportion of heavy positive ions present to that observed by Narcisi and Bailey (1965). The results from a sequence of integrations are shown in Table 4. 1. The time constant τ is defined as above
(equation)

Table 4. 1.

$K/\alpha_c = 1.0\ cm^{-3}$

$q_o = 10^3\ cm^{-3}sec^{-1}$

$N_o = 5 \times 10^3\ cm^{-3}$

$t_{\frac{1}{2}} = 1.0$ sec

$\Delta q(cm^{-3}sec^{-1})$	$N(cm^{-3})$	τ(sec)	A(dB)
10	14.1	10.2	3×10^{-4}
10^2	153	12.4	.003
10^3	1.57×10^3	14.9	.031
10^4	1.75×10^4	49.3	.351
10^5	1.75×10^5	12.3	3.49

It can be seen that τ can, in fact, increase with increasing absorption pulse amplitude. The relationship is a square root one however; τ increases only threefold for a tenfold increase in A. Integration for various combinations of K/α_c, q_o and $t_{\frac{1}{2}}$ showed that, while under some circumstances there was no increase of τ with A, where increases did occur, they were never more than threefold for a tenfold increase in A.

The shape of pulses in the range which has τ increases with A can be seen in Fig. 4. 12. The pulses have two relaxation times corresponding to an initial rapid decay followed by a much slower decay. The relaxation time of the slower decay is given by $1/2\alpha_D N$, while the steeper component of the slope is the one from which τ was actually calculated.

It can be shown analytically that if $\alpha_D = 0$ the effect of a pulse in q is a stepped change in both N and C after which a new equilibrium is established. When α_D is not zero but much smaller than α_C there is a slow decay back to the original equilibrium at a rate controlled by α_D.

This simple model involving a constant (decoupled) source of rapidly recombining ions can be discounted as an explanation of the observed A - τ relationship for the following reasons:

(i) τ cannot be made to increase rapidly enough with increasing A;

(ii) The increase in τ with increasing A does not become significant until A is at least equal to the steady background in absorption (unlike the observed pulsations);

(iii) the predicted pulse shapes do not resemble those observed experimentally.

Some interesting features of this analysis were that τ is a strong function of the half width of the pulse in q and is also sensitive to the extent of the departure of the cluster ion concentration from its equilibrium value.

We cannot entirely rule out a multiple positive ion system as an explanation of the observed A - τ relationship, since this model studied here was a highly simplified one. To continue this line of enquiry further we would need more information about the relative proportions of the various positive ion species and of the rate constants of the reactions by which they are formed and destroyed.

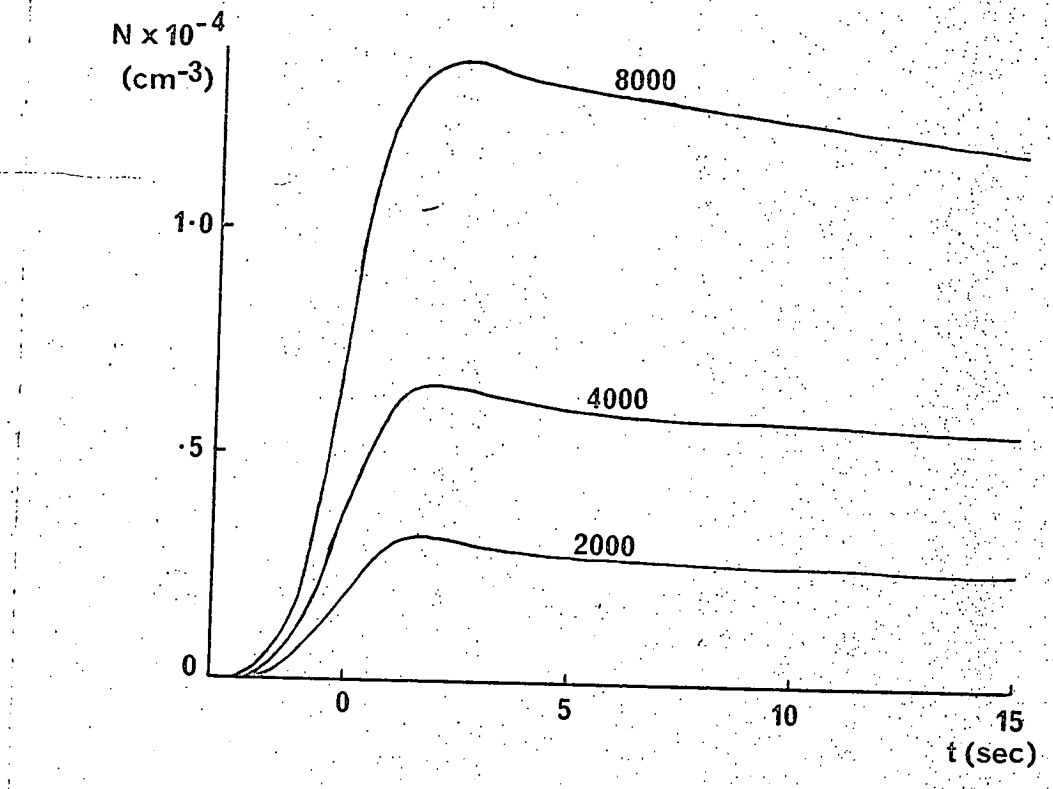

Fig. 4.12

Variation of electron density N as a function of time for the two-ion model described in Section 4.4.1. The pulses correspond to values of Δq of 2000, 4000 and 8000 $cm^{-3}sec^{-1}$ superimposed on a background q_o of 1000 $cm^{-3}sec^{-1}$. The respective relaxation times as defined by (3.2) are 18.0, 25.6 and 43.5 seconds. This apparent increase in τ with ΔN is due solely to the small region of steeper slope which occurs just after the peak in N.

At the moment the observed positive correlation between absorption pulse amplitude and relaxation time is best explained in terms of variability of penetration depth of pulses in primary electron flux rather than by a two ion theory.

4. 4. 2 Variability in Penetration Depth.

In Fig. 3. 2 the locus of pulses of constant parent electron flux and varying e - folding energy indicated by the filled circles has a positive slope of about .5 for the softer parent electron spectra. This slope is less than that of the experimental A - τ diagrams. However, if the flux of the parent electrons were to be inversely related to their e - folding energy, the slope of their locus on the A - τ diagram would be steeper and could be made similar to the trend in the experimental scatter diagrams. What is more, such a curve describing pulses of increasing e - folding energy and decreasing flux would pass through a maximum in a similar way to the points in the A - τ diagram of Fig. 4. 8.

An inverse relationship between intensity and spectral hardness has been reported by Barcus and Rosenberg(1966) for (background) bremmstrahlung X-ray spectra although the actual pulsation observed by them appeared to have consistently soft spectra. A greater than tenfold variation in e - folding energy from pulse to pulse would be necessary to yield the spread in τ of from 1 to 30 sec. manifested by the observed c. n. a. pulsations. Such a large pulse to pulse variation in hardness would be very obvious on any multichannel recording of bremmstrahling x- rays. While spectral variations in fast x - ray pulsations have been observed with multichannel detectors by Brown and Weir (1967), the peak to peak variation was small. There could have been very little variation in energy spectrum from pulse to pulse.

The essential feature which gives rise to the increase in τ with increasing spectral hardness is the bulge in the background profile of ion - pair production rate which peaks at 105Km. This bulge brings about a similar bulge in the profile of steady state electron density, N, and a

corresponding depression in τ which is inversely proportional to N above about 80 Km (Figs. 3. 8 and 3. 9). Below the peak in q at 105 Km τ increases with decreasing height and so succesively harder spectra achieving greater and greater penetration depths will yield increasingly large values τ. It is not so much spectral hardness which is important but penetration depth. The rate at which τ increases with increasing energy of the primary pulse will be determined by the slope of the profile in q below its maximum and this in turn will depend on the hardness of background spectrum. Soft background spectra will give rise to $\tau(h)$ profiles which vary rapidly with height. Small variations in the height of penetration of pulses superimposed on this background would then yield large variation in relaxation time. It may not even be necessary for the e - folding energy or top - of- the - atmosphere flux to vary greatly. For a suitably soft background spectrum small variations in mean height of penetration due to variations in pitch angle or mean energy could bring about the relationships between A - τ seen in the scatter diagrams of Figs. 4. 6 to 4. 11.

4. 5 Relaxation Time and Recombination Coefficient.

All but one of the experimental scatter diagrams show pulsations with relaxation times of 2 seconds or less. When comparing these scatter diagrams with Fig. 3. 2 (omitting Figs. 4. 6 and 4. 7 which had large background absorptions) we see that the predicted relaxation times are about five times too large to account for observed pulses.

In Fig. 3. 2 there is the obvious tendency for relaxation time to decrease with decreasing pulse spectral hardness. One might expect to obtain relaxation times from the model of less than 2 seconds merely by choosing a sufficiently soft primary pulse spectrum. Fig. 3. 9 shows that 10 seconds is the minimum relaxation time which can be obtained with this profile. Spectra with e - folding energy less than 5KeV would

have maxima above the 105 Km minimum in $\tau(h)$ and the pulse relaxation time would increase with decreasing spectral e - folding energy.

This argument applies only to this profile and only to small perturbations. In order to produce pulses with relaxation times as small as those observed all that is required is that the electron density in the absorbing region be made sufficiently large. For $\alpha = 2 \times 10^{-7} cm^3 sec^{-1}$ and $\tau = 1$ sec, N would be required to have a value of 2.5×10^6 cm^{-3}. The specific absorption for 32 MHz at 105 Km is 6×10^{-8}dB. $Km^{-1}(el.cm^{-3})^{-1}$ and so the absorption per Kilometre due to this electron density would be about .15dB. The region of enhanced electron density would need to be confined to a strip 3 Km wide in order to yield height integrated cosmic noise absorption of .5dB.

Fifteen kilometres higher, at 120 Km, the specific absorption is an order of magnitude less and the narrowness of the absorbing region is no longer a problem. It is interesting to note that the peak in precipitation flux observed near 6keV by O'Brien and Reasoner (1971) and by Westerlund (1969) would give rise to a peak in ion pair production rate near this height according to the rate profiles of Rees (1963).

Observations by O'Brien and Reasoner (1971) using spectrometers and differential energy detectors carried aloft by rockets measured auroral zone electron bursts having complex energy spectra with strong peaks near 40eV and near 6 keV and pitch angle distributions which were almost isotropic at some energies. The peak energy of the 6keV peak varied in time in a non-systematic way. Had fast response riometers been in operation on the ground in the course of this rocket flight it seems almost certain that some sort of c. n. a. pulsations would have been observed. Possibly they would have been the complex type of Fig. 4. 2 with amplitude and relaxation time variability corresponding to the

variability in the 6 keV peak detected by the rocket instruments.

Another possibility is that the recombination coefficient has a value larger than the one used above. Increasing α by an order of magnitude to $2 \times 10^{-6} cm^3 sec^{-1}$ has the effect of lowering the curves of Fig. 3. 2 into the range of values of τ observed experimentally (Fig. 3. 4). This is a rather high value of α to use in the E-region where most experiments have lead to the adoption of a value 2×10^{-7} or less (Mitra, 1968)

If we go a step further and use the height dependant values of α due to G. C. Reid (1970) (Figs. 3. 5 and 3. 6) we find that there is now insufficient spread in τ to account for the observations. The reason for this is apparent when we examine height profiles of τ for the given conditions (Figs. 3. 10 and 3. 11). There is a greater than tenfold spread in τ as a function of height but taking the weighted mean of this with respect to the pulse absorption distribution A(h) reduces this spread to that of Figs. 3. 5 and 3. 6. If the height spread in A(h) were to be reduced by assuming a narrow region of ion pair production rate for the pulses then τ (h) would be averaged over a smaller height range, the smoothing effect of averaging would be reduced and there would result a greater spread in τ as a function of primary spectral hardness.

For the soft background case (Figs. 3. 5 and 3. 10) we are left with the same problem. The minimum in τ(h) still occurs at 105 Km although its actual value has been reduced (in inverse proportion to α) to a value of 4 seconds. Using the same argument as before, in order that τ be as small as one second, the electron density N would need to be $10^6 cm^{-3}$. Such an electron density would bring about .06 dB per kilometre absorption of cosmic noise at 105Km and the pulse region would still need to be less than 9 Km in width. For this harder background (Fig. 3. 11) τ(h) has a minimum at 86 km

of 1.6 seconds but an absorption pulse with this relaxation time arising from this $\tau(h)$ profile would once again need to occupy only a small range in height.

To sum up, the relaxation times of less than two seconds exhibited by some of the pulsations are explicable if either

(i) the height range of absorption is small,

or (ii)the recombination coefficient has a value greater than the currently accepted value, at the heights concerned

or (iii)the pulse in absorption occurs at greater heights than expected ie: above 105 Km.

4. 6 Relaxation time and Auroral Luminosity.

Measurements of pulsations in auroral luminosity at times of c. n. a. pulsation activity yield additional information. Observations of the simultaneous occurence of the two types of pulsations are described in Appendix I . The pulsations in luminosity at λ 4278 A^{o} were between 1 and 2 kR in amplitude superimposed in a background of 2kR. All-sky camera photographs indicate that, while the luminosity background was almost uniform over the field of view of the photometer, the patchy, diffuse auroral forms superimposed on this background were quite variable in shape and size and impossible to relate to the photometer record. This was only to be expected since the photometer pulsations occured on a smaller time scale than the one minute cycle time of the all-sky camera.

The c. n. a. pulsations recorded simultaneously varied from .02 dB to .2 dB in amplitude and were superimposed on a background which varied between .45 and .65 dB. Their relaxation times varied from 1 sec. to 15 sec. There were four c. n. a. pulsations with relaxation times of less than two seconds of which three corresponded to light pulsations much smaller than average, (although too much attention ought not to be given to this since the field of view of the photometer differed from that of the riometers). An example is the

light pulsation corresponding to the west beam c. n. a. pulsation occuring at 1406.05 U.T. in Fig. 4 of Appendix I.

This quantitative luminosity data places further constraints on the alternative models suggested in the previous section. There are five such constraints, viz:

$$\Delta A = \int_0^\infty \Delta N \, \mu \, dh \qquad (4.11)$$

$$A_o = \int_0^\infty N_o \, \mu \, dh \qquad (4.21)$$

$$\frac{\Delta L}{\sigma} = \int_0^\infty \Delta q \, dh \qquad (4.3)$$

$$\frac{L_o}{\sigma} = \int_0^\infty q_o \, dh = \int_0^\infty \alpha N_o^2 \, dh \qquad (4.4)$$

and from equation (3.20)

$$\frac{\Delta A}{\tau} = \int_0^\infty \frac{\Delta N \, \mu \, dh}{\tau(h)} \qquad (4.5)$$

where the zero subscript refers to the steady background, and the prefix Δ to the pulse amplitude above background of A, L, N and q, the absorption, luminosity, electron density and ion pair production rate respectively. The quantity, σ is dependant on the photon emission rate. If we assume that one photon at λ 4278 $\mathring{A}$ is emitted for every fifty ion pairs formed (Omholt, 1968) we have

$$\sigma = 2 \times 10^{-3} \text{ Rayleighs.}(\text{cm}^{-3}\text{sec}^{-1})^{-1}\text{Km}^{-1}$$

μ, which is a function of height, is the specific absorption in $\text{dB.Km}^{-1}(\text{cm}^{-3})^{-1}$. For an operating frequency of 32 MHz above 60Km μ is proportional to the collision frequency.

There are, of course, an infinity of possible distributions of N_o, N and q which will satisfy equations (4. 1) to (4. 5) but by using some approximations and inequalities we can reach some general conclusions about the event of 12 March 1969.

Firstly, let us assume that the bulk of the pulse absorption occurs within a height interval (h_1, h_2) such that

$$\tau(h) \simeq \tau \quad \text{for } h_1 \leqslant h \leqslant h_2$$

Then from (4. 5)

$$\Delta A \simeq \int_{h_1}^{h_2} \Delta N \mu \, dh$$

$$< \mu_1 \cdot \int_{h_1}^{h_2} \Delta N dh \qquad (4. 6)$$

where $\mu_1 = \mu(h_1)$ and $\Delta h = h_2 - h_1$.

Let us further assume that attachment processes are negligible in the pulse absorbing region. Then

$$\tau = \frac{1}{\alpha(2N_o + \Delta N)}$$

and at $t = t_1$, the time of maximum of the pulse in electron density

$$q(t_1) - \alpha N(t_1)^2 = \left(\frac{dN}{dt}\right)_{t_1} = 0$$

i.e.

$$q(t_1) = \alpha (N_o + \Delta N)^2$$

Since the pulse in N lags the pulse in q we have

$$q_o + \Delta q_1 > q(t_1)$$

i.e.
$$q_o + \Delta q > \alpha(N_o + \Delta N)^2 \qquad (4.8)$$

since

$$q_o = \alpha N_o^2$$

$$\Delta q > \alpha(2N_o + \Delta N)\,\Delta N$$

i.e.
$$\Delta q > \frac{\Delta N}{\tau(h)} \qquad (4.9)$$

From (4.3)

$$\frac{\Delta L}{\sigma} > \int_{h_1}^{h_2} \Delta q \; dh$$

$$> \int_{h1}^{h_2} \frac{\Delta N}{\tau(h)} \; dh$$

$$= \frac{1}{\tau} \int_{h1}^{h_2} \Delta N \; dh$$

$$> \frac{\Delta A}{\mu_1 \tau} \qquad \text{by (4.6)}$$

Thus

$$\mu_1 > \frac{\sigma \Delta A}{\Delta L \tau} \qquad (4.\ 10)$$

For the pulses of the event of 12/3/69

$$\frac{\Delta A}{\tau} \simeq .01 \text{ dB/sec}$$

and

$$\Delta L \simeq 2 \times 10^3 \text{ Rayleighs}$$

Hence,

$$\mu_1 > 10^{-8} \text{ dB.km}^{-1}\text{cm}^3$$

The specific absorption at 32 MHz has this value at 116 km. We may conclude that the <u>lower</u> boundary of the pulse absorption region lay below 116 km.

From (4. 3) and (4. 4)

$$\frac{L_o + \Delta L}{\sigma} \geqslant \int_{h_1}^{h_2} (q_o + \Delta q)\, dh$$

$$\geqslant \int_{h_1}^{h_2} \alpha (N_o + \Delta N)^2\, dh$$

$$\geqslant \int_{h_1}^{h_2} \frac{dh}{4 \alpha \tau (h)^2}$$

$$\simeq \frac{\Delta h}{4 \alpha \tau^2}$$

Hence,

$$\frac{\alpha}{\Delta h} \geq \frac{\sigma}{\tau^2 (L_o + \Delta L)} \qquad (4.11)$$

Taking $\tau = 2$ sec. and $L_o + \Delta L = 3$ KR we have

$$\frac{\alpha}{\Delta h} \geq 4 \times 10^{-8} \text{cm}^3 \text{ sec}^{-1} \text{.km}^{-1}$$

Once again, a limit can be placed, jointly, on the values of α and the "effective" width of the pulse absorbing region Δh, this time by considering only the c. n. a. pulsation relaxation time and the accompanying level of luminosity. The minimum value of $\alpha/\Delta h$ derived in this way is independant of height since the specific absorption, μ, is not involved. Even if the short relaxation time c. n. a. pulsations recorded during the event of 12/3/69 are presumed to have occurred in the E-region the thickness of the absorbing region would still need to have been small (ie: $\lesssim$10km) if a "conventional" value of α of less than $5 \times 10^{-7} \text{cm}^3 \text{sec}^{-1}$ is assumed.

Of course, we cannot preclude the possibility, discussed in Section 2 that α may have a dynamic value which differs from its steady state value. Also, during auroral activity the temperature of the E-region can attain temperatures in excess of 2,000^{o}K (Walker and Rees,1968). Such temperatures would no doubt have a major effect on α, changing its value by, perhaps, orders of magnitude. Nevertheless the temperatures are not likely to be this high below 120 km and there is no justification at this stage for assuming a value for α outside of the range of values reported in the literature.

SECTION 5

Conclusion

5.1 An E-region Phenomenon.

Fast c. n. a. pulsations observed in the southern auroral zone exhibit two unexpected properties which require explanation.

(i) there was a strong tendency for the relaxation times of the pulsations to increase with increasing pulse amplitude

(ii) some of the pulsations had exceptionally short relaxation times, some being less than two seconds, in magnitude.

The original assumption, made when this work was commenced, was that the pulsations in cosmic noise absorption took place in the D-region i.e.: below 100 km in height. Following other workers (Eather and Jacka,1966; Hultqvist 1964,1965,1966; Bailey 1968) it was assumed that absorption was brought about at these heights by the ionization produced by the high-energy,exponential tail of the primary electron flux. This view was supported by the simultaneous observation of c. n. a. pulsations and fast x-ray pulsations of greater than 25 keV energy.

Height profiles of ion - pair production rate for primary spectra with a variety of e-folding energies were determined and the relaxation times of the resulting absorption pulses were computed via the Bates and Massey (1946) rate equations (1. 1) for a variety of rate equation parameters and primary spectra. In no case were the relaxation times predicted by this model as small as some of those observed experimentally even when the large, height-dependant values of the recombination coefficient deduced by G. C. Reid (1970) were used in (1. 1). The model can only be made compatible with the observations if it is assumed that, for the fast relaxation time pulsations,

the absorbing region is either thinner or higher than was originally assumed or if the recombination coefficient has values higher even, than those proposed by G. C. Reid.

Comparison with auroral luminosity pulsations recorded simultaneously with c. n. a. pulsations on 12/3/69 indicated that the short relaxation time pulsations observed on that occasion were compatible with the accompanying level of luminosity if the bottom of the absorbing region lay below 116 km. On the other hand, the low levels of accompanying luminosity resulted in an upper limit being placed on the quantity $\alpha/\Delta h$ of $4 \times 10^{-8} cm^3 sec^{-1} Km^{-1}$ once again implying that the effective height width of the absorbing region is relatively small ie: of the order of 10km or less for "conventional" values of α.

Thus all of the available evidence, both that obtained from the D-region model based on equation (1. 1) and that obtained from simultaneous observations of auroral luminosity leads to the conclusion that the height width of the pulse absorbing region is small, of the order of 10 kilometres or less. Such a small range in height of enhanced electron density implies one of two things

either (i) the ionizing primary flux was nearly mono-energetic and nearly monodirectional

or (ii) a mechanism was operating whereby ionization created by the primary electron flux was being stratified and compressed into a small region - the wind shear theory of sporadic E comes to mind.

We cannot exclude alternative (ii), just as we cannot positively exclude the possibility that α has values even higher than those deduced by G. C. Reid. The simplest alternative is (i) however.

Examination of Fig. 3. 11 indicates that an absorption pulse with a half width of of 10 km centred at about 84km is barely able to yield a suitably small relaxation time of less

than two seconds. Background spectra with e-folding energies either greater or less than 20keV will not be so fortuitous. This spectrum only gives rise to such a small value of $\tau(h)$ because the peak in ion pair production rate coincides with the 87 km discontinuity in α. Harder spectra cause more ionization lower down where the collision frequency is higher; the background electron density necessary yield 0.5dB background absorption would be less leading to larger values of $\tau(h)$. On the other hand, softer spectra give rise to maxima in N and minima in $\tau(h)$ above the ledge where α is higher (Fig. 3. 10)

It appears then, that the pulse absorbing region is not likely to lie below 87km where a high value of the recombination coefficient could be invoked to explain the short relaxation times. In any case, a thin layer at 84km would require a monoenergetic primary flux near 50 keV. Such a flux has not been observed by means of rockets or satellites.

If we are to avoid the region of high recombination coefficient in seeking to explain the shorter relaxation times we need to look at the E-region, above 105km. where a layer of enhanced electron density of say 10^6electrons cm^{-3} of thickness 10km will give rise to a suitably short relaxation time but will not give rise to an unreasonably large amount of background absorption because of the lower specific absorption at these heights.

The picture which emerges, the simplest model to fit the observations, is that of an absorbing region about 10km thick with a lower border between about 105km and 116km in height. Such a layer would be brought about by a nearly monoenergetic peak in the flux of primary electrons with peak energies in the range of from 10keV down to 4 keV. The short relaxation time pulsations would be brought about by an intensification of the peak itself, while the longer relaxation time pulsations would be brought about by a broadening or movement of the peak towards the high energy end of the spectrum.

Alternatively, we can conceive of a relatively stable peak with pulsations in primary flux superimposed upon it. If these flux pulsations approximate the energy of the background the resulting absorption pulse will be rapidly decaying On the other hand, flux pulsations with energies higher than the background peak will penetrate to greater atmospheric depth and give rise to greater pulse absorption but the absorption pulses will have longer relaxation times because of the smaller ambient electron densities at these depths.

Pulses in primary flux with energies on the high side of an energy peak in the primary background flux would in this way give rise to c. n. a. pulsations whose relaxation times increase with increasing amplitude. Pulses in primary flux with energies less than the background peak should give rise to c. n. a. pulsations which show the opposite effect. That such an effect is not observed is hardly surprising when one considers that the small fast c. n. a. pulsations have amplitudes of only .02 dB. The resolution of the fast response riometer would need to be improved before we could expect to resolve pulsations on the low energy side of such a background peak.

Quasi-monoenergetic, non-isotropic peaks in the primary electron flux in the energy range 1 keV to 10 keV have been observed by means of rocket borne differential energy detectors by a number of workers (Evans, 1968; Westerlund, 1969; Chase, 1970 O'Brien and Reasoner, 1971). Furthermore sudden shifts in the position of these peaks with a time scale of seconds have also been observed (Chase, 1970; O'Brien and Reasoner, 1971).

Surely we need look no further in seeking an explanation of the occurrence and observed behaviour of fast cosmic noise absorption pulsations.

5. 2 Further work.

Much of the above discussion is tentative and circumstantial; not enough information was available for it to be

possible to draw any unequivocal conclusions. The obvious requirement is that fast response riometers, which are cheap and easy to build, be operated in conjunction with sounding rockets measuring the differential energy spectrum and pitch angle distribution of the primary particle flux. Once a relationship between c. n. a. pulsations and shifts or pulses in the primary spectrum becomes more firmly established a good deal of morphological data becomes available. The spatial size and time of occurence of the c. n. a. pulsations are known; all that is needed is to connect up c. n. a. pulsations with the precipitation phenomena for this data to provide us with more quantitative information about magnetospheric processes.

The smaller pulsations with the shorter relaxation times were those on which much of the above discussion was based. These pulsations are close to the resolution limit of the instrument. The resolving power of the fast response riometer needs to be increased and this can only be done by widening the bandwidth. Unfortunately the sensitivity of the instrument to cosmic noise absorption falls off as the square of the frequency and the intensity of the cosmic noise itself falls off rapidly with frequency as well. It would probably not be worthwhile widening the bandwidth to more than 40 MHz (ie: from 30MHz to 70 MHz in pass band).Even so this would result in a fivefold increase in amplitude sensitivity which would have a number of advantages, viz.

(i) relaxation times of the smaller pulses could be measured with much greater accuracy;

(ii) it would be possible to check to see if the relaxation times started to increase with further decreases in pulse amplitude below .02 dB as suggested in section 5. 1; and (iii) the detailed shape of an individual absorption pulse could be measured. Comparison with the detailed shape of the corresponding luminosity pulse might be made to yield a height profile of electron density via the equations

$$A(t, H) = \int_0^{\alpha} N(t, h)\ \mu(h)\ dh \qquad (5.\ 1)$$

$$L(t, h) = \sigma \int_0^{\alpha} \left\{ N(t, h) + \alpha\ N(t, h)^2 \right\} dh \qquad (5.\ 2)$$

Even with the existing instrument a number of fields are worthy of further study. For example:

(i) a more precise analysis of the relationship between luminosity pulsations and c. n. a. pulsations using instruments with similar fields of view. More stringent limits might be placed on the quantities $\alpha/\Delta h$ and μ_1 in equations (4. 10) and (4. 11);

(ii) a more detailed study of the relationship between c. n. a. pulsations and Pi 1 and Pi 2 micropulsations. The hypothesis presented by Campbell (1970) to explain the observed time lags between micropulsations and luminosity pulsations in terms of the time of propogation of hydromagnetic waves through the ionosphere could be tested. An alternative concept could also be examined according to which the micropulsations are not propogated from the magnetosphere but are created in the ionosphere itself when fluctuations in secondary electron density create changes in conductivity and hence in current density in the E-region during a magnetic bay. A group of fast response riometers with beams directed to different parts of the sky would enable the position and orientation of enhancements in electron density to be ascertained and their relationships to the micropulsation disturbance vector examined;

(iii) a study of the relationship between the time structure of V. L. F. emissions and the time structure of particle precipitation. A relationship between the intensity

of V. L. F. emissions and auroral absorption events has already been established (Vershinin and Ponomarev 1966; Hayashi and Kokubun 1971; Payne 1972). A fast response riometer operated in conjunction with suitable V. L. F. receiving equipment would reveal whether a similar relationship exists between the fine structure of such events, ie: do c. n. a. pulsations correspond to individual emissions such as risers or groups of risers in the dawn chorus? If so, then more quantitative data could be brought to bear upon the nature of the wave-particle interactions believed to be responsible for both V. L. F. emissions and some types of electron precipitation.

Acknowledgements

I would like to express my gratitude and thanks to my supervisor, Prof. G. R. A. Ellis of the University of Tasmania for his guidance and encouragement. I would like to thank the Antarctic Division of the Department of Supply for the logistic support which made this project possible. I am indebted to Prof. K. D. Cole of Latrobe University for reading the manuscript and offering his advice and comment and to Prof. E. J. G. Pitman of Hobart for reading Appendix II and correcting my rather rusty formalism.

I would also like to thank Mrs. A. Montgomery for her excellent diagrams and the members of the photographic section of the Antarctic Division for reproducing them so well. I am also grateful to Mrs. R. Thacker for taking over the typing and to Mr. F. Bond and Mr. P. Sulzberger of the Antarctic Division for their encouragement in completing this project.

References

Ansari, Z. A.(1964). J. Geophys. Res. 69, 4493.

Apostol, T. M.(1969). Ch.7 of "Calculus", Blaisdell..

Arnold, F., J. Kissel, D. Krankowsky, H. Wieder and J. Zahringer (1971). J. Atm.Terr.Phys. 33, 1169.

Arnold, F. and D. Krankowsky (1971). J. Atm.Terr.Phys. 33, 1693.

Bailey, D. K.(1959). Proc. I. R. E. 47 , 255.

Bailey, D. K.(1968). Rev. Geophys. 6, 289.

Barcus, J. R. and T. J. Rosenberg.(1966). J. Geophys. Res. 71, 803.

Barth, C. A.(1966). Ann.Geophys. 22, 198.

Bates, D. R. and H. S. Massey(1946). Proc.Roy.Soc. A187,261.

Benson, R. F.(1964). Rad.Sci. J. Res. 68D, 129.

Berger, M. J., S. M. Seltzer and K. Maeda(1970). J. Atm. Terr.Phys. 32, 1015.

Bewersdorf, A., J. Dion, J. P. Legrand, E. Keppler, G.Kremser and W. Riedler (1967). Space Res. VII, 645.

Bowman, M. R., L. Thomas and J. E. Geisler (1970). J. Atm. Terr. Phys. 32, 1661.

Brown, R. R. and R. A. Weir (1967). J. Geophys.Res. 72, 5357.

Campbell, W. H.(1970). J. Geophys. Res. 75, 6182.

Catchpoole, J. R.(1970). Can.J. Phys. 48, 2537.

Chamberlain, J. W.(1961). "Physics of the Aurora and Airglow", Academic Press, London.

Chanin, L. M.,A. V. Phelps and M. A. Biondi (1959). Phys. Rev. Lett. 2, 344.

Chase, L. M.(1970). J. Geophys.Res. 75, 34.

Dingle, R. B., D. Arndt and S. K. Roy (1957). App.Sci.Res. B6, 155.

Eather, R. H. and F. Jacka (1966). Aust.J. Phys. 19, 215.

Evans, D. S.(1968). J. Geophys.Res. 73, 2315.

Fehsenfeld, F. C., E. E. Ferguson and A. L. Schmeltekopf (1966). J. Chem.Phys. 45, 1844.

Fehsenfeld, F. C., A. L. Schmeltekopf, H. I. Schiff and E. E. Ferguson (1967). Plan.Space Sci. 15, 373.

Ferguson, E. E.(1971). Rev.Geophys.Space Phys. 9, 997.

Ferguson, E. E. and F. C. Fehsenfeld (1969). J. Geophys. Res. 74, 5743.

Fritz, T. A.(1968). J. Geophys.Res. 72, 7245.

Gunton, R. C. and T. M. Shaw (1965). Phys.Rev.140A, 756.

Hargreaves, J. K.(1969). Proc. I. E. E. E. 57, 1348.

Hayashi, K. and S. Kokubun (1971). Rep.Ion.Space Res. Japan 25, 369.

Hesstvedt, E.(1968). Geofysiske Publikasjoner 27, 1.

Hultqvist, B.(1964). Plan. Space Sci. 12, 579.

Hultqvist, B.(1964). Plan.Space Sci. 12, 1035.

Hultqvist, B.(1965). Space Res. 5, 91.

Hultqvist, B.(1966). Space Sci. Rev. 5, 771.

Hunt, B. G.(1971). J. Atm.Terr.Phys. 33, 929.

Hunten, D. M. and M. B. McElroy (1968). J. Geophys.Res.73,2421

Jacobs, K. G., R. Kist and K. Rawer (1969).Space Res. IX, 246.

Kamiyama, H.(1967). J. Geomag.Geoélect. 19, 1.

Kane, J. A.(1962). J. Atm.Terr.Phys. 23, 338.

Kirkpatrick, P. and L. Weidmann (1945).Phys.Rev. 67, 321.

Lerfald, G. M., C. G. Little and K. Parthasarathy (1964). J. Geophys.Res. 69, 2857.

Le Levier R. E. and L. M. Branscomb (1968). J. Geophys.Res. 73, 27.

Little, C. G. and H. Leinbach (1958). Proc. I. R. E. 46, 334.

Manson, A. H. and M. W. J. Merry (1970). J. Atm.Terr.Phys. 32, 1169.

Mitra, A. P.(1968). J. Atm.Terr.Phys. 30, 1065.

Moruzzi, J. L. and A. V. Phelps (1966). J. Chem.Phys.45,4617.

Narcisi, R. S. and A. D. Bailey (1965). J. Geophys.Res. 70, 3687.

Narcisi, R. S., A. D. Bailey, L. Della Lucca, C. Sherman and D. M. Thomas. J. Atm.Terr.Phys. 33, 1147.

O'Brien, B. J.(1962). J. Geophys. Res. 67, 3687.

O'Brien, B. J.(1964). J. Geophys.Res. 69, 1.

O'Brien, B. J., F. R. Allum and H. C. Goldwire (1965). J. Geophys.Res. 70, 161.

O'Brien, B. J. and C. D. Loughlin (1963). Space Res.3, 399.

O'Brien, B. J. and D. L. Reasoner (1971). J. Geophys.Res. 76, 8258.

Ogawa, T. and T. Tohmatsu (1966). Rep.Ion.Space Res.Japan 20, 395.

Omholt, A.(1968). Ann.Geophys.24, 215.

Pack, J. L. and A. V. Phelps (1966). J. Chem.Phys. 44, 1870.

Paulikas, G. H., J. B. Blake and S. C. Freden (1966). J. Geophys. Res. 71, 3165.

Payne, R. - private communication.

Pearce, J. B.(1969). J.Geophys.Res. 74, 853.

Phelps, A. V. and J. L. Pack (1959). Phys.Rev.Lett. 3, 340.

Potemra, T. A. and A. J. Zmuda (1970). J.Geophys.Res.75, 7161.

Rees, M. H.(1963). Plan.Space Sci. 11, 1209.

Rees, M. H.(1964a). Plan. Space Sci. 12, 722.

Rees, M. H.(1964b). Plan. Space Sci. 12, 1093.

Reid, G. C.(1961). J. Geophys. Res. 66, 4071.

Reid, G. C.(1970). J. Geophys. Res. 75, 2551.

Reid, John (1967). Nature 214, 5095, 1321.

Reid, J. S. and J. Phillips (1971). Plan.Space Sci. 19, 959.

Sen, H. K. and A. A. Wyller (1960). J. Geophys.Res. 65,3931.

Tulinov, V. F.(1967). Space Res. VII, 386.

Tulinov, V. F., L. V. Shibaera and S. G. Jakovlev (1969). Space Res. IX, 231.

Ulwick, J. C., W. P. Reidy and K. D. Baker (1967). Space Res. VII, 656.

Vershinin, Ye. F. and Ye. A. Ponomarev (1966) Izv. SibIZMIR, No.1

Walker, J. C. G. and M. H. Rees (1968). Plan. Space Sci. 16, 459.

Walt, M., W. M. MacDonald and W. P. Francis (1967). "Physics of the Magnetosphere" p.543 (Ed. by Carovillano, McClay and Radoski) Reidel, Dordrecht, Holland.

Watanabe, K. and H. E. Hinteregger (1962). J. Geophys. Res. 67, 999.

Webber, W. (1962). J. Geophys. Res. 67, 5091.

Westerlund, L. H. (1969). J. Geophys.Res. 74, 351 (1969).

Whitten, R. C. and I. G. Popoff (1965). "The Physics of the Lower Ionosphere", Prentice-Hall, Englewood Cliffs N.J.

Whitten, R. C., I. G. Popoff, R. S. Edmunds and W. W. Berning (1965). J. Geophys. Res. 70, 1737.

APPENDICES

Appendix I.

Planet. Space Sci. 1971, Vol. 19, pp. 959 to 969. Pergamon Press. Printed in Northern Ireland

TIME LAGS IN THE AURORAL ZONE IONOSPHERE

J. S. REID and J. PHILLIPS
Physics Department, University of Tasmania, Hobart, Tasmania

(*Received in final form* 31 *December* 1970)

Abstract—Fast response riometers were operated at Macquarie Island (invariant latitude 64°S) in conjunction with balloon-borne X-ray scintillators, a λ4278 Å photometer, and a loop for detecting micropulsations. The pulsations in cosmic noise absorption (CNA) observed with the riometers were found to lag behind pulsations in bremmstrahlung X-rays, auroral luminosity and micropulsations occurring at the same time. These phase lags and the time asymmetry characteristic of CNA pulsations are shown to be consistent with the ionospheric rate equation.

INTRODUCTION

The relationship between electron density, N, and ion pair production rate, q, in the ionosphere in the presence of ionizing radiation may be described by the well known ionospheric rate equation:

$$\frac{dN}{dt} = \frac{q}{1+\lambda} - \alpha N^2 \tag{1}$$

where λ is the ratio of negative ions to electrons and α is the effective recombination coefficient.

Equation (1) implies that there will be a time lag between changes in q and changes in N. Appleton (1954) showed that, to the first order, the 'ionospheric time constant', τ, is given by

$$\tau \simeq 1/2\alpha N. \tag{2}$$

Brown (1964) dealt with equation (1) by considering the behaviour of N if q is a step function. Based on his work Eather and Jacka (1966) computed τ_{90}', the time taken for the absorption of cosmic noise to attain 10 per cent of its equilibrium value following a sudden decrease in the intensity of the ionizing radiation. They assumed that both cosmic noise absorption (CNA) and auroral luminosity were caused by fluxes of electrons with exponential spectra precipitated into the ionosphere from the magnetosphere. The CNA would be a function of N in Equation (1) and the luminosity a function of q. τ_{90}' then depends on the spectral index of the primary electrons and on the parameters α and λ.

Eather and Jacka examined 30 fast recovery CNA events for which simultaneous luminosity data were available. In each case the riometer recovery rate was limited either by the auroral luminosity dacay rate or by the instrumental rise-time. They concluded that their experimental result $\tau_{90}' < 31$ sec for all of the events, implied that the spectral indices of the primary electron spectra were all less than 5 keV. They found that peaks in luminosity and absorption were simultaneous to better than 5 sec, the time resolution of their instruments.

Simultaneous pulsations in CNA and auroral luminosity have been observed by Roldugin (1967). He also placed an upper limit of 5 sec on any lag which may occur between the two phenomena.

Holt and Omholt (1962) observed lags of from 4 to 8 min but this result can more readily be attributed to large differences in the fields of view of their instruments rather than to a genuine consequence of the rate Equation (1) (Eather and Jacka, 1966; Ansari, 1963).

It will be shown in this paper that, by using instruments of sufficient time resolution, it is possible to observe time lags of the order of a second in the auroral zone ionosphere. The cosmic noise absorption pulsations observed with fast response riometers lag behind fast bremmstrahlung X-ray pulsations, auroral luminosity pulsations and micropulsations occurring at the same time.

THE FAST-RESPONSE RIOMETER

The time and amplitude resolution of a riometer (Little and Leinbach, 1958) are determined by the bandwidth and output time-constant of the instrument. In a conventional riometer the bandwidth is usually restricted to 20 kHz, in order to avoid interference from broadcast stations and other sources. However, in the fast-response riometer the bandwidth was widened to 1·4 MHz and the output time-constant decreased from about 3 sec to 0·05 sec. The statistical fluctuation in output power was similar to a conventional riometer, about 0·05 dB.

The riometer consisted of an antenna, a low noise wideband radio receiver at 32 MHz centre frequency and output devices: a chart recorder with appropriate d.c. amplifier and a frequency modulation system for recording the data on magnetic tape. The output from the receiver detector was passed through a high-pass filter with a time-constant of two minutes to eliminate the large, slowly varying component of CNA events. Time-calibration pulses were superimposed on the record by shorting out a small, constant fraction of the signal in the receiver. Each antenna consisted of a broadside array of four half-wave dipoles suspended eight feet above a conductive ground plane. Their beams were tilted by using coaxial cable instead of open wires to interconnect the dipoles. The phase lag introduced by the velocity factor of the polythene causes the beam to tilt through 30° from the vertical.

As one would expect, the instrument has little long term stability and is subject to a good deal of interference from man-made sources. Nevertheless, the interference is readily identified and did not occur for more than 30 per cent of the time that the instrument was operated in the field.

Instruments of this type were operated at Macquarie Island (geographic 54·5°S, 159°E) in the Southern Auroral Zone during the summers of 1967, 1968 and 1969.

OBSERVATIONS

CNA pulsations

The most striking features of the records obtained were the trains of cosmic noise absorption pulsations which occurred in the midnight to noon sector (Reid, 1967; Yuan and Jacka, 1969). They were frequently asymmetrical in shape, having a rapid onset and slow decay and varied from 5 to 20 sec in duration. They were sometimes periodic for 5–10 cycles with periods of 7–9 sec.

The pulsations were usually superimposed on a steady background of absorption of 1 or 2 dB and had amplitudes of up to 0·8 dB. They occurred during SVIA events or late in the post break-up phase of auroral absorption. They were never observed during the pre break-up and break-up phase of auroral absorption events. These latter showed little fine structure which was not also discernable on a conventional riometer record.

Out of a total of 104 days of observation in the first three months of 1967 and 1969, CNA pulsations were observed on 35 days. There were 55 events lasting more than 15 min of which 35 contained asymmetrical pulsations.

CNA pulsations and X-ray pulsations

Various features of the CNA pulsations such as their time scale and time of occurrence suggest that they are associated with the fast bremmstrahlung X-ray pulsations observed with balloon borne instruments. Early in 1969 a number of X-ray detectors were flown by balloon from Macquarie Island in conjunction with four fast response riometers on the ground.

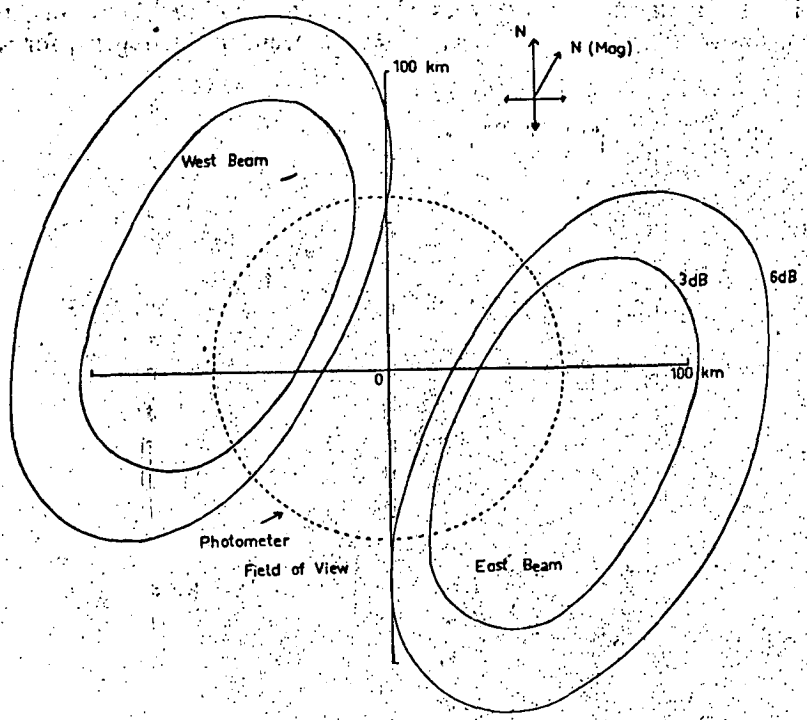

FIG. 1. 3dB AND 6dB CONTOURS OF TWO RIOMETER BEAMS SHOWING WHERE THEY INTERSECTED THE 100 km LEVEL IN THE ATMOSPHERE.
The dotted circle shows where the edge of the photometer field of view intersected this level. The North and South riometer beams are not shown.

Each X-ray detector consisted of a Harshaw integral line 1 in. by 1 in. NaI (Tl) crystal mounted on a RCA 6199 phototube. The crystals were uncollimated and all pulses corresponding to X-ray photon energies greater than 25 keV were counted. The balloons floated between the 9 and 11 millibar levels in the atmosphere.

The radiation patterns computed for two of the riometer antennas are shown in Fig. 1. The positions of the balloons were largely unknown, but it is most likely that they were between 100 and 200 km away from the antennas when most of the events occurred. Thus the X-ray detector would have been looking at a region of the ionosphere outside of the region covered by any of the antenna beams.

There were 12 X-ray balloon flights of which eight were successful, giving a total of 80 hr during 1969 during which X-ray and fast response riometer data were simultaneously available.

During this time 16 trains of fast X-ray pulsations were observed containing individual

pulsations with peak to valley ratios of greater than 2:1. These can be grouped into five major events lasting more than twenty minutes plus four small isolated trains lasting only a few minutes each. Four out of five of the major pulsation events were accompanied by CNA pulsations observed from the ground.

CNA pulsations in excess of 0·1 dB were observed on six occasions during the eighty hours when usable flight data was available. Five of these trains of pulsations occurred during the major X-ray pulsation events mentioned above.

While it is apparent that the two types of events are associated there was little peak to peak correlation of individual pulsations. The best event in this regard, for which good

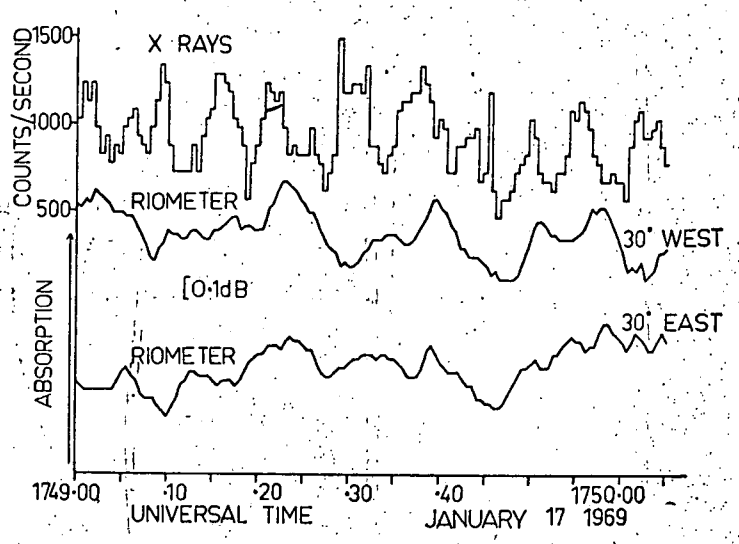

FIG. 2. A SAMPLE OF RECORD TAKEN FROM THE FIRST PULSATION EVENT OF 17 JANUARY 1969, SHOWING SIMULTANEOUS X-RAY AND CNA PULSATIONS.
Absorption is increasing upwards.

data were simultaneously available, was the first event of 17 January, 1969 when CNA pulsations occurred for 7 min in the course of an X-ray pulsation event. Part of this record is shown in Fig. 2. Some peak to peak correlation with a time lag is observable without further reduction of the data.

The data from this event were reduced by the method of superposed epochs. The zero epochs were taken at the peak of all the west beam CNA pulsations larger than 0·2 dB in amplitude consistent with successive intervals not overlapping. The result of superposing 16 epochs is shown in Fig. 3. There is a significant peak in X-ray intensity which occurs some seconds before the maximum in the mean cosmic noise absorption for the 16 epochs.

CNA pulsations and auroral luminosity pulsations

Pulsating auroras are known to exhibit at times a high degree of coherence with X-ray pulsations (Scourfield *et al.*, 1970; Rosenberg *et al.*, 1967; Pilkington *et al.*, 1968; Pettersen *et al.*, 1968). It seems likely that a similar relationship may be found between auroral pulsations and CNA pulsations.

A photometer with a 4278 Å interference filter of bandwidth 70 Å was operated in conjunction with the riometers between 8th and 13th March, 1969. The photometer had a 30° field of view and was pointed vertically (Fig. 1). One would expect almost all absorption

occurring within the field of view of the photometer to be detected by at least one of the four riometers.

The only clear night during this time was the night of 12 March, 1969 when CNA pulsations were observed in conjunction with pulsations in luminosity at λ4278 Å. March 12 was a night of intense auroral activity. Following the breakup of an IBC III to IV aurora early in the evening at 1010 U.T. the sky became extremely confused. Pulsating arcs and patches were observed intermittently until 1420 U.T. when the sky clouded over completely. Auroral luminosity pulsations were recorded by the photometer from 1357 to

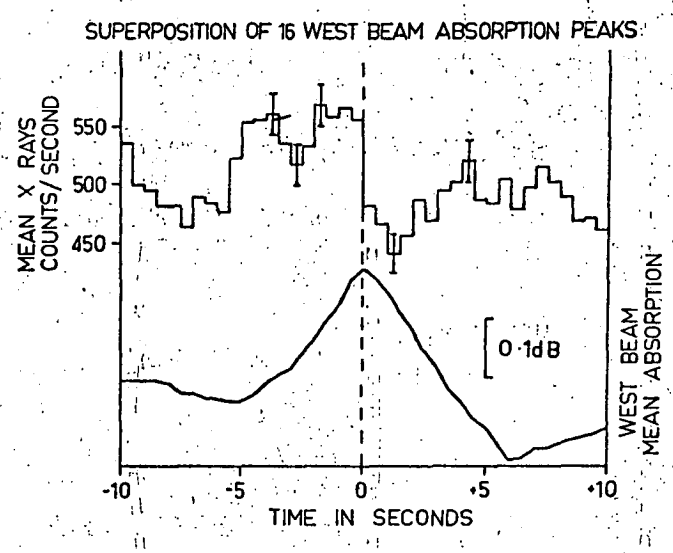

FIG. 3. DATA FROM THE FIRST EVENT OF 17 JANUARY 1969, REDUCED BY THE METHOD OF SUPERPOSED EPOCHS.
The error bars show 95 per cent confidence limits.

1420 U.T. CNA pulsations were observed from 1103 to 1110 U.T. and again from 1355 to 1408 U.T. when the riometers stopped working because of interference from a local transmitter. Thus good simultaneous data were obtained between 1357 and 1408 U.T.

The region near the zenith within the field of view of the photometer was initially occupied by a fragmented homogeneous band until 1400 U.T. when the band became a series of irregularly fading patches (condition a_4 in the International Auroral Atlas).

A sample of the photometer and riometer records obtained during this event is shown in Fig. 4. A degree of coherence between the photometer record and the three riometer records is evident. The data obtained between 1357 and 1408 U.T. were reduced by the method of superposed epochs (Fig. 5).

The lag of 2·5 sec between luminosity and absorption shown in Fig. 5 is similar to that observed for the mean X-ray pulsation of Fig. 3, but the mean absorption pulse shows a greater degree of asymmetry.

MODEL FOR THE ABSORPTION PULSE

In computing the absorption of cosmic noise as a function of time, $A(t)$, which will arise from a given height distribution in the ionization rate $q(t, h)$, difficulty arises from the fact that Equation (1) is nonlinear. The pulse in electron density, N, arising from a given

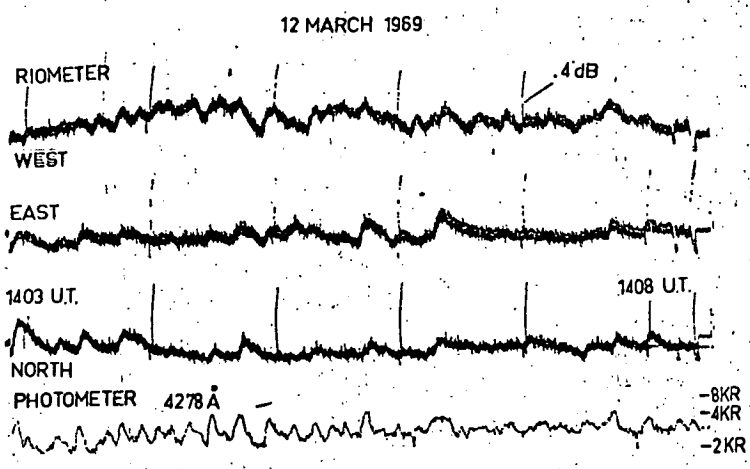

FIG. 4. A SECTION OF THE RECORD OF THE EVENT OF 12 MARCH 1969, SHOWING THE SIMULTANEOUS OCCURRENCE OF CNA PULSATIONS AND AURORAL LUMINOSITY PULSATIONS AT λ4278 Å.

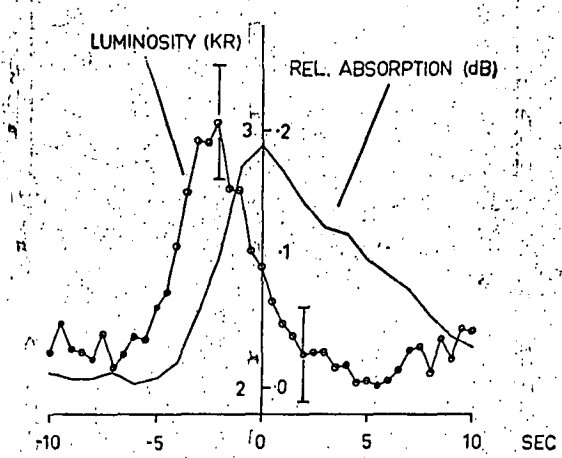

FIG. 5. DATA FROM THE EVENT OF 12 MARCH, 1969 REDUCED BY SUPERPOSING 18 NORTH BEAM ABSORPTION PULSES OF GREATER THAN 0·1 dB AMPLITUDE. The tails show the 95 per cent confidence limits of the mean in luminosity.

pulse in ionization will have a shape which depends on the magnitude of N itself and hence on the magnitude of q. Since q is a function of height as well as time the shape of the pulse in N will depend on height in the ionosphere. The ionospheric time-constant implicit in (1) and approximated to by (2) is a function of height.

Nevertheless, it is possible to integrate (1) numerically for any small range in height in the ionosphere for which q will be substantially constant. When the various pulses obtained in this way are summed over the whole of the relevant portion of the ionosphere a total pulse will be obtained which is independant of height. The component pulses will need to be weighted by the collision frequency during this summation in order to convert from electron density to absorption.

Assumptions

It was assumed that X-ray pulsations, auroral luminosity pulsations and CNA pulsations all have a common origin: viz, the impulsive precipitation of electrons from the magnetosphere into the upper atmosphere. This pulse of primary particles was taken as a gaussian function of time superimposed upon a steady background of precipitation. The ion pair production rate, q, can be expressed as

$$q(t, h) = Fq_0(h)\,[\mathrm{Exp}\,(-\tfrac{1}{2}bt^2) + B] \tag{3}$$

where F is the amplitude of the pulse, $q_0(h)$ is the height profile of ion pair production rate for a steady flux of primary electrons, t is the time measured from the precipitation peak in seconds, b controls the width of the pulse and B results from the steady background of precipitation.

In practice b was taken as unity and B as 0·5 which yields a pulse of 2·4 sec half maximum width, with a peak to valley ratio of 3:1. The model pulse of q then resembles the fast X-ray pulses observed experimentally.

Rees' (1963) curves were used for $q_0(h)$.

Using this function (3) for q, Equation (1) was integrated for $N(h, t)$ by the fourth order Runge Kutta process assuming

$$\alpha = 2 \times 10^{-7}\ \mathrm{cm^3\ sec^{-1}} \quad \text{and} \quad \lambda = 0.$$

The height h was varied in 2 km steps from 80 to 200 km and the integration of (1) carried out separately for each range of h.

Finally the absorption pulse was computed using a modified Appleton–Hartree formula for non-deviative absorption:

$$\begin{aligned} A(t) &= 2{\cdot}5C\int N(h, t)\nu(h)[(\omega \pm \omega_L)^2 + \nu(h)^2]^{-1}\,\mathrm{d}h \\ &\simeq 2{\cdot}5C\int N\nu\,\mathrm{d}h \qquad (\text{since } \omega \gg \omega_L) \end{aligned} \tag{4}$$

Where C is the Appleton–Hartree coefficient, ω is the operating frequency, ω_L is the electron gyro frequency and where

$$\nu = 1{\cdot}5 \times 10^6\ \mathrm{Exp}\ [-(h - 80)/6{\cdot}8]\ \mathrm{sec^{-1}}$$

was used for the collision frequency.

Since $\omega > 10\nu$, the disparity between (4) and the Sen-Wyller expression is less than 5 per cent (Sen-Wyller, 1960; Benson, 1964).

Because of the non-linearity of (1) the time lag and decay time of $N(t)$ and hence of $A(t)$ are functions of the amplitude of the pulse. For this reason the magnitude of F in (3) was adjusted so as to yield an absorption pulse of 0·8 dB in amplitude.

The luminosity pulse

Since the excited state of N_2^+ which gives rise to the λ4278 Å line is excited by collisions with primary and energetic secondary electrons and since the lifetime of this state is of the order of microseconds, we can assume that the pulse in luminosity at λ4278 Å is proportional to q, the ion pair production rate.

Thus the luminosity pulse $L(t)$ will be given by

$$L(t) = 2 \times 10^{-8}\int q(t, h)\,\mathrm{d}h\ (\text{Rayleighs})$$

where we have assumed that 1 photon at λ4278 Å is emitted for every fifty ion pairs formed (Omholt, 1968).

It should be noted that where a line is excited by low energy secondary or ambient electrons, the luminosity pulse will depend on N the electron density rather than q, and will show a similar lag and asymmetry to those predicted by this model for the absorption pulse.

Predictions of the model

The computations were performed for two exponential primary electron spectra with spectral indices of 8·3 keV and 3·0 keV respectively. The quantitative results are set out in Table 1 and the shapes of the pulses are shown in Fig. 6.

TABLE 1

Spectral index	8·3 keV	3·0 keV
Time lag of CNA pulse maximum	1·3 sec	0·8 sec
Value of luminosity maximum	17·6 kR	180 kR

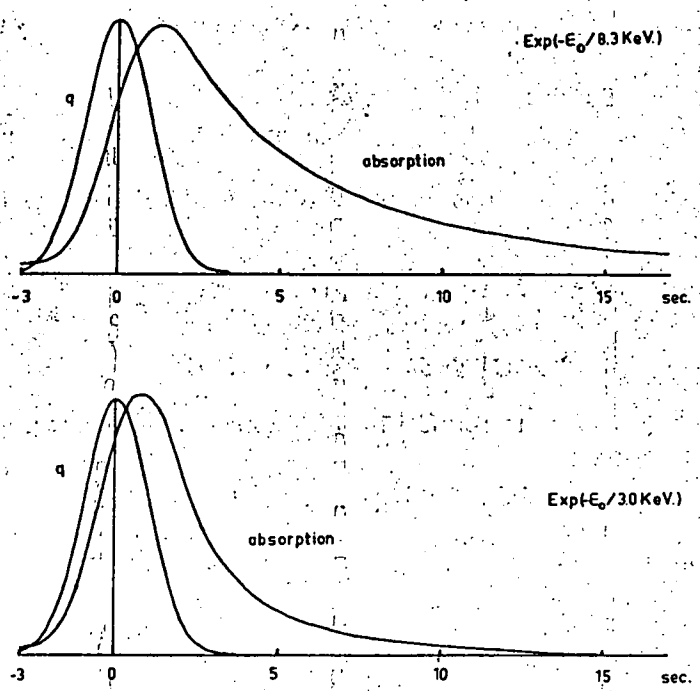

FIG. 6. THEORETICALLY DERIVED CURVES SHOWING THE PULSES IN ABSORPTION BROUGHT ABOUT BY A GAUSSIAN PULSE IN ION PAIR PRODUCTION RATE (q) FOR TWO EXPONENTIAL PRIMARY SPECTRA.

The harder of the two spectra yields an absorption pulse which is in good agreement with the observations as summarised in Figs. 3 and 5. This time lag and asymmetry are of the right order. For the 3·0 keV case, however, the luminosity maximum of 180 kR does not agree with observations since CNA pulsations were not observed at times of strong aurora. We can assume that any absorption pulsations which might result from pulsating primaries with this spectral index must be too small to be observable.

Limitation of the model

The model is intended as a first approximation and as such suffers from a number of limitations. The parameters α and λ are certainly not independent of height although this approximation may be adequate above 80 km. The ionizing effect of bremmstrahlung X-rays at lower altitudes has also been ignored. Although the number density of secondary electrons derived from this source is likely to be small, the weighting effect of the collision frequency may be sufficiently large to create a significant amount of absorption at heights of 40 or 50 km.

The time lag and asymmetry of the absorption pulse are quite strong functions of the background term B in (3). In a real situation the background of primary radiation may have a spectrum which differs considerably from that of the pulse. In addition the pulse itself may change in spectrum with time resulting in a changing height distribution in q. In either case a hardening or softening of the X-ray spectrum in the course of a pulse would be seen. Such an effect has been observed by Brown and Weir (1967). This model will not hold when this is the case since Equation (3) will not be an adequate description of the ionization pulse.

Finally, the area of the absorbing region is unknown and perhaps variable. However, the high degree of coherence between pulsations observed by different riometer beams indicates that most of the pulses are large compared with the separation of the antenna beams, i.e. of the order of 50 km or more across. (Compare East and West beams in Figs. 2 and 4.) Despite these limitations the model predicts CNA pulsations which closely resemble those observed experimentally. A more sophisticated analysis, taking many of the above points into account, will be the subject of a further paper.

CNA PULSATIONS AND MICROPULSATIONS

During all but one of the 55 CNA pulsation events observed at Macquarie Island with fast response riometers, marked micropulsation activity occurred. The activity was always of the Pil type characteristic of disturbed conditions in the auroral zone.

In March 1967 a micropulsation detector consisting of a large air-cored loop, a d.c. amplifier and an audio-frequency modulation system were used to record the vertical component of micropulsations on magnetic tape simultaneously with the output of a fast response riometer. On replaying the tape a sufficiently high time resolution could be obtained to enable a phase comparison to be made between CNA pulsations and micropulsations.

During the 11 days in which this system was operating only two CNA pulsation events were observed. A sample record from the event of 1 March is shown in Fig. 7. A marked degree of coherence between the two records is immediately obvious. The event of 5 March was similar in character.

The times between each CNA pulsation peak and the nearest peak in dZ/dt were measured and a histogram showing the distribution of these lags is shown in Fig. 8. The median lag was 1 sec.

Discussion

Micropulsations of the Pil type have previously been observed in association with auroral pulsations (Victor, 1965; Campbell and Rees, 1961) and with X-ray pulsations (McPherron *et al.*, 1968) and so must be related to impulsive electron precipitation in the early morning hours. It is hardly surprising that they should be associated with CNA

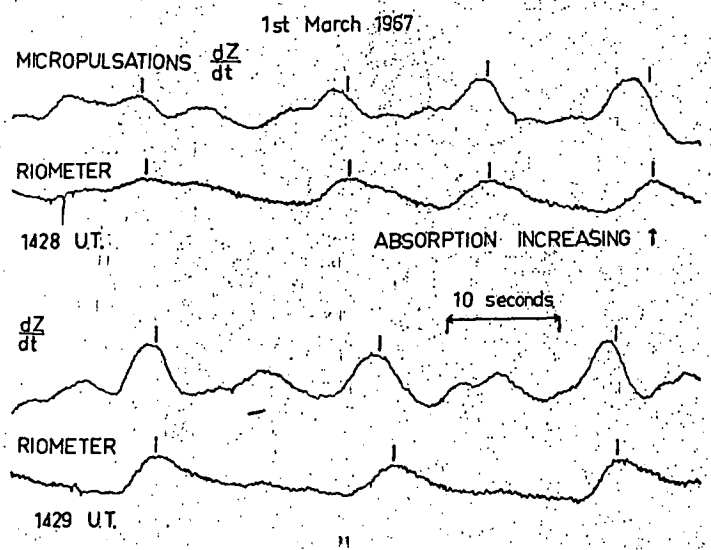

FIG. 7. A SECTION OF THE RECORD OF THE PULSATION EVENT OF 1 MARCH, 1967 SHOWING THE RELATIONSHIP BETWEEN MICROPULSATIONS dZ/dt AND SIMULTANEOUSLY OCCURRING CNA PULSATIONS.
The vertical bars indicate time simultaneity.

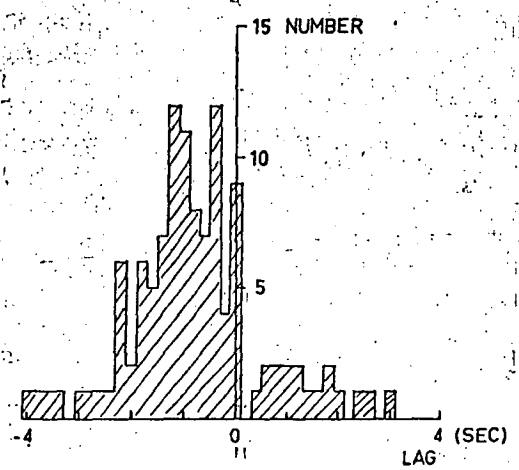

FIG. 8. DISTRIBUTION OF TIME LAGS BETWEEN PEAKS IN dZ/dt AND PEAKS IN ABSORPTION FOR THE EVENT OF 1 MARCH, 1967.
The lag was taken as negative when the dZ/dt peak preceded the absorption peak.

pulsations. Victor plotted a similar histogram to Fig. 8 showing phase shifts between luminosity pulsations and micropulsations. The median phase shift was zero and about half of the pulses had phase shifts between 1 and −1 sec. Figure 8 is consistent with Victor's result when the observed lag between CNA and luminosity is taken into account.

CONCLUSION

The cosmic noise absorption pulsations observed with a fast response riometer lag behind pulsations observed simultaneously with other instruments. This time lag and the time

asymmetry characteristic of the pulsations are, to a first approximation, consistent with the ionospheric rate Equation (1). Thus, high time resolution riometry makes possible the direct observation of the time delay which can occur in the auroral zone ionosphere between N, the electron density and q, the ion pair production rate.

An 'ionospheric time-constant' is measurable.

Acknowledgements—We wish to thank the Antarctic Division of the department of Supply for its support in this project.

We would also like to thank Professor G. R. A. Ellis for his helpful guidance and comment.

REFERENCES

ANSARI, Z. A. (1963). *Geophys. Inst. Univ. Alaska. Sci. Rept.* UAG-R138.
APPLETON, E. (1954). *J. atmos. terr. Phys.* **3**, 282.
BENSON, R. F. (1964). *Radio Science* **680**, 219.
BROWN, R. R. (1964). *Features of auroral energy spectrum inferred from observations of ionospheric absorption.* Kiruna Geophys. Observ. Scient. Rep.
BROWN, R. R. and WEIR, R. A. (1967). *J. geophys. Res.* **72**, 5357.
CAMPBELL, W. H. and REES, M. H. (1961). *J. geophys. Res.* **66**, 41.
EATHER, R. H. and JACKA, F. (1966). *Aust. J. Phys.* **19**, 215.
HOLT, O. and OMHOLT, A. (1962). *J. atmos. terr. Phys.* **24**, 467.
LITTLE, C. G. and LEINBACH, H. (1958). *Proc. I.R.E.* **46**, 334.
MCPHERRON, R. L., PARKES, G. K., CORONITI, F. V. and WARD, S. M. (1968). *J. geophys. Res.* **73**, 1697.
OMHOLT, A. (1968). *Annls. Geophys.* **24**, 215.
PILKINGTON, G. R, ANGER, C. D. and CLARK, T. A. (1968). *Planet. Space Sci.* **16**, 815.
REES, M. H. (1963). *Planet. Space Sci.* **11**, 1209.
REID, J. S. (1967). *Nature* **214**, 1321.
ROLDUGIN, V. K. (1967). *Geomag. and Aeron.* **7**, 454.
ROSENBERG, T. J., BJORDAL, J. and KVIFTE, G. J. (1967). *J. geophys. Res.* **72**, 3504.
SCOURFIELD, M. W. J., CRESSWELL, G. R., PILKINGTON, G. R., and PARSONS, N. R., (1970). *Planet. Space Sci.* **18**, 495.
SEN, H. K. and WYLLER, A. A. (1960) *J. geophys. Res.* **65**, 3931.
VICTOR, L. J. (1965). *J. geophys. Res.* **70**, 3123.
YUAN F. F. F. and JACKA F. (1969). *Nature* **222**, 653.

Appendix II

Abstract

The observation of impulsive phenomena by means of physically separated detectors of low resolution is a situation frequently met with in geophysics. After making certain simplifying assumptions, this paper explores a relationship between the normalized sample product moments (rather than correlation coefficients) obtaining between pairs of detectors and the spatial auto-correlation function of the impulses under observation. Further simplifying assumptions can be made which allow an "ellipse of concentration" of the impulse to be deduced from observations made with three detectors.

The technique is applied to fast cosmic noise absorption pulsations observed at Macquarie Island in 1969. The spatial patterns of precipitation giving rise to the pulsations are found to be elongated and inclined in azimuth to the auroral oval.

APPENDIX II

Random Sampling with Low Resolution Detectors

1. Introduction

Owing to the pulsating nature of many geophysical phenomena and the low spatial resolution of the instruments recording these phenomena, we frequently are faced with the situation in which a large number of observations are made with a small number of low-resolution detectors.

Observation of a single pulsation with a small number of spaced detectors reveals little information about the scale size of the pulsation. It is intuitively obvious that a larger number of observations should reveal a good deal more information about the size and shape of the pulsating regions.

Indeed, many workers have drawn conclusions about the mean size of individual pulsations from the correlation coefficients obtaining between time series recorded simultaneously with physically separated detectors. This had been done in an intuitive way without resort to any quantitative statistical model of the experimental situation.

An example is in the estimation of the scale size of fast bremmstrahlung x-ray pulsations observed with balloon-borne detectors (Barcus et al, 1966).

This paper is an attempt to place such estimations of spatial size, based on time series correlation, on a more secure statistical footing.

11. Assumptions of the Model

Let D_1, D_2, ... be measuring instruments whose sensitivities, P_1, P_2, ..., are functions of two spatial

variables, ξ , η

The variables, ξ, and η, may be angular displacements, or, for example, cartesian coordinates of position in the plane of the ionosphere.

Let $\mathcal{A} = \mathcal{A}(\xi, \eta, t)$ be the "event" distribution in which we are interested, and let $g_1(t)$, $g_2(t)$, ... be measurements of $\mathcal{A}(\xi, \eta, t)$ obtained at each of the detectors D_1, D_2, ... at time t. Then

$$g_i(t) = \int_{-\infty}^{\infty}\int_{-\infty}^{\infty} \mathcal{A}(\xi, \eta, t)\, P_i(\xi, \eta)\, d\xi\, d\eta \qquad (1)$$

Let us restrict ourselves to the case where $\mathcal{A}$ takes the form of a series of discrete pulses in such a way that the presence or absence of each pulse is clearly discernible on each of the records $g_i(t)$. Let us further assume that each of these pulses always has the same shape, $A(\xi, \eta)$, i.e. the same spatial distribution of (relative) intensity, and that coordinates of the centre of this distribution (x_j, y_j) and the amplitude of the j th pulse, h_j, are particular values of the random variables X, Y, and H. Thus the spatial distribution of the jth pulse is given by

$$\mathcal{A}(\xi, \eta, t) = h_j\, A(\xi - x_j, \eta - y_j)$$

The intensity of the j th pulse as measured with detector D_i will then be given by

$$g_{ij} = g_i(t_j) = \int_{-\infty}^{\infty}\int_{-\infty}^{\infty} h_j\, A(\xi - x_j, \eta - y_j)\, P_i(\xi, \eta)\, d\xi\, d\eta \qquad (2)$$

The right-hand side of (2) is the "cross-correlation" of the functions A and P. Let the cross-correlation function $r(x, y)$ of two functions $p(x, y)$ and $q(x, y)$ be written

$$r(x,y) = p * q \Big|_{x,y}$$

i.e., by definition

$$p * q \Big|_{x,y} = \int_{-\infty}^{\infty} \int_{-\infty}^{\infty} p(\xi - x, \eta - y)\, q(\xi, \eta)\, d\xi\, d\eta$$

Then

$$g_{ij} = (h_j A) * P_i \Big|_{x_j, y_j}$$

$$= h_j \left(A * P_i \Big|_{x_j, y_j} \right)$$

which will be written

$$g_{ij} = h_j A * P_i \Big|_{x_j, y_j}$$

For greater generality let us include further random variables, B_i, each with zero mean, associated with each of the detectors D_i and representing any randomness which may be present in the data collection process. For example, where the pulsations are distributions of bremmstrahlung x-ray intensity, the B_i describe the photon counting statistics. Thus (3) becomes

$$g_{ij} = h_j A * P_i \Big|_{x_j, y_j} + b_{ij}$$

where b_{ij} is the particular value that the random variable B_i takes for the jth pulse.

Our problem is to relate the pulse shape A to the observations g_{ij} after making certain general assumptions about the random variables X, Y, H, and B_i.

These assumptions will be as follows:

i. For any pair of detectors D_i, D_j, the random variables X, Y, H, B_i, B_j, have a probability function, ϕ, defined over the space R_5 with a frequency function, f, which is continuous everywhere in R_5.

ii. All the random variables are statistically independent of one another.

iii. The functions $A(\xi, \eta)$, $P_i(\xi, \eta)$ are only non-zero within a certain finite range of ξ and η, i.e., there exists a number, K, such that

$$A(\xi,\eta) = P(\xi,\eta) = 0 \quad \text{if } |\xi| > K, \text{or } |\eta| > K$$

Then

$$A * P_i\Big|_{x,y} = 0 \quad \text{if } |x| > 2K \text{ or } |y| > 2K$$

iv. The frequency functions of X and Y, f_x and f_y are constant over the region viewed by the detectors, i.e., for $|x_i| < 2K$ and $|y_i| < 2K$. This will be true only if the region in which the pulses are occuring is larger than the region viewed by the detectors.

v. Any pair of observations, g_{ik}, g_{jk}, made with the detectors D_i, D_j, is equivalent to making a random selection of the point $(x_k, y_k, h_k, b_{ik}, b_{jk})$ from the space R_5 and then computing g_{ik}, g_{jk} from the coordinates using (4) above.

In the experimental situation we only know the values of the functions g_{ik}, g_{jk}; the calculations (4) are effected by the detecting instruments. Thus g_{ik} and g_{jk} can be regarded as sample characteristics of the sample $(x_k, y_k, h_k, b_{ik}, b_{jk})$ as defined by (4) above. In other words, each of the g_{ik} is a particular value of the random variable G, which is a function of the other random variables as defined by

$$G_i = HQ_i(X,Y) + B_i \qquad (5)$$

where

$$Q_i = A * P\Big|_{X,Y}$$

vi. The integral $\int_{R_5} G_i G_j \, d\Phi$ is finite. This will be true

if H and the B_i have finite 1st, 2nd, 3rd and 4th moment, and if the various moments of $A * P_i|_{X,Y}$ also exist.

III. The Product Moments

In an experimental situation, the data we have available consists of our knowledge of the detector characteristics and a sample of n sets of readings of pulse height obtained from m detectors, viz., we know g_{ij}, where $i = 1, 2 \ldots m$, $j = 1, 2 \ldots n$. We wish to utilise these mn readings to provide an estimate of some of the properties of the spatial distribution $A(\xi, \eta)$.

Consider the population parameter γ_{ij} defined by

$$\gamma_{ij} = E(G_i G_j) = \int_{R_S} G_i G_j \, d\phi \qquad (6)$$

γ_{ij} is the population product moment of the random variables G_i and G_j.

Consider the sample characteristic c_{ij} defined by

$$c_{ij} = \frac{1}{n} \sum_{k=1}^{n} g_{ik} g_{jk} \qquad (7)$$

c_{ij} is the product moment of the sample of n pairs of readings g_{ik}, g_{jk} obtained from D_i, D_j.

Then

$$\lim_{n \to \infty} c_{ij} = \gamma_{ij} \qquad \text{a.s.}$$

by the strong law of large numbers (Breiman, P. 52).

Here "a. s." means "almost surely", or "with unit probability".

IV. Normalised Product Moments

Let

$$C_{ij} = c_{ij} / \sqrt{c_{ii} c_{jj}}$$

then

$$\lim_{n \to \infty} C_{ij} = \gamma_{ij} / \sqrt{\gamma_{ii} \gamma_{jj}} \qquad \text{a.s.}$$

providing none of the factors in the denominators are zero.

let $\Gamma_{ij} = \gamma_{ij} / \sqrt{\gamma_{ii}\,\gamma_{jj}}$

The normalised sample product moment tends to the normalised population product moment, Γ_{ij}, as the number in the sample tends to infinity.

C_{ij} is a consistent estimator of Γ_{ij}.

An expression will now be derived for the population product moments in terms of the event and detector distributions A and P.

$$\begin{aligned}\gamma_{ij} &= E(G_i G_j) \\ &= E\{(HQ_i + B_i)(HQ_j + B_j)\} \\ &= E(H^2)E(Q_i Q_j) + E(B_i B_j)\end{aligned}$$

since

$$E(B_i) = E(B_j) = 0$$

Now

$$E(Q_i Q_j) = \int_{-\infty}^{\infty}\int_{-\infty}^{\infty} Q_i Q_j f_x f_y \, dX\, dY$$

$$= \int_{-2K}^{2K}\int_{-2K}^{2K} Q_i Q_j f_x f_y \, dX\, dY$$

by condition (iii).

Hence

$$E(Q_i Q_j) = f_x f_y \int_{-2K}^{2K}\int_{-2K}^{2K} Q_i Q_j \, dX\, dY$$

by condition (iv)

$$= f_x f_y \int_{-\infty}^{\infty}\int_{-\infty}^{\infty} Q_i Q_j \, dX\, dY$$

by condition (iii)

Now $E(B_i B_j) = 0$ if $i \neq j$

Let $E(B_i^2) = \sigma_i^2$

Hence, when $i \neq j$,

$$\gamma_{ij} = E(H^2) f_x f_y \int_{-\infty}^{\infty}\int_{-\infty}^{\infty} Q_i Q_j \, dX\, dY \qquad (10)$$

and

$$\gamma_{ii} = E(H^2) f_x f_y \int_{-\infty}^{\infty}\int_{-\infty}^{\infty} Q_i^2 \, dX\, dY + \sigma_i^2 \qquad (11)$$

The existence of the terms σ_i^2, and σ_j^2 in the righthand side of (9) creates some difficulties. We therefore will define "adjusted normalised product moments" C_{ij}^*, Γ_{ij}^*, where

$$C_{ij}^* = c_{ij} \Big/ \sqrt{(c_{ii} - \sigma_i^2)(c_{jj} - \sigma_j^2)} \qquad (12)$$

and

$$\Gamma_{ij}^* = \gamma_{ij} \Big/ \sqrt{(\gamma_{ii} - \sigma_i^2)(c_{jj} - \sigma_j^2)} \qquad (13)$$

Once again we have with unit probability

$$\lim_{n \to \infty} C_{ij}^* = \Gamma_{ij}^*$$

providing that the factors in the denominators are non-zero.

In most practical cases, σ_i and σ_j will either be known to be sufficiently small to ignore or they can be computed in advance from a knowledge of the bandwidth and output time-constant or similar parameters of the detecting instruments.

Substituting (10) and (11) in (13) yields

$$\Gamma_{ij}^* = \int_{-\infty}^{\infty}\int_{-\infty}^{\infty} Q_i Q_j \, dX \, dY \Big/ \sqrt{\int_{-\infty}^{\infty}\int_{-\infty}^{\infty} Q_i^2 \, dX \, dY \cdot \int_{-\infty}^{\infty}\int_{-\infty}^{\infty} Q_j^2 \, dX \, dY} \qquad (14)$$

It should be noted that if the sample correlation coefficients were to be used instead of simply the product moments, they would not lead to a function like Γ_{ij}^*, which is independent of f_x, f_y, $E(H)$, and $E(H^2)$. This is because the sample means $\sum g_{ij}/n$ are estimators of population characteristics which are linear functions of f_x and f_y.

These factors would no longer cancel in the expressions for the correlation coefficients since the means appear as second degree terms in these expressions. Similarly $(E(H))^2$ appears in these terms rather than $E(H^2)$.

We can use the properties of the convolution operation which is associative and commutative to simplify (14) still further. The cross-correlation and convolution operations are related as follows:

$$p * q\big|_{x,y} = \bar{p} \odot q\big|_{x,y}$$

where, by definition, $\bar{p}(\xi, \eta) = p(-\xi, -\eta)$

The expression $p \odot q$ means "the convolution of p with q". By definition

$$p \odot q\big|_{x,y} = \int_{-\infty}^{\infty}\int_{-\infty}^{\infty} p(\xi,\eta)\, q(x-\xi, y-\eta)\, d\xi\, d\eta$$

$$= q \odot p\big|_{x,y}$$

It can easily be shown that

$$(p \odot q) \odot r = p \odot (q \odot r)$$

and if $q'(\xi, \eta) = q(\xi - x_0, \eta - y_0)$

then $p \odot q'\big|_{x,y} = p \odot q\big|_{x-x_0,\, y-y_0}$

(see Bracewell, 1965, for a discussion of convolution and cross-correlation).

Now

$$\int_{-\infty}^{\infty}\int_{-\infty}^{\infty} Q_i Q_j\, dX\, dY = \int_{-\infty}^{\infty}\int_{-\infty}^{\infty} A * P_i\big|_{X,Y} \cdot A * P_j\big|_{X,Y}\, dX\, dY$$

Let us represent the spatial sensitivity functions of the detectors, $P_i(\xi, \eta)$, in terms of the coordinates (x_i, y_i) of the centres of the fields of view of each of the detectors, i.e., let

$$P_i(\xi, \eta) = p_i(\xi - x_i, \eta - y_i)$$

Then

$$\int_{-\infty}^{\infty}\int_{-\infty}^{\infty} Q_i Q_j \, dX\,dY = \int_{-\infty}^{\infty}\int_{-\infty}^{\infty} (A * p_i)\big|_{X-x_i,\,Y-y_i} \cdot (A * p_j)\big|_{X-x_j,\,Y-y_j} \, dX\,dY$$

$$= \int_{-\infty}^{\infty}\int_{-\infty}^{\infty} (A * p_i)\big|_{x',y'} \cdot (A * p_j)\big|_{x'-(x_j-x_i),\,y'-(y_j-y_i)} \, dx'\,dy'$$

$$= (A * p_i) * (A * p_j)\big|_{\Delta x,\,\Delta y}$$

where $x' = X - x_i$, $y' = Y - y_i$

and $\Delta x = x_j - x_i$, $\Delta y = y_j - y_i$.

Thus

$$\int_{-\infty}^{\infty}\int_{-\infty}^{\infty} Q_i Q_j \, dX\,dY = (A^- \odot p_i)^- \odot (A^- \odot p_j)\big|_{\Delta x,\,\Delta y}$$

$$= (A \odot p_i^-) \odot (A^- \odot p_j)\big|_{\Delta x,\,\Delta y}$$

$$= (A \odot A^-) \odot (p_i^- \odot p_j)\big|_{\Delta x,\,\Delta y}$$

$$= (A^- \odot A)^- \odot (p_i^- \odot p_j\big|_{\Delta x,\,\Delta y}$$

$$= (A * A) * (p_i * p_j)\big|_{\Delta x,\,\Delta y}$$

and

$$\Gamma_{ij}^{*} = \frac{(A * A) * (p_i * p_j)\big|_{\Delta x,\,\Delta y}}{\sqrt{(A * A) * (p_i * p_i)\big|_{0,0} \cdot (A * A) * (p_j * p_j)\big|_{0,0}}}$$

When $p_i = p_j = p$ (16)

i.e. when the detector fields have the same shape and orientation but different centres, (15) becomes

$$\Gamma_{ij}^{*} = \frac{(A * A) * (p * p)\big|_{\Delta x, \Delta y}}{(A * A) * (p * p)\big|_{0,0}} \qquad (17)$$

ie.

$$C_{ij}^{*} = \frac{\alpha_A * \alpha_p\big|_{\Delta x, \Delta y}}{\alpha_A * \alpha_p\big|_{0,0}} \qquad (18)$$

where α_A is the autocorrelation function of the event distribution, and α_p is the autocorrelation function of the detector field pattern.

The sample characteristics, C_{ij}^{*}, are each estimates of one value of the mormalised cross-correlation function $\alpha_A * \alpha_p$ viz, the value that this function has at the point $(\Delta x, \Delta y)$, where $(\Delta x, \Delta y)$ is the displacement of one detector field with respect to the other. Each pair of detectors will yield one value of this function providing the $(\Delta x, \Delta y)$ for the pair is unique. If there are sufficient detectors of sufficiently high resolution, the function $\alpha_A * \alpha_p$ can be constructed graphically and then corrected for the smoothing effect of α_p (Bracewell, 1956) to obtain a set of sample points for α_A. If A is assumed to be band-limited, and an even function of (x, y), A itself can be reconstructed (Bracewell, 1965, Ch. 10). If there are sufficient detectors for this to be possible, it also may be possible to reconstruct each individual pulse $h_j A(x - x_j, y - y_j)$ directly from each set of observations g_{ij}. Reconstruction after computing $\alpha_A * \alpha_p$ may still be favoured, however, for the following reasons -

i. Phase (i.e., position) information has been conveniently removed.

ii. The effects of instrumental noise have been statistically reduced.

iii. In general, there will be $\frac{1}{2} m (m-1)$ data points available for reconstruction of α_A compared with data from only m detectors available for reconstruction of A itself.

This paper is intended to apply to situations where only a small number of low resolution detectors are in use, and any total reconstruction of A or α_A is out of the question. Here, the best that can be done is to make assumptions about the form of distribution $A(\xi,\eta)$ and solve the equations (18) for the model parameters.

V. A Gaussian Model

Consider the functions:

$$P(x,y) = \exp(-X' \mathbf{P} X)$$

$$Q(x,y) = \exp(-X' \mathbf{Q} X)$$

where $$\mathbf{X} = \begin{Bmatrix} x \\ y \end{Bmatrix}$$

and $\mathbf{P}$ and $\mathbf{Q}$ are two by two symmetric definite positive matrices. The surfaces corresponding to P and Q will be hills above the (x, y) plane of elliptical contour and gaussian section. It can readily be shown that the cross-correlation of P and Q is given by

$$P * Q\big|_{x,y} = \frac{\pi \exp(-X' \mathbf{R} X)}{\sqrt{|\mathbf{P} + \mathbf{Q}|}}$$

where $$\mathbf{R}^{-1} = \mathbf{P}^{-1} + \mathbf{Q}^{-1}$$

Thus $$P * P\big|_{x,y} = \frac{\pi \exp(-\frac{1}{2} X \mathbf{P} X)}{\sqrt{|2\mathbf{P}|}} \qquad (20)$$

Let us make the assumption that the event distribution is of the form (19). Suppose the detector field patterns also are of this form, i.e.,

$$A(x,y) = \exp(-\mathbf{X}'\mathbf{A}\mathbf{X})$$

$$p(x,y) = \exp(-\mathbf{X}'\mathbf{P}\mathbf{X})$$

Then

$$(A * A) * (p * p)\Big|_{x,y} = \frac{\pi^3 \cdot \exp\left(-\frac{1}{2}\mathbf{X}'\mathbf{R}\mathbf{X}\right)}{\sqrt{|2\mathbf{A}|\,|2\mathbf{P}|\,\left|\frac{1}{2}\mathbf{A} + \frac{1}{2}\mathbf{P}\right|}}$$

and

$$(A * A) * (p * p)\Big|_{0,0} = \pi^3 \Big/ \sqrt{|2\mathbf{A}|\,|2\mathbf{P}|\,\left|\frac{1}{2}\mathbf{A} + \frac{1}{2}\mathbf{P}\right|}$$

where

$$\mathbf{R}^{-1} = \mathbf{A}^{-1} + \mathbf{P}^{-1} \qquad (21)$$

Substitution in (17)

$$C_{ij}^{*} = \exp\left(-\tfrac{1}{2}\mathbf{X}_{ij}'\mathbf{R}\mathbf{X}_{ij}\right)$$

where $\mathbf{X}_{ij} = \begin{Bmatrix} x_i - x_j \\ y_i - y_j \end{Bmatrix} = \begin{Bmatrix} \Delta x \\ \Delta y \end{Bmatrix}$

i.e. $$-2 \log C_{ij}^{*} = \Delta x^2 r_{11} + \Delta y^2 r_{22} + 2\Delta x \Delta y\, r_{12} \qquad (22)$$

where r_{11}, r_{22} and r_{12} are the elements of $\mathbf{R}$.

There will be one equation (22) for each pair of detectors D_i, D_j. Three such equations will be sufficient to solve for the elements of $\mathbf{R}$. The elements of $\mathbf{A}$ can then be obtained from (21). Should there be more than three equations (22), the set is overdetermined. Different sets of solutions can then be obtained by solving all the different triplets of equations. The consistency of different solutions obtained in this way is a measure of the degree to which the initial assumptions are justified, in particular the assumptions that $\mathbf{A}$ was of the form (19), and that the "event position" probability density functions f_x and f_y are constant over the field of view of the detectors.

Strictly speaking, a gaussian form for A and the detector patterns does not satisfy condition (iii) that the non-zero domain of A and P_i is bounded. This implies that errors will be introduced when f_x and f_y are taken outside the integral in the expression for $E(G_i G_j)$. Gaussian functions tend to zero rapidly, however, and providing f_x and f_y are constant over a sufficiently large domain, the errors introduced in this way will be negligible.

VI. Application to Fast Response Riometer Data

Unfortunately, the four riometer antenna patterns used on Macquarie Is. in 1969 did not satisfy condition (16). Their shapes were similar, being roughly elliptical in contour, but two were oriented North-South and two were oriented East-West (Fig. II.1). Thus, for any triplet of antennas, only one pair will satisfy (16). We will make the same assumptions as in the previous section -- that the event patterns and the antenna patterns are gaussian quadratic forms, but we must substitute these in equation (15) rather than in (17).

Let the antenna patterns relative to their centres $P_1(x, y)$, $P_2(x, y)$, $P_3(x, y)$ be given by

$$P_i = \exp(-X' \mathbf{P} X)$$

where

$$X = \begin{Bmatrix} x \\ y \end{Bmatrix}$$

Since two out of three of the antennas must have the same orientation, let

$$\mathbf{P}_1 = \mathbf{P}_3$$

Let the event autocorrelation function be given by

$$A * A = \exp(-\mathbf{X}' \mathbf{A} \mathbf{X})$$

Then $$C_{ij}^{*} = N_{ij} \exp(-\mathbf{X}'_{ij} \mathbf{S} \mathbf{X}_{ij}) \quad (23)$$

where $$N_{ij} = \frac{\left(|\mathbf{A} + \mathbf{R}_{ii}| \cdot |2\mathbf{P}_i| \cdot |\mathbf{A} + \mathbf{R}_{jj}| \cdot |2\mathbf{P}_j| \right)^{\frac{1}{4}}}{\left(|\mathbf{A} + \mathbf{R}_{ij}| \cdot |\mathbf{P}_i + \mathbf{P}_j| \right)^{\frac{1}{2}}} \quad (24)$$

$$\mathbf{S}_{ij}^{-1} = \mathbf{R}_{ij}^{-1} + \mathbf{A}^{-1} \quad (25)$$

and $$\mathbf{X}_{ij} = \begin{Bmatrix} x_i - x_j \\ y_i - y_j \end{Bmatrix}$$

where (x_i, y_i) are the coordinates of the centre of the pattern of the ith antenna, and

$$\mathbf{R}_{ij}^{-1} = \mathbf{P}_i^{-1} + \mathbf{P}_j^{-1}$$

Thus $$\mathbf{R}_{ii} = \tfrac{1}{2} \mathbf{P}_i$$

Since $$\mathbf{P}_1 = \mathbf{P}_3$$

$$\mathbf{R}_{13} = \tfrac{1}{2} \mathbf{P}_1$$

Hence $$N_{13} = 1 ,$$

and $$N_{12} = N_{13} = N \text{ say} ,$$

and $$\mathbf{S}_{12} = \mathbf{S}_{23} .$$

Let $$\mathbf{S}_{12} = \begin{Bmatrix} p & r \\ r & q \end{Bmatrix} \quad (26)$$

and

$$S_{13} = \begin{Bmatrix} s & u \\ u & t \end{Bmatrix} \tag{27}$$

and let us normalise all the distances so that the distance from the centre of the group of four antenna patterns to the centre of each antenna is unity. If we take North and East as the positive directions of x and y in a cartesian coordinate system and let P_1, P_2, and P_3 describe the patterns of the North, East, and South antennas respectively, we have

$$X_{12} = \begin{Bmatrix} 1 \\ -1 \end{Bmatrix} \tag{28}$$

$$X_{23} = \begin{Bmatrix} 1 \\ 1 \end{Bmatrix} \tag{29}$$

$$X_{31} = \begin{Bmatrix} 0 \\ 2 \end{Bmatrix} \tag{30}$$

Substituting (26) through (30) into (23) yields:

$$p + q + 2r = -\log C^*_{12} + \log N \tag{31}$$

$$p + q - 2r = -\log C^*_{23} + \log N \tag{32}$$

$$4t = -\log C^*_{31} \tag{33}$$

From (25) we have the matrix equation

$$S_{12}^{-1} + S_{23}^{-1} = R_{12}^{-1} + R_{23}^{-1} \tag{34}$$

Equation (34) represents a further three equations and we have six equations for the six unknowns, p, q, r, s, t, and u. Equations (31), (32), and (33) can be solved for r and t immediately. If we forget about N for the moment (i. e., set N = 1), p and q also can be obtained.

S_{12} can now be expressed as a function of p:

$$S_{12}(p) = \begin{Bmatrix} p & r \\ r & H-p \end{Bmatrix}$$

$$\text{where} \quad H = p + q = \frac{1}{2}\left(\log N^2 - \log C_{12}^* C_{13}^*\right)$$

For any given value of p, (34) can be solved for s, t, and u. Thus by trial and error a value of p can be found yielding a value of t in (34) which satisfies equation (33). The elements of $\mathbb{A}$ can then be found from (25) and substituted in (24) to obtain N. The equations (31) through (34) can be solved again with this new value of N and the process repeated until successive solutions differ by less than a predetermined tolerance.

In practice, a simple computor programme can be written which includes procedures for extracting determinants, inverting two by two symmetric matrices, and for finding the zeros of functions by an iterative method.

If the event distribution $A(x, y)$ is also assumed to be a gaussian quadratic form, its form matrix elements are double those of the event autocorrelation $A * A\big|_{x,y}$ (See equation (20).)

$$\text{If} \quad A(x,y) = A_0 \exp\left(-X' \begin{Bmatrix} a & c \\ c & b \end{Bmatrix} X\right)$$

$$= A_0 \exp\left[-(ax^2 + by^2 + 2cxy)\right]$$

then the contours of points of constant cosmic noise absorption are ellipses. Let the ellipse for which $A = A_0 e^{-1}$

be termed the "ellipse of concentration". This ellipse has the equation

$$a x^2 + b y^2 + 2 c x y = 1$$

Putting $x = r \cos\theta$, $y = r \sin\theta$, we have

$$r^2 = 1 / (a \cos^2\theta + b \sin^2\theta + 2 c \sin\theta \cos\theta)$$

which can be written

$$r^2 = 2 / (a + b + R \cos (2\theta - \delta))$$

where $R = \sqrt{(a-b)^2 + 4c^2}$

and $\sin\delta = 2c / R$

The semi-minor and smi-major axes of the ellipse of concentration are given by

$$r^2 = 2 / (a + b \pm R)$$

corresponding to values of θ of $\frac{1}{2}\delta \pm n\pi$ and $\frac{1}{2}\delta \pm (2n+1)\pi$.

VII. Experimental Results

This type of analysis was applied to two fast c.n.a. pulsation events: Those of 13 February 1969, and 14 March, 1969. The normalised product moments, C_{ij}, were not corrected for detector randomness, i.e., the σ_i were taken as zero. The antenna sensitivity patterns and the event distribution patterns are referred to a height of 100km. No attempt has been made to allow for the finite thickness of the absorbing region, nor for the different angles between antenna beams and the local geomagnetic field.

Values of the semi-minor and semi-major axes of the antenna patterns were chosen so that the 3dB contour ellipse would fit, as closely as possible, the computed 3dB contour of the antennas as shown in Fig. II.1. The smi-minor axis, semi-major axis, and zenith distance of the centre of each antenna's ellipsoid of concentration projected on an horizontal plane at 100km. height

were taken as 43km., 84km. and 63km. respectively. For the event of 13 February, 77 pulse heights were used to compute the C_{ij}, and for the 14 March event, 80 pulse heights were used. The results are set out in Table 1..

The four different ellipses of concentration of the four event distributions computed for the 13 February event are reasonably consistent in size, shape, and orientation. Those for the event of 14 March are not quite as good, particularly with regard to the orientation. The salient features are as follow -

TABLE 1

Antenna designations			Product moments			Absorption ellipse of concentration		
						Semi-minor axis	Semi-major axis	Azimuth (major axis)
P_1	P_2	P_3	C_{12}	C_{23}	C_{31}			
(a) Event of 14 March 1969 (1843-1913 U. T.)								
N	W	S	.641	.929	.622	68km	237km	15 deg. W of N
N	E	S	.705	.773	.622	78 "	126 "	41 " E of N
W	S	E	.929	.773	.729	106 "	229 "	21 " W of N
W	N	E	.641	.705	.729	49 "	155 "	57 " W of N (geographic)
(b) Event of 13 February 1969 (2219-2245 U. T.)								
N	W	S	.741	.952	.675	94km	287km	17 deg. W of N
N	E	S	.926	.769	.675	104 "	225 "	16 " - "
W	S	E	.952	.769	.812	101 "	325 "	31 " "
W	N	E	.741	.926	.812	89 "	290 "	37 " " (geographic)

i. The event ellipses of concentration are much larger than those of the antennas. Indeed, in five out of eight cases, the minor axis of the event ellipse is larger than the major axis of the antenna ellipse.

ii. The event ellipses are two to three times as long as they are wide.

iii. For the 13 February event, the event ellipse is inclined at an angle of about 25 deg. West of geographic North. This computed inclination is brought about by high values of C_{ij} obtaining between the North and East, and between the South and West riometer records. The azimuth of the L-shell passing through Macquarie Is. is 73 deg. West of North (Kilfoyle and Jacka, 1968), and the azimuth of the contours of the auroral oval for $K_p = 3$ varies between about 73 deg. West of North at 1800 U. T. and 55 deg. West of North at 2200 U. T. (Bond and Payne, 1970). That the pattern of precipitation observed as c. n. a. pulsations should be elongated is hardly surprising, but their inclination to the directions of the L-shell ($>30°$) and of the auroral oval is a matter of some interest, and may have significance in studies of the magnetosphere and of precipitation mechanisms.

Sufficient time was not available to subject other c. n. a. pulsation events to this type of analysis. However, visual examination of the records of the other events indicates that the degree of correlation between pulsations observed with different antennas is unlikely to be less than for the events analysed. The high degree of correlation existing between the North and East, and South and West, records, associated with the corresponding high values of C_{ij} in Table 1, also is readily discernible by visual inspection.

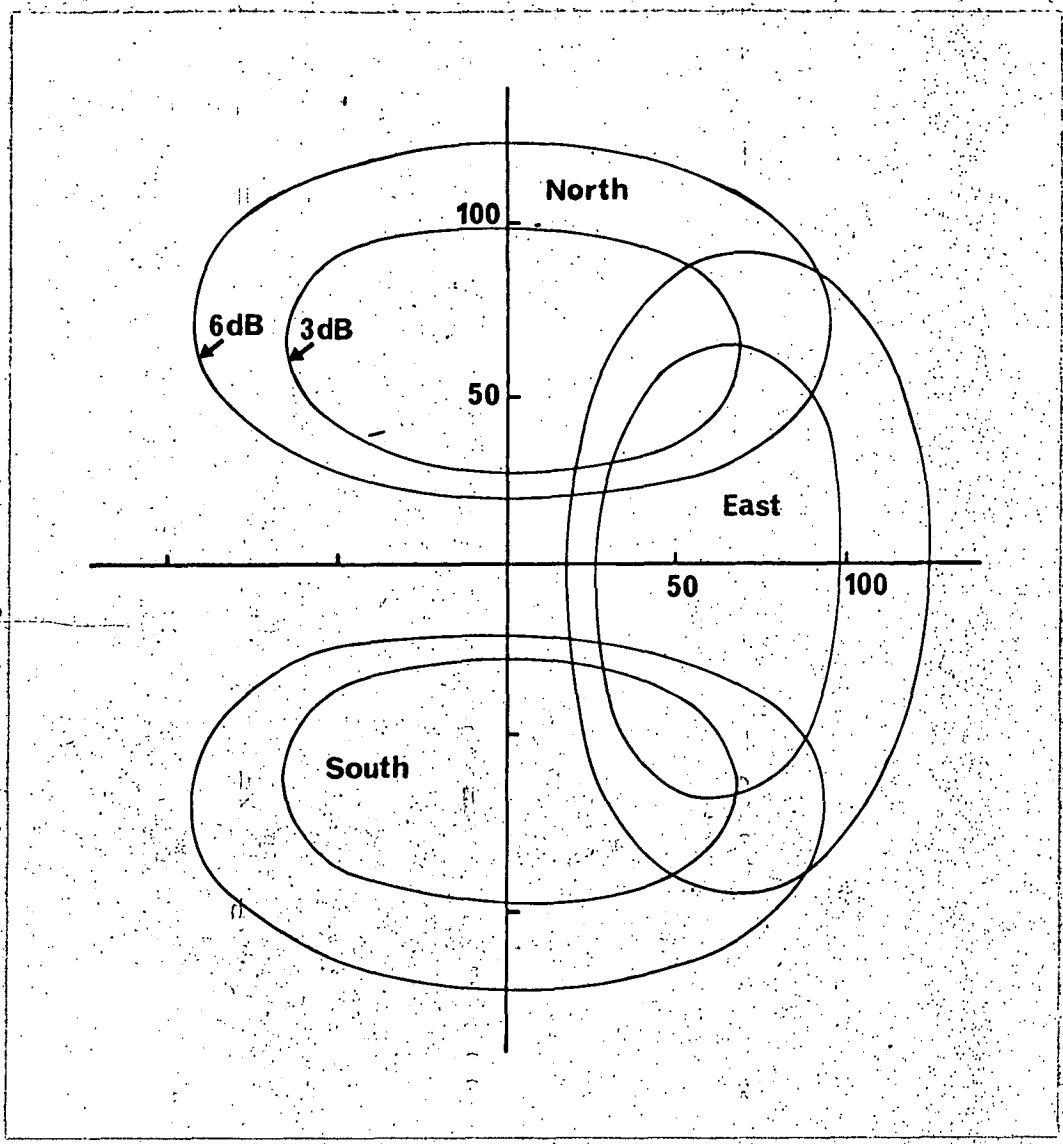

Fig. II.1

3 dB. and 6 dB. contours as they intersect the 100 km level for three of the four fast response riometer antenna beams operated at Macquarie Island in 1969. The fourth beam pattern was similar but is omitted for simplicity and because these three beam orientations illustrate the discussion set out in Section VI.

References

Barcus, J. R., R. R. Brown and T. J. Rosenberg (1966). J. Geophys. Res. 71, 125.

Bond, F. R. and R. L. Payne (1971). Technical Note 7. Antarctic Division, Dept. of Supply, Melbourne, Vic.

Bracewell, R. N.(1956). Aust. J. Phys 9, 298.

Bracewell, R. N.(1965)."The Fourier Transform and its Applications". McGraw-Hill, N.Y.

Breiman, L.(1968)."Probability". Addison Wesley, N.Y.

Kilfoyle, B. P. and F. Jacka (1968). Nature 220, 773.

Appendix III

Electronic Techniques

III. 1. Theory.

The root mean square fluctuation in detector voltage, ΔV, about its mean value, V, for a receiver measuring white noise is given by

$$\Delta V = K V (\Delta f \tau)^{-\frac{1}{2}}$$

providing $\Delta V << V$. (1)

Here, Δf is the band width of the receiver, τ is the detector time constant and K is a constant of proportionality. Similar relationships hold for power and for measured temperature etc. K is approximately unity and depends on the detector characteristic. Equation (1) is based on a discussion by Machin, Ryle and Vonberg (1952) and quoted by Little and Leinbach (1958) in their original description of the riometer.

It is immediately obvious from (1) that the frequency resolution and time resolution of such a noise measuring device can only be improved at the expense of each other unless the bandwidth, Δf, is increased.

The resolution of a standard 30 MHz riometer is about 3 seconds in time and .1 dB in amplitude for a receiver bandwidth of 20 KHz. Thus for the same amplitude resolution the time resolution can be reduced to .05 seconds by increasing Δf to 1.2 MHz.

The minimum reader, which controls the time constant for rising signals needs to be removed, of course.

The sluggish response of the servo noise diode due to the time taken to heat the filament is an obstacle but this can be removed and the riometer operated without any concern for its long term stability. Edwards (private communication) has pointed out that, in fact, the servo diode can be retained and a broad band riometer operated as both a conventional and as a fast response instrument. The conventional record can be obtained by recording the noise diode current in the usual way, while the fast component can be taken from the difference signal which appears at the output of the phase sensitive detector.

This method was not used although the theoretical importance of the background of absorption may make such a system worth trying in the future.

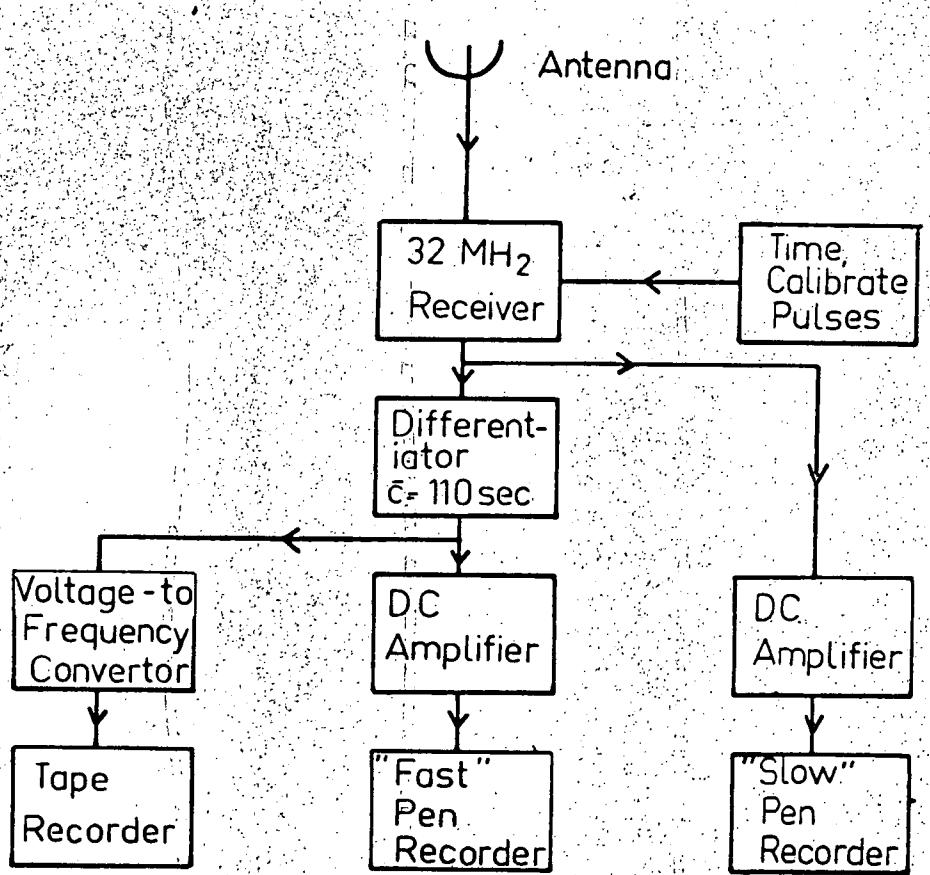

Fig. III.1

Fast response riometer - block diagram.

III. 2. General Description

A block diagram of one of the four fast response riometers used in 1969 is shown in Fig. III.1. The equipment was, basically, a low noise wide band receiver at 32MHz. connected to an antenna and to recording equipment. There was no servo noise diode feedback loop as in a conventional riometer nor was there a minimum reader to protect the record against impulsive interference.

The output from the detector was fed to a DC amplifier via a simple RC integrator with a time-constant of two minutes. This served to eliminate the sidereal cosmic noise variation and the slow background of cosmic noise absorption and so to keep the record on scale for the relatively high amplifications used. The detector voltage was also made to drive a DC amplifier directly at lower gain and slower chart speeds so as to produce a crude version of a conventional riometer record. This slow record was used to check the antenna beam directions and enabled quick estimates to be made of the absolute size of absorption events.

The final output was recorded both on paper charts at 0.5 in.sec.$^{-1}$ and as frequency modulated tones multiplexed on to one track of a Philips Stereo Tape-recorder at 15/16 in.sec.$^{-1}$ The other track was used for simultaneous recording of photometer or balloon X-ray data when this was available. The tape recorder ran for just over eight hours without attention. At the end of each tape the charts were examined for c. n. a. pulsation activity. If no pulsations had occurred the tape was used again. Three or four good events were lost due to their occurence in the interval between the tape running out and the author finishing breakfast.

On returning to Australia all interesting portions of the tape were played back at the same speed at which they were recorded and the four tones separated out and demodulated via the same filters and DC amplifiers used in the original recording process. This time though the chart was run at speeds ranging from 1 mm.sec.$^{-1}$ to 10 mm.sec.$^{-1}$ Thus high time resolution could be achieved without wasting miles of paper. The monitor charts made on Macquarie Island were necessary for identifying when events had occurred and for locating events easily on the tapes.

Time marks which also served as calibration marks were superimposed on the record itself by shorting out .4 dB of signal in the I.F. section of the receiver. Pulse amplitudes were measured by comparing them with these marks. The logarithmic nature of a riometer output is of no concern since the pulses constitute such a small fraction of the signal that the device is, to all intents and purposes, linear. This calibration technique enabled the frequency response of the whole system forward from the I.F. section to be checked by examining the shape of the timing pulses as they appeared on the demodulated record. The leading edge of the (initially square) pulses had the appearance of having been fed through an integrating circuit with a time constant of about .03 sec. Since the differentiating time constant was known to be 110 sec., the output bandwidth of the system was .0015 Hz. to 5 Hz.

Each section will now be discussed in more detail.

III.3 The Antennas.

The beam of each antenna was directed thirty degrees from the vertical and the four beams were directed magnetic north, south, east and west in azimuth respectively. The 3dB and 6 dB. contours projected on to an horizontal plane at 100 Km. are shown in Fig II.1

The relative received power as a function of zenith angle in a plane perpendicular to the dipole elements is shown in Fig.III.2. The effect of a conducting ground is taken into account in computing the curve of Fig.III.2.

Each antenna consisted of four half-wave dipoles made from 16 gauge hard drawn copper wire stretched between guyed poles (Fig.III.3). The separation of the two parts of the dipoles was 2 inches and their length was .94 of a half wavelength to allow for end effect. The dipoles were strung at half wavelength intervals eight feet above the ground which was made conducting by placing lengths of wire at quarter wavelength intervals parallel to the dipoles.

The dipoles were interconnected via pairs of 75 ohm coaxial cables with the outer braid earthed. The cables thus formed balanced lines with characteristic impedance of 150 ohm. The method of interconnecting dipoles is shown schematically in Fig.III.4. The electrical distance between adjacent dipoles is 3/4 λ since the velocity factor of the polythene spacing is, fortuitously, .67. Alternate dipoles are $1\frac{1}{2}\lambda$ apart electrically and can be connected together without mismatch whatever the impedance of the line. Each pair of alternate elements now presents an impedance of 150 ohms and they can be connected together via any length of 150 ohm line, in this case with $.3/4\lambda$ electrical length of line. The four dipoles now present an impedance of 75 ohm and can be matched to a 75 ohm cable via a 1:1 transformer.

The above argument was borne out by actual measurements of the antenna impedances and by observation of the sidereal changes in signal level recorded on the slow chart. The peak in signal level occured four hours earlier for the east pointing antenna than for the west pointing antenna.

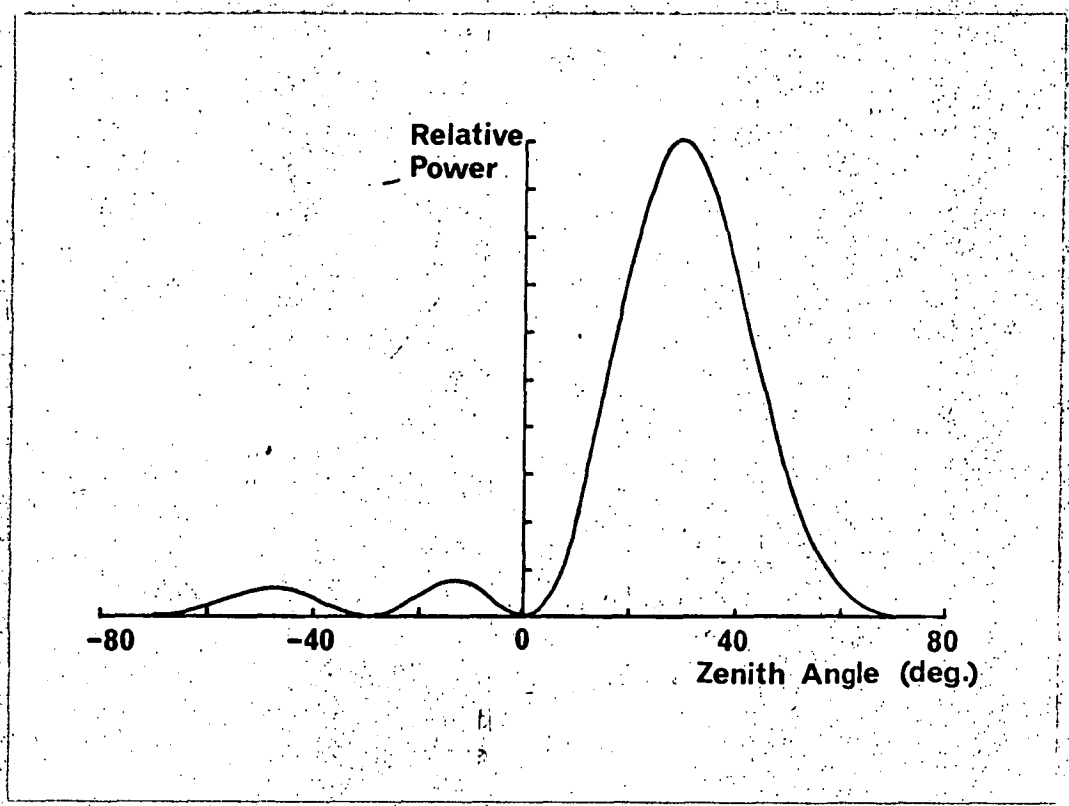

Fig. III.2

Antenna pattern in a plane perpendicular to the dipoles.

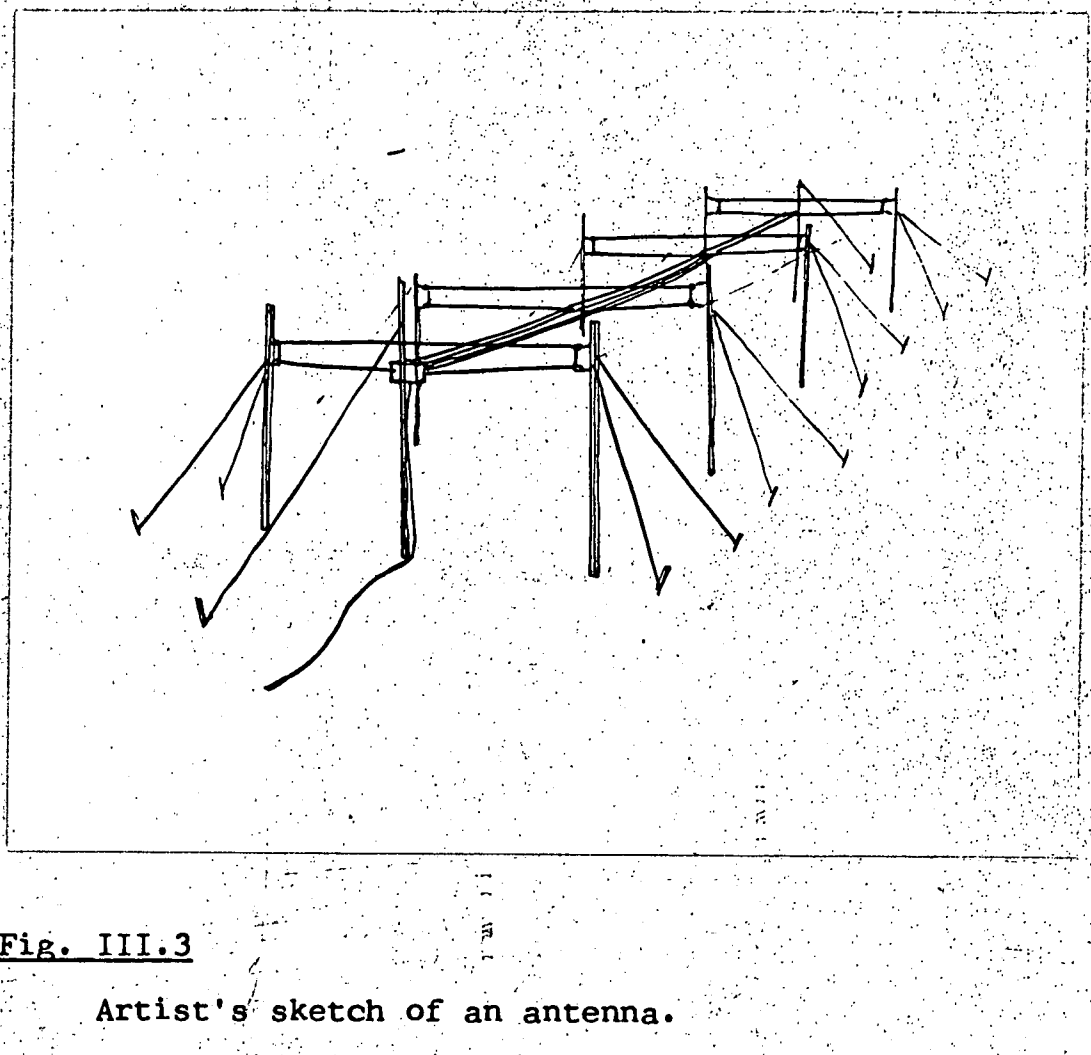

Fig. III.3

Artist's sketch of an antenna.

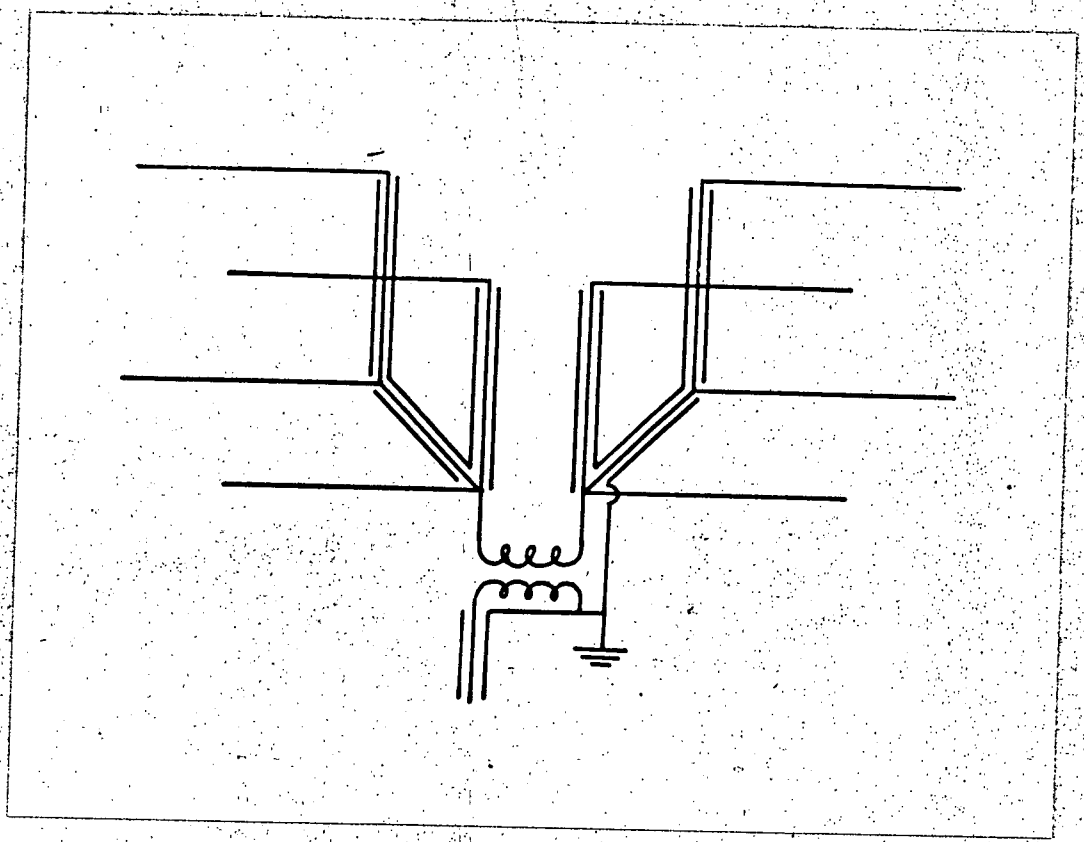

Fig. III.4

Schematic diagram illustrating the way in which the transmission lines were connected to the dipoles.

Phased arrays of this type are much easier to build and are more reliable and more broad band than Yagi-Udah arrays which are higher Q and unwieldly at riometer frequencies. A structure a little more robust than the one described is desirable, however, in the high wind and seal harem environment of Macquarie Island.

III.4 The Receivers.

The RF and IF sections of the receivers are shown in Figs.III.5 and III.6. Their centre frequencies were in the range 32.2 MHz to 32.4 MHz, their 3 dB pass bands varied between 1 and 1.4 MHz and their 10dB passbands were in the range 1.9 to 2.5 MHz. A common oscillator, suitably decoupled was used to drive all four receivers. Cross talk between receivers was better than 60 dB.

The front end tuned circuit was loaded with a resistor so as to keep the antenna matching constant and independent of input transistor and antenna parameters over the bandwidth of the receivers.

Each cascode pair was housed in a separate brass compartment to avoid parasitics and each I.F. section was built on a different chassis from the R.F.section.

The circuit for providing timing calibration pulses can be seen at the front end of the I.F. in Fig.III.6.

The wide bandwidth and absence of a minimum reader and servo noise diode makes the system temperature sensitive and subject to interference. The temperature sensitivity was too slow to affect the differentiated output but prevented absolute absorption measurements of any but the smallest events from being made from the slow chart. The remote location of Macquarie Island helped the interference problem but solar noise in the middle of the day and interference from the station transmitter were considerable.

A relay was installed which earthed the inputs to the DC amplifiers during local transmissions. This at least prevented the pen recorders from being damaged during "scheds".

Use of an antenna with a null at the horizon and a centre frequency of 32 MHz rather than 30 MHz avoided distant broadcast station interference.

III.5 The Recording Section.

The differentiator and DC amplifier are shown in Fig.III.7. Their operation should be obvious.

The voltage to frequency converter is shown in Fig.III.8. The leftmost four transistors comprise the transistor equivalent of a Miller oscillator. The input transistor is a Miller integrator. The top two transistors make up a switch which at an appropriate voltage switches on the lowest transistor which discharges the Miller capacitor by analogy with the positive grid current of the valve circuit. The circuit is linear to within about two percent over its range of operation and the output consists of short spikes of constant width.

The rest of the circuit consists of two band pass filters in series. Each filter consists of an amplifier with negative feedback through a band stop parallel T network. The precise values of the components of the parallel T filters have to be found by trial and error. They require a good deal of fiddling around but take up less room on a circuit board than would inductances at these frequencies.

The circuits are drawn for the 270 Hz subcarrier. The response for the 800 Hz subcarrier is shown in Fig.III.10. The subcarrier centre frequencies used were 100, 270, 800 and 2,000 Hz. Each had a $\pm$ 20 percent swing corresponding to full scale deflection on the pen recorder chart.

Despite the fact that the frequencies are so close together no cross talk was discernible although because of the small swing in frequency tape recorder "wow" was a problem. In addition dropout often occurred on the top channel and extra filtering was required when demodulating the bottom channel so that its frequency response was not quite as good as that specified in section III.2.

When demodulating the filters were disconnected from the oscillator at the input end and connected to the tape recorder. Their outputs were connected to demodulators (Fig.III.9) which drove the pen recorders via the DC amplifiers.

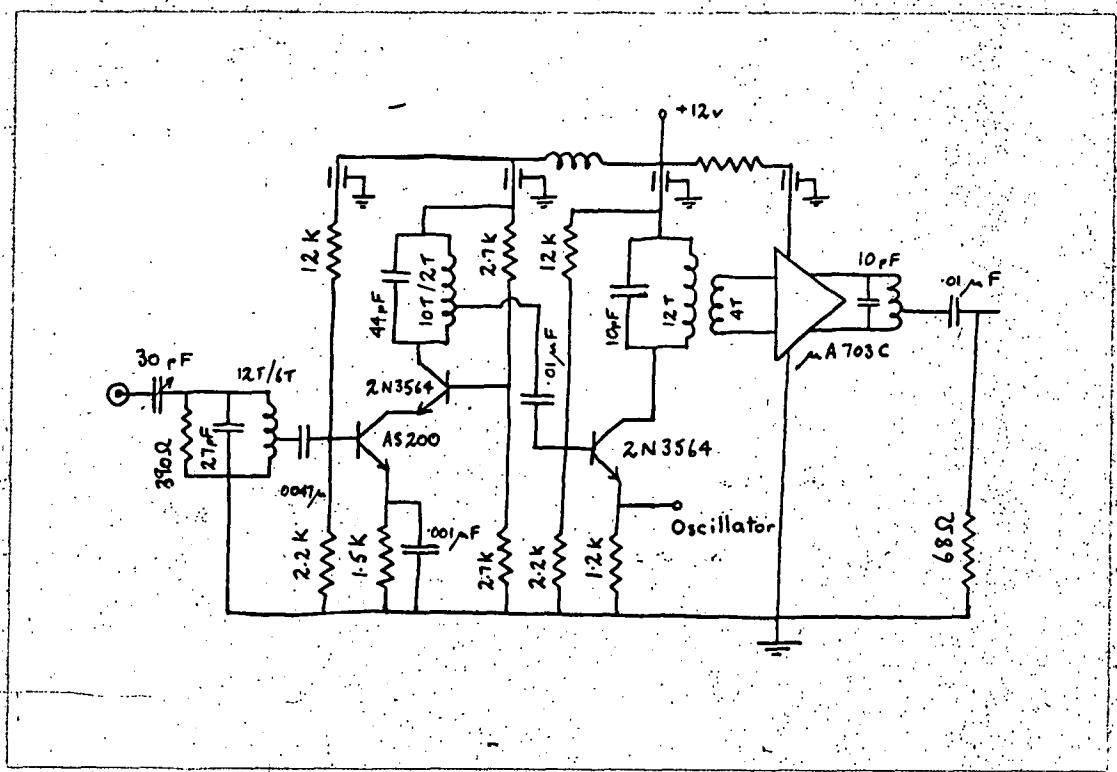

Fig. III.5

Fast response riometer - R.F. and first I.F. stages.

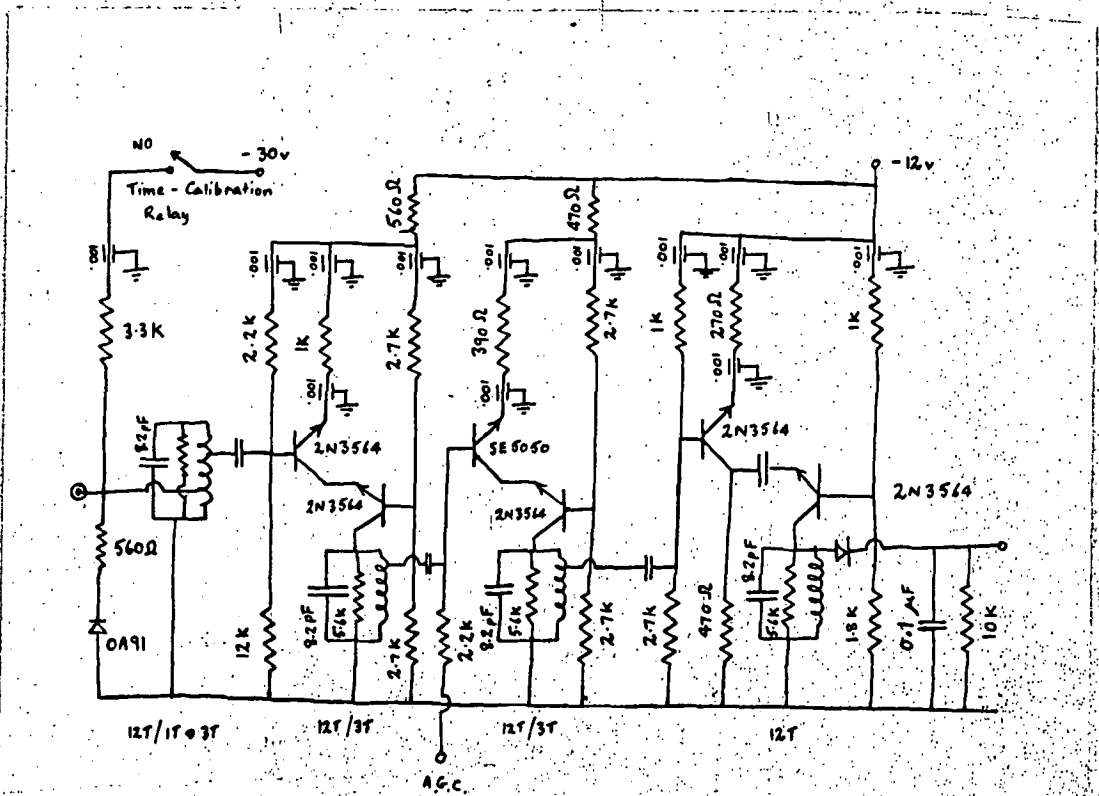

Fig. III.6

Fast response riometer - I.F. stage showing calibrator.

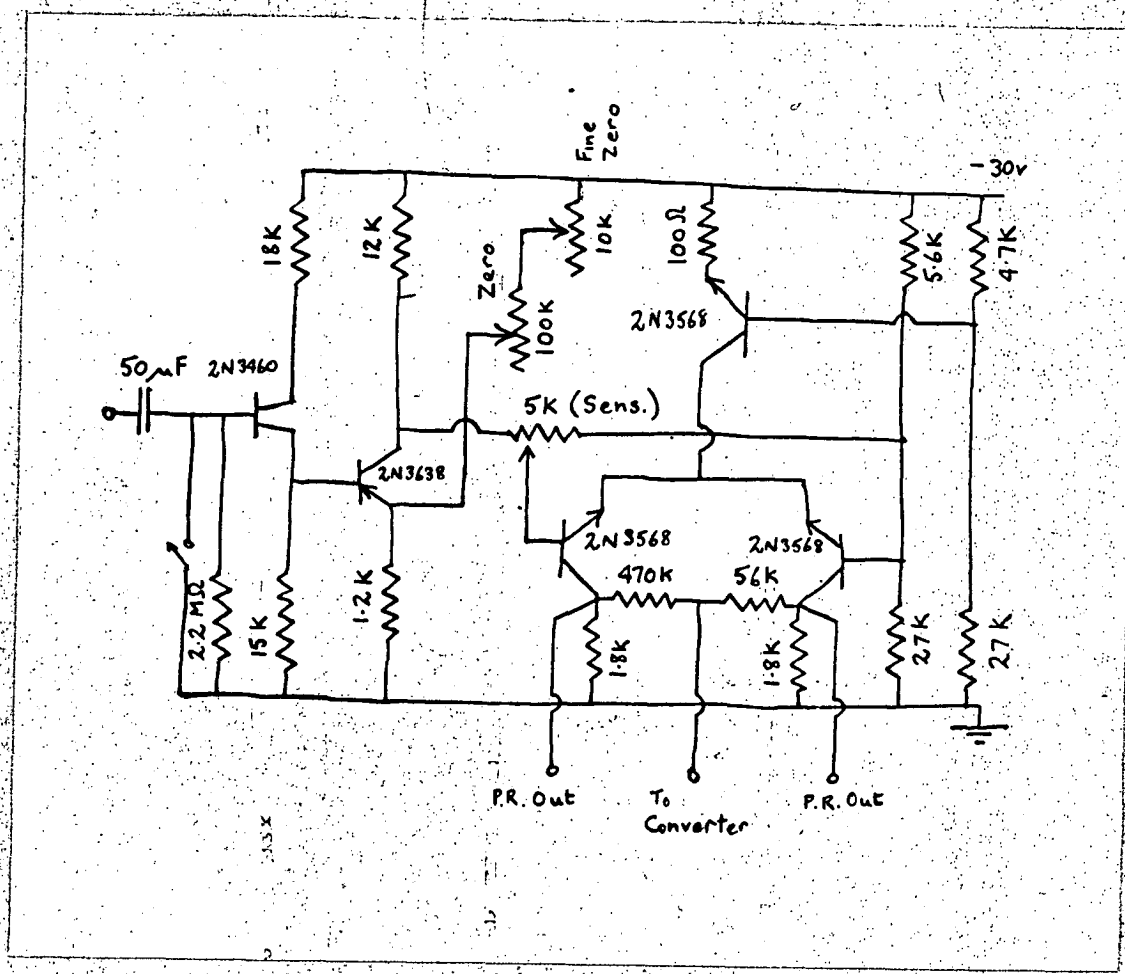

Fig. III.7

D. C. amplifier and differentiator.

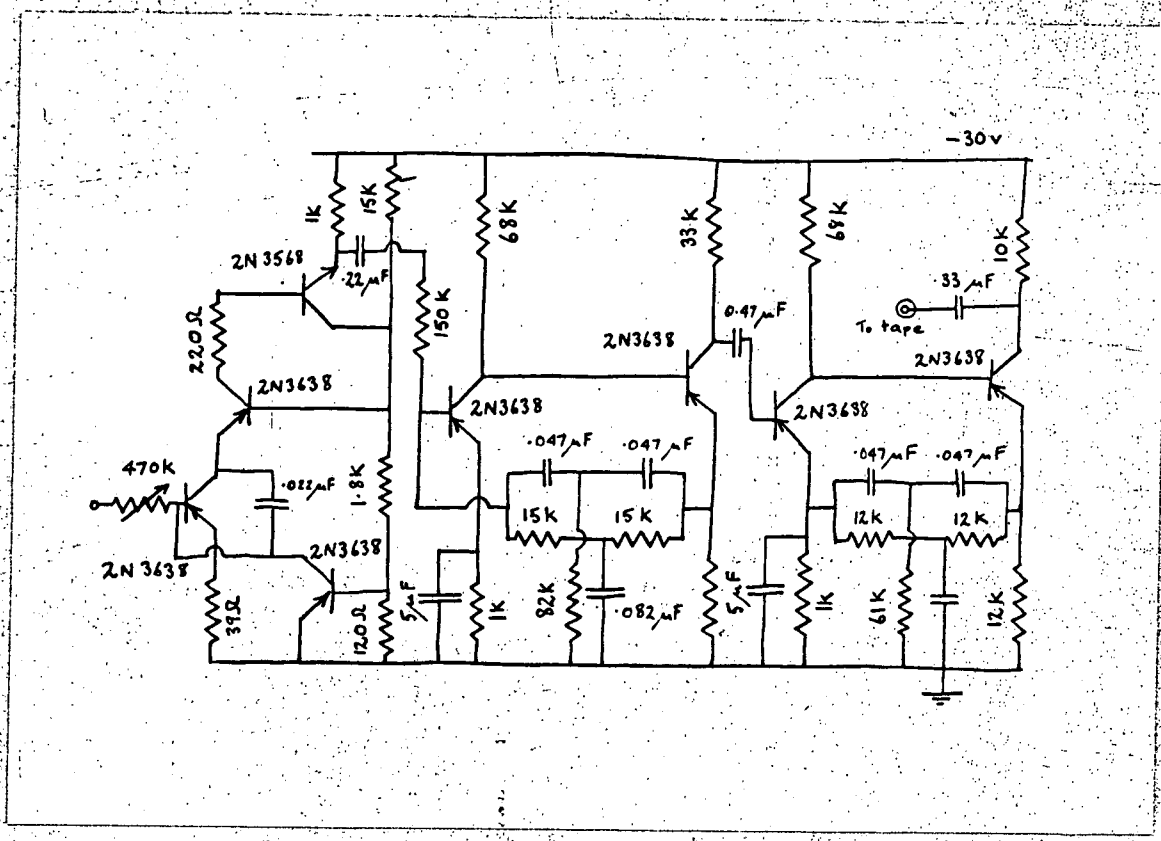

Fig. III.8

Voltage to frequency converter showing variable frequency oscillator and two stage band - pass filter.

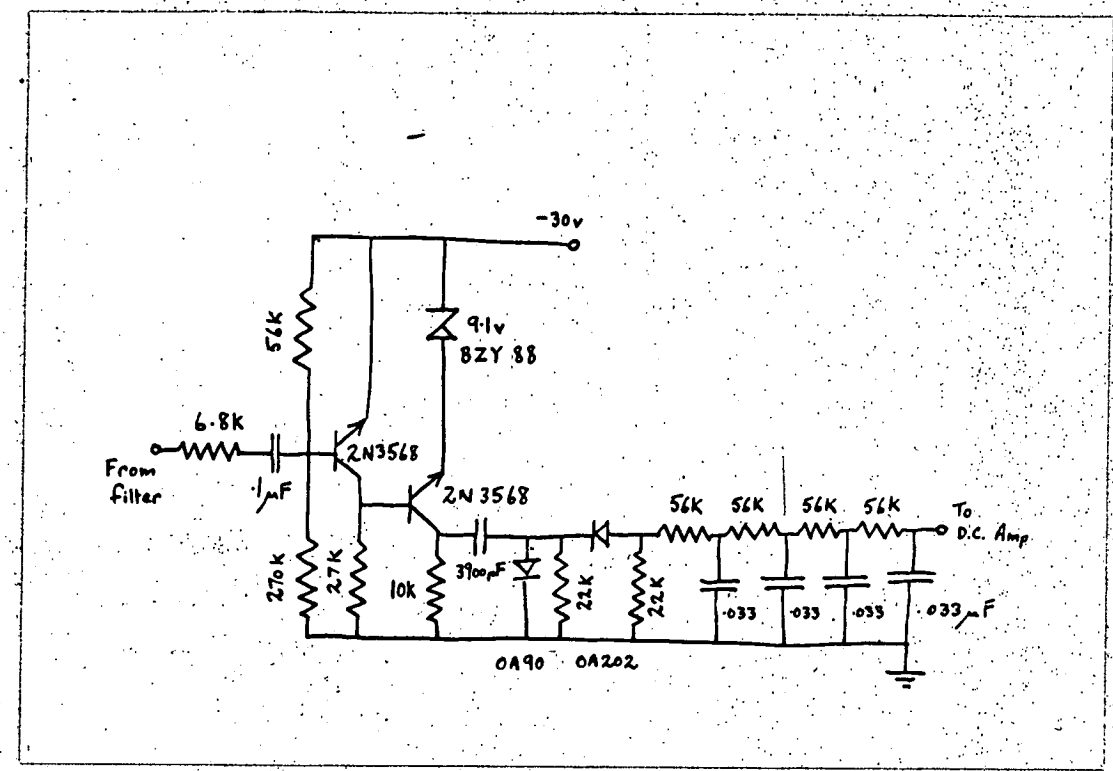

Fig. III.9

Frequency demodulator.

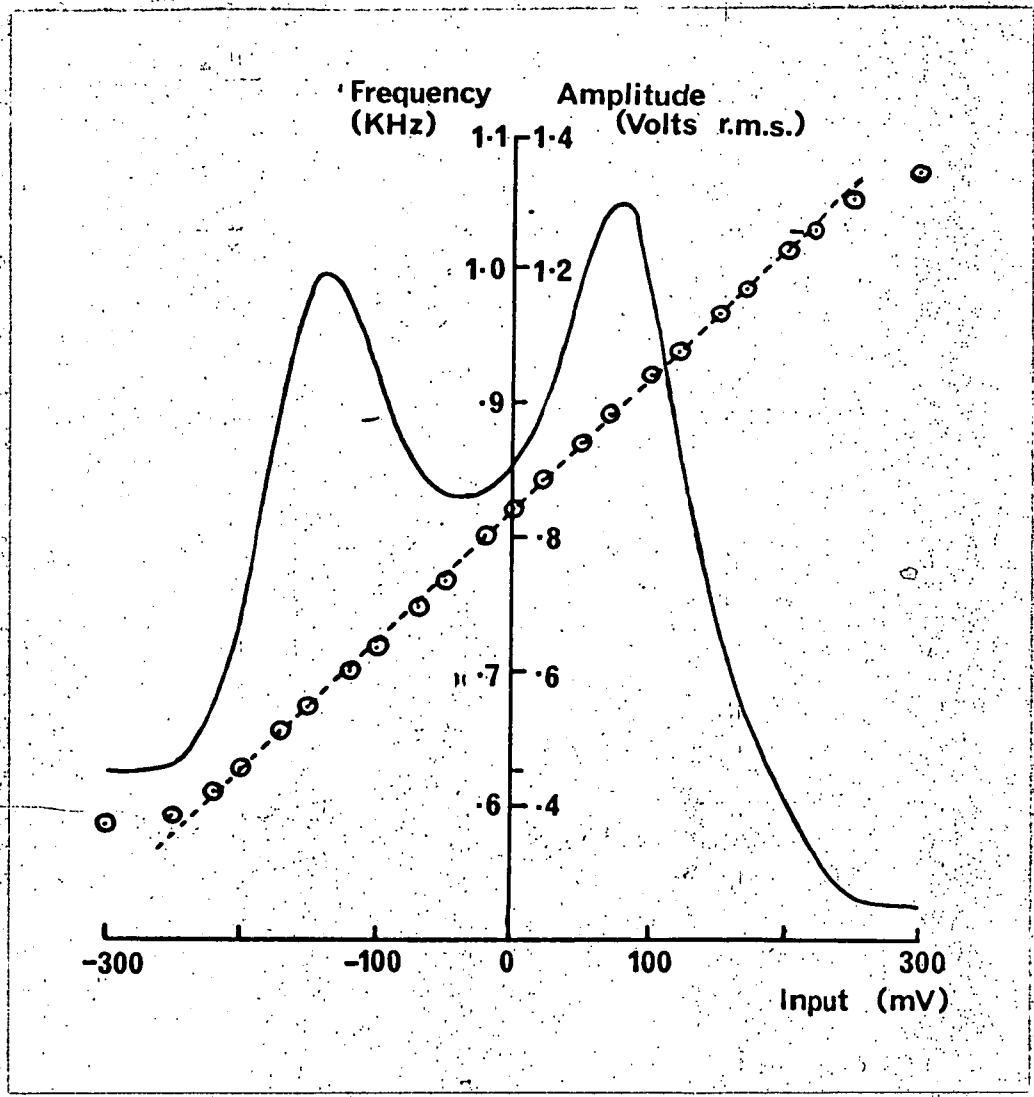

Fig. III.10

Response curve for the 800 Hz subcarrier voltage to frequency converter and D.C. amplifier. The frequency and amplitude of the tape - recorded signal are shown as a function of input voltage to the DC amplifier.

References

Little, C. G. and H. Leinbach (1958). Proc.I. R. E.46, 334.

Machin, K. E., M. Ryle and D. D. Vonberg (1952). Proc. I. E. E. 99, pt. III, 127. 127.

Appendix IV

Ionization Rate Profiles: The Effect of Bremmstrahlung.

IV.1 Introduction

This work was carried out before the work of Berger and Seltzer (1972) and of Pilkington and Anger (1971) was known to the author, in fact before Berger and Seltzer's later paper became available in Tasmania. It is included here because it resolves the problem of the conflicting results of Rees (1964) and Kamiyama (1967) mentioned in Section 2.5.2 of this thesis, because it yields an estimate of the effect of multiple Compton scattering on X-ray photon transport in the atmosphere and because it is a description of the way in which the ionization rate profiles used in the body of the thesis were actually calculated.

The method used is based on that of Faust and Johnson (1949) in that an approximation was used which allowed the discretization of the problem of multiple Compton scattering viz: that scattering of photons can be approximated to by assuming that photons of initial energy E_o, after scattering, all assume the mean energy $\bar{E}$ where $\bar{E}$ is given by

$$\bar{E} = \frac{\sigma_s}{\sigma} E_o \quad \ldots\ldots\ldots\ldots\ldots \quad (1)$$

Here σ is the Klein-Nishina cross-section which can be decomposed into the sum of $\sigma_a + \sigma_s$, where σ_s/σ is the (mean) fraction of the incident energy given to the scattered quantum while σ_a/σ is the (mean) fraction of the incident energy given to the recoil electron.

The method used here differs from that of Faust and Johnson though, in that the approximation was made that the photons are always scattered isotropically whereas they used a one dimensional technique whereby photons are either scattered

through 180^{o} or continue in a straight line. The assumption of isotropic scattering is more suited to an isotropic source of photons and is a little more sophisticated in that it enables the absorption of photons travelling along oblique paths to be properly taken into account.

The electron flux giving rise to ion-pairs in the atmosphere was assumed to be isotropic over the downward hemisphere and infinite in horizontal extent. The differential flux of the primary electrons at the "top of the atmosphere" was assumed to be flat from 1 to 10 KeV and to fall off exponentially from 10 KeV to 511 KeV. Energies above 511 KeV were not considered.

The normalized energy dissipation function $\lambda(x)$ due to Spencer (1959) and to Grün (1957) as used by Rees (1964 b) was used to determine the energy deposition rate of the electrons themselves and with some crude simplifying assumptions, to give the gross flux of electrons from which the bremmstrahling production rate could be calculated. This was thought to be more realistic than the method of Kamiyama (1966) who used Heitler's (1944) formula for the degradation of electron energy but who ignored electron scattering.

This method is based on the concept of " order of scattering". Bremmstrahling X-rays created by electron collisions are regarded as being absorbed in proportion to the total cross-section $\sigma_p + \sigma_c$, but as creating in any region of space bremmstrahling photons in proportion to the Compton scattering cross - section, σ_c and ion electron pairs in proportion to the absorption part of the total cross - section, $\sigma_p + \sigma_a$. Here σ_p is the photo-electric cross section and the Compton cross section σ_c is regarded as being composed of two parts σ_a and σ_s.

The total electron flux and the bremmstrahling cross section were used to compute the bremmstrahling production rate as a function of height in the atmosphere and photon energy. The production rate was then used to compute the flux of unscattered photons at each height and energy and this flux was used to determine the production rate of singly scattered, i.e. first order, photons. The first order photon production rate was integrated to obtain a first order flux which in turn yielded a second order production rate and so on.

The ion - pair production rate due to each order of scattering at each height were then added to yield a total ionization rate. In practice this function converged quite rapid -ly.

In reality the intensity of the scattered flux is not isotropic but is a function of the angle between the direction of the photon before and after scattering. The final energy is also a function of this angle. Errors must have been introduced by the approximation of isotropic scattering with constant energy. These errors will not be too serious since:

(i) at say E = 90 KeV the scattered intensity varies only by a factor of 3 with scattering angle,

(ii) the bulk of the photons under consideration have energies less than this and are scattered more isotropically,

(iii) the fluxes of photons being scattered are far from mono-directional and this will smooth out the angular dependance of intensity and energy.

Nevertheless the effect of the approximation will be to underestimate the fluxes of photons low down in the atmosphere since photons travelling vertically downward have a higher probability of continuing downward than has been expressed in the model.

IV.2 Electron Flux and Energy Dissipation Function

A graph of energy vs. distance travelled by an electron is approximately rectangular in shape, since an electron penetrating matter loses most of its energy near the end of its range i.e. near $s = r_o$ where r_o is the range and is a function of the initial energy of the electron and s is the distance travelled measured along the path of the electron. The normalized energy dissipation function of Grün (1957), $\lambda(x)$, does not resemble a rectangle and for a mono directional source of electrons in air and has a peak near x=0.4. Here $x = r/r_o$ is the fractional range measured in the initial direction of the electrons. $\lambda(x)$ does not resemble a rectangle because its shape is controlled by scattering. Electrons entering the target material are scattered away from the initial direction and reach the end of their range at intermediate values of x.

The enrgy deposition rate $\lambda(x)dx$ is, by definition the fraction of the energy lost by the electron beam between x and $x + dx$. If we assume that electrons lose all of their energy at $s = r_o$ then $\lambda(x)dx$ represents the number of electrons which come to rest between x and $x + dx$. This or an equivalent assumption must have been made by Rees (1964 b) since equation (7) of that paper implies that there is no continuous degradation of electron energy with decreasing height.

In order to compute the bremmstrahlung emitted by the electron stream we need to know the gross flux of electrons as a function of height and energy. Let $F_1(x)$ be the flux of downward moving electrons and let $F_2(x)$ be the flux of upward moving electrons, then the gross and net fluxes of electrons F_G and F_N are given by

$$F_G(x) = F_1(x) + F_2(x)$$

$$F_N(x) = F_1(x) - F_2(x)$$

Let $F_1{}^s dx$ and $F_2{}^s dx$ be the number of electrons in the

downward and upward streams respectively which are stopped between x and x + dx and let F_{12} be the net number of electrons deflected from the downward stream into the upward stream. Then

$$dF_1 = - F_1{}^s dx - F_{12} dx$$

and

$$dF_2 = F_2{}^s dx - F_{12} dx$$

Hence

$$d(F_1 - F_2) = - (F_1{}^s + F_2{}^s) dx$$

i.e.

$$\frac{dF_N}{dx} = \lambda(x)$$

Thus $\lambda(x)$ is related to the downward net flux of electrons. In order to obtain F_G in terms of λ let us assume that

$$F_2(x) = AF_1(x) \text{ for } x \geq 0$$

where A is a constant.

Then

$$F_N(x) = (1 - A)F_1(x)$$

hence

$$(1 - A)(F_1(x) - F_1(11) = - \int_1^0 \lambda dx$$

i.e.

$$(1 - A)F_1(x) = \int_x^1 \lambda dx$$

since $F_1(1) = 0$

hence

$$(1 - A)\, F_1(o) = \int_o^1 \lambda dx$$

If we assume that the number of forward moving electrons is negligible for $x < 0$ compared with the source then $F_1(o)$ is unity and

$$A = 1 - \int_o^1 \lambda dx$$

$$= \int_{-1}^o \lambda dx$$

Thus

$$F_G(x) = \frac{1+A}{1-A} \int_x^1 \lambda dx$$

$$= \frac{2 - B}{B} \left(B - \int_o^x \lambda dx\right)$$

where $B = 1 - A$

$$= \int_o^1 \lambda dx$$

With these simplifying assumptions then, the differential total electron flux of electrons at height h with energy E_o can be written

$$F(E,h)dE = \frac{2 - B}{B} \left\{ B - \int_o^x \lambda(t)dt \right\} F_o(E)dE \qquad (2)$$

where $F_o(E)$ is the differential flux at the top of the atmosphere.

Here $x = z(h)/z_o(E)$

where h' is the optical depth at height h and $z_o(E)$ is the range in the same units

$$z_o(E) = N_A R / M$$

where N_A is Avogadro's number. M the mean molecular weight and R is the range in $gm.cm^{-2}$. R is given by Grün(1957) and Rees (1964 a) as

$$R = 4.57 \times 10^{-6} E^{1.75}$$

for E in KeV

In the computer program, λ was taken from the curve given by Rees (1964 b) for electrons which are isotropic

over the range 0 to 80°. For this curve B has the value .81. Equation (1) above resembles equation (7) of Rees' paper, but has the advantage that the flux becomes zero at atmospheric depths such that $x \geq 1$ i.e. such that $h < h_o$ where h_o is the range. This is not the case in Ree's formula which does not account for electrons back-scattered out of the atmosphere.

The rate at which ion pairs are created by electrons q(h) is given by

$$q(h) = \int_o^\alpha N(h)\, \bar{\lambda}(x)\, E\, F\, (E)\, dE/\ .0355 \qquad (3)$$

where F(E) is the flux at the top of the atmosphere, N(h) is the number density of atoms and molecules at height, h, and .0355 KeV is the mean energy lost by an electron in the formation of an ion pair.

IV.3 Scattering Energies.

Some form of discretization is usually necessary in performing computations with a digital computor. In this case the height in the atmosphere, h, and the electron and photon energies, E, were made discrete quantities. Following Faust and Johnson (1949) the energies were made discrete in such a way that, for energies above 20 KeV, energy E_k was expressed in terms of E_{k-1} in accordance with equation (1) as follows:

$$E_k = (\sigma_s/\sigma)\, E_{k-1} \qquad (4)$$

The maximum energy was chosen, more or less arbitrarily as 510.8 KeV the rest mass of an electron.

Below 20 KeV the ratio of σ_s/σ is close to unity and in this region the discrete energies were chosen to be 1 Kev

apart. 1 KeV was the minimum energy used.

IVa. Top of The Atmosphere Flux.

The flux of electrons was assumed to be of the form (for reasons discussed in the body of this thesis):

$$G(E)dE = A \exp(-E/E_o)\, dE \quad \text{for } E > 10 \text{ KeV}$$

and $$G(E)dE = A \exp(-10/E_o)dE \quad \text{for } E \leq 10 \text{ KeV} \qquad (5)$$

where A is a normalizing factor chosen such that

$$\int_o^\alpha G(E)\, dE = 1$$

Thus $$A = \exp(10/E_o) / (9 + E_o)$$

This continuous flux G was converted to a discrete flux F by assigning to $F(E_k)$ the number of electrons in an interval around $G(E_k)$ i.e.

$$F(E_k) = \int_{E_1}^{E_2} G(E')\, d\, E'$$

where $E_1 = \frac{1}{2}(E_k + E_{k+1})$

and $E_2 = \frac{1}{2}(E_k + E_{k-1})$

IV.6 The Bremmstrahling Cross-Section.

IV.6.1 Angular Dependance.

This discussion is based on formulae given by

Heitler (1944). The differential bremmstrahlung cross-section is given in the non-relativistic case by

$$d\Phi = K \sin\theta \sin\theta_o \, (p^2\sin^2\theta + p_o{}^2\sin^2\theta_o \qquad (6)$$

$$- 2p\, p_o \sin\theta \sin\theta_o \cos\phi \,) \, d\theta_o d\theta d\phi$$

where K is a constant independant of the angles, and p_o and p are the initial and final relativistic momenta of the electron. θ_o is the angle between the photon direction, $\underline{k}$ and the direction of p_o, θ is the angle between $\underline{p}$ and $\underline{p_o}$ and is the angle between the planes $\underline{p}$, $\underline{k}$ and $\underline{p_o}$, $\underline{k}$.

$d\Phi$ can be obtained as a function of θ_o alone by integrating over θ and

$$d\Phi(\theta_o) = K\left(2p^2 + \frac{4p_o{}^2}{3}\sin^2\theta_o\right)\sin\theta_o d\theta_o$$

Let Pdw_o be the cross-section associated with a certain solid angle dw_o. Then the number of photons scattered into dw_o, N is given by

$$N = Pdw_o = P\sin\theta_o d\theta_o d\phi_o$$

P is related to $d\Phi(\theta_o)$ by

$$d\Phi(\theta_o) = \int_o^{2\pi} (P\sin\theta_o d\theta_o) d\phi_o$$

Hence

$$P = \frac{K}{2\pi} \quad (2p^2 + \frac{4p_o^2}{3} \sin^2\theta_o) \qquad (7)$$

P is the differential cross-section relative to the initial direction of the electron only for a given photon energy.

Let θ, ϕ be the coordinates of the electron direction relative to a z-axis and let θ', ϕ' be the coordinates of the photon relative to this z-axis.

Let $F(\theta, \phi\ )$ be the angular distribution of initial directions of electrons and let $N^* dw' dw$ be the number of photons emitted in solid angle dw' due to electrons in solid angle dw.

Then

$$N^* dw' dw = P(\theta_o, \phi_o)\ dw_o\ F(\theta, \phi\ )\ dw$$

The number of photons emitted with directions in solid angle dw' due to electrons coming from all directions is given by

$$N(\theta', \phi')\cdot dw = \int_W N\ dw' dw$$

$$= \int_W P(\theta_o, \phi_o) dw_o F(\theta, \phi\ )\ dw \qquad (8)$$

Rotating axes so that P is measured from the spatially fixed z-axis we have

$$dw_0 = dw' \qquad (9)$$

and

$$\cos\theta_o = \cos\theta' \cos\theta - \sin\theta' \sin\theta \cos(\phi' - \phi) \qquad (10)$$

Substituting (10) into (7), and (7) and (9) into (8) and integrating with F constant over the downward hemisphere and zero for $\theta < \pi/2$ we find that N is independant of θ and ϕ

Thus the flux of bremmstrahlung X-ray photons emitted by electrons which are isotropic over only one hemisphere is isotropic over the whole sphere.

This discussion applies only to non-relativistic electrons but since the bulk of the electrons lie below 511Kev the conclusion is justified for the model under discussion.

IV6.2 The Total Bremmstrahlung Cross Section.

The total relativistic cross section, that is the differential cross section integrated over all angles, derived using the Born approximation was used to derive the photon production rate as a function of height. At low (non - relativistic) electron energies the formula is not exact due to the inadequacy of the Born approximation for this condition However, the non-relativistic formula can be made exact by multiplying it by a factor derived by Sommerfeld (1931). In the program this factor was used to multiply the relativistic general cross section. This results in a non - zero value of ϕ_k, the cross section, at the short wave length limit i.e. when all of the energy of the electron is transferred to the photon.

The effect of screening was neglected. This results in the divergence of $k\phi_k$ at the long wave length limit. Here k is the energy of the photon, $k\phi_k$ is an energy cross - section while ϕ_k is, of course, the cross - section in terms of the number of photons emitted per unit normalized energy interval. The effect of screening for small photon energies

and for light elements can be seen by comparing the two curves for aluminium in Fig 14, page 170 of Heitler's book. Had screening been taken into account as well, the energy cross - section, $k\phi_k$, would closely resemble those derived by Sauter's method and computed by Kirkpatrick and Weidman (1945). As it is the neglect of screening only introduces errors greater than twenty percent of photon energies of less than one percent of the initial electron energy and for our purposes this can be neglected since we are not dealing with energies outside the range 1 KeV to 510.8 KeV.

The formula used in the program for the bremmstrahlung cross - section ϕ , which is a function of both the electron energy and photon energy i.e. as follows

$$\phi = \frac{\bar{\Phi} \; B \; p \; S}{K \; p_o}$$

where

$$\bar{\Phi} = \frac{z^2 \; r_o^2}{137}$$

$$= 2.96 \times 10^{-26} \text{ cm}^2$$

where Z is given a mean value of 7.2 for air.
K is the energy of the photon, and p and p_o are the relativistic energies of the electron before and after the interraction respectively.

S is the Sommerfeld factor:

$$S = \bar{z} z_o / ((1 - e^{-\bar{z}}) (e^{\bar{z}_o} - 1))$$

where $\bar{z} = \frac{2\pi Z}{137\beta} = \frac{0.33}{\beta}$ for $Z = 7.2$

$\beta = v/c$ where v is the velocity of the electron after the collision and c is the velocity of light. Similarly for $\bar{z}_o$.

B is a complicated function of the relativistic electron energies E, E_o and momenta, p, p_o before and after the collision. B is dimensionless and is the bracketed factor in equation (16), p166 of Heitler (1944).

Note that the ϕ used here is not the same as the ϕ_k used by Heitler which is the cross section referred to a normalized photon energy. In fact

$$\phi = \frac{\phi_k}{T_o}$$

where T_o is the initial kinetic energy of the electron. ϕ is in units of $cm.^2\ KeV^{-1}$ or $cm.^2\ erg^{-1}$ depending on the units of K whereas, ϕ_k, is in units of $cm.^2$

IV. 7 Bremmstrahlung Production Rate.

For a mono-energetic electron flux, F_o, with energy E the number of photons, RdE', radiated from unit volume with energies between E' and $E' + dE'$ is given by

$$RdE = \phi(E,E')\ N\ F_o\ dE'$$

When the electron flux is continuous, F(E), all the electrons with energies greater than or equal to E' make a contribution to RdE' hence

$$RdE' = \left(\int_{E'}^{\infty} \phi(E,E').N.F(E)\ dE\right) dE'$$

In accordance with the basic idea of photons having only discrete energies we must assign to each photon energy E_k' all of the bremmstrahlung radiated at all the energies over an interval on either side of E_k'. Let the discrete bremmstrahlung flux, S, at energy E_k' be given by

$$S(E_k') = \int_a^b R(E')\, dE'$$

where $a = \frac{1}{2}(E_k' + 1 + E_k)$

and $b = \frac{1}{2}(E_k + E_k - 1)$

Thus $S(E_k') \simeq R(E_k') \Delta K$

where $\Delta K = b - a$

i.e. $$S(E_k') = \int_{E_k'}^{\infty} \phi(E, E_k')\, N\, F(E)\, dE\, \Delta K \qquad (11)$$

Since F(E) is itself discrete and since S, N and F are also functions of h we can write (11) as

$$S(E_k, h) = N(h) \sum_{m=1}^{k} (\phi(E_m, E_k)\, F(E_m)\, \Delta K) \qquad (12)$$

For convenience later on we will write this in the form

$$S(E_k, h) = N(h)\, S'(E_k, h)$$

where S' is the sum in (12)

Following Kamiyama (1966), once the photon production rate S is known at each height the flux $B(E_k, h)$ as a function of height and energy can be computed

$$B_o(E_k,h) = \tfrac{1}{2} \int_o^\infty S(E_k,h') \; Ei\left\{ \sigma_t(Z(h) - Z(h')) \right\} dh'$$

$$= \tfrac{1}{2} \int_o^\infty S'(E_k,h') \; Ei\left\{ \sigma_t(z(h) - z(h')) \right\} dz(h')$$

since $dz(h) = - N(h)dh$

Here Ei(x) is the exponential integral

$$Ei(x) = \int_x^\infty \frac{e^{-t}}{t} \; dt$$

N(h) is the number density in atom $cm.^{-3}$ end, z is the optical atmospheric depth in atom $cm.^{-2}$. σ_t is the total cross section

$$\sigma_t = \sigma_p + \sigma$$

where σ_p is the photo electric cross section and σ is the Klein - Nishina cross- section. The radiation is treated as if even the scattered component is lost on the way from height h' to height h; B_o is a measure of the flux of unscattered photons.

The various photon cross-sections and the ratio σ_s/σ used to compute the E_k were taken from Leipunskii et al (1965)

In the computer program h and h' were of course discrete quantities. The function Ei(x) diverges as x tends to zero while its integral remains finite. The contribution to $B_o(E_k,h)$ from the same height layer was therefore treated separately in the summation viz.

$$B_o(E_k,h_i) = \sum_{j \neq i} S'_o(E_k,h_j) \; Ei(\sigma_t(z_i - z_j))\Delta z_j \; + B_z$$

where

$$B_z = S_o'(E_k, h_j)\sigma_t\left(Ei(x) + \frac{1 - e^{-x}}{x}\right)$$

where $x = \sigma_t \Delta z_i$

IV.8 Multiple Scattering

The photon flux array, B_o, can be used to compute both the ion pair production rate and the production rate of first order, i.e. singly scattered, photons.

q_o is given by

$$q_o(h) = \int_o^\infty (E)\, B_o(E,h)\, N(h)\, dE$$

where $(e) = (\sigma_p(E) + \sigma_a(E)).(E - 0.8)/.0355$

The constant 0.8 is the approximate energy required to eject the K electron from a nitrogen atom. It is assumed that this electron once ejected is responsible for most of the ion pairs formed.

The first order source array, i.e. the production rate of singly scattered photons was computed as follows

$$S_1'(E_k, h) = B_o(E_m, h)\sigma(E_m)$$

where $m = k - 1$ if $E_k > 20$ KeV, and $m = k$ if $E_k \leq 20$ KeV.

Below 20 KeV the mean energy loss of scattered photons is less than 1 KeV and so they were treated as if no energy were lost at all. Any errors introduced in this way would be

negligible since the photo electric effect soon swamps the effects of scattering of energies below 25 KeV.

From the first order source array $S_1'(E_k,h)$ a first order flux array, $B,(E_k,h)$ and a first order ion pair production rate, $q_1(h)$, were computed in the same manner as above. From $B_1(E_k,h)$ the doubly scattered photon production rate $S_2'(E_k,h)$ can be computed and so on. Since the contribution to q(h), of successive scatterings falls off rapidly only four iterations were carried out. The values of q(h), due to each order of scattering were summed at each height to give a total ionization rate profile.

IV.9 Results.

The total bremmstrahlung ionization rate profile and the component profiles due to each order of scattering resulting from a primary electron spectrum with e-folding energy, E_o = 80KeV are shown in Fig. IV.1. The total ionization rate profiles including the effect of electrons are shown in Fig. IV.2 for E_o = 5KeV and E_o = 80 KeV. Even for the harder spectrum the bremmstrahlung ionization rate is five orders of magnitude less than the peak due to electrons. The effect of ionization produced by multiple scattered bremmstrahlung X-rays can thus be completely neglected in discussing cosmic noise absorption pulsations. Its effect is negligible when compared with the ionizing effect of the electro -ns themselves.

For comparison with the results of other workers as summarized by Berger and Seltzer (1972), the program was re-run with the primary electron spectrum given by (5) replaced by a monoenergetic spectrum at 100 KeV. The differential bremmstrahlung flux as a function of photon energy at various heights in the atmosphere as computed in the manner described above is shown superimposed on the results brought together

by Berger and Seltzer. The results obtained here compare favourably with the results of other workers at 50 Km and above but are somewhat low at 40 Km and 32 Km. This is no doubt due to our approximation that the photons are scattered isotropically (IV.3).

The ionization rate profiles due to electrons are shown for a number of primary spectra in Fig. 2.1.

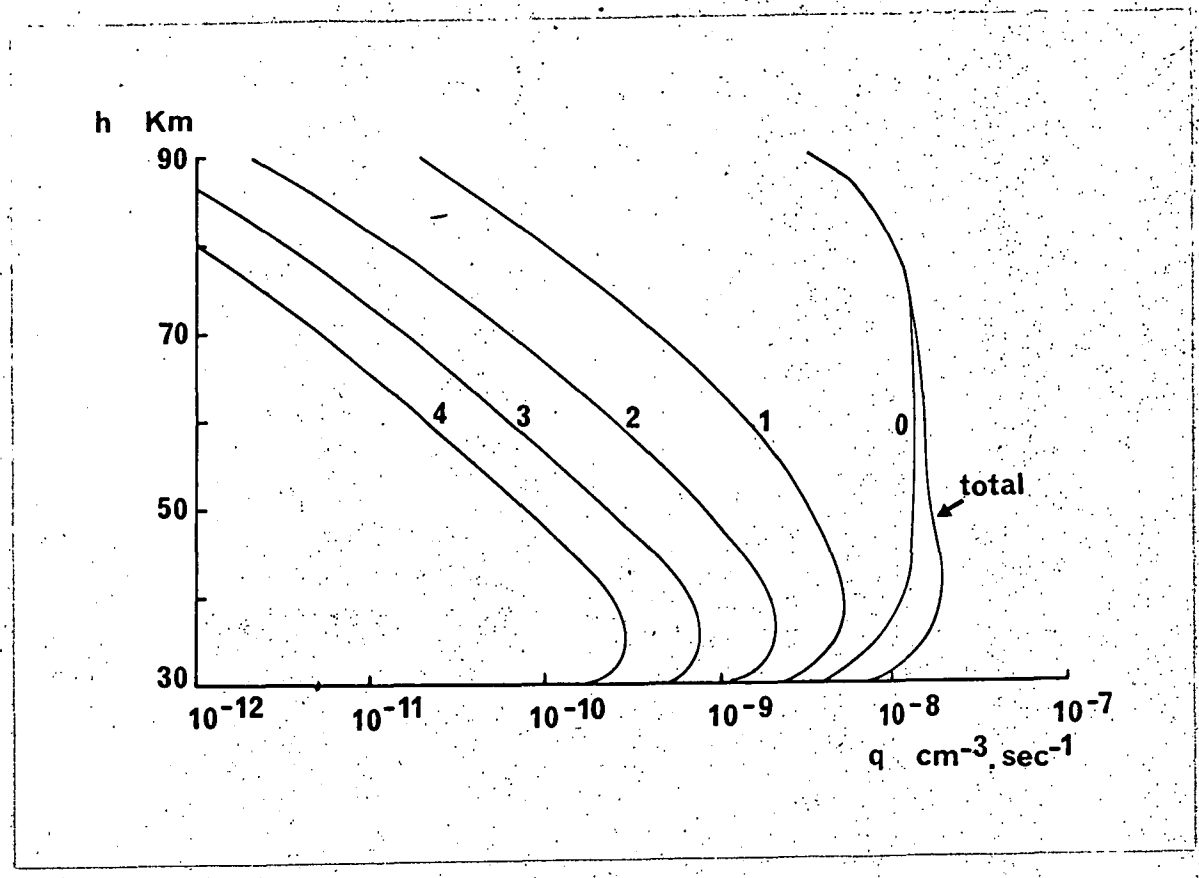

Fig. IV.1

Ion-pair production rate due to bremmstrahlung produced by flux of electrons from 1 to 510.8 keV in energy with e - folding energy of 80 keV. The numbers labelling the curves represent the number of times the photons have been scattered. The total production rate due to all five orders of scattering is also shown.

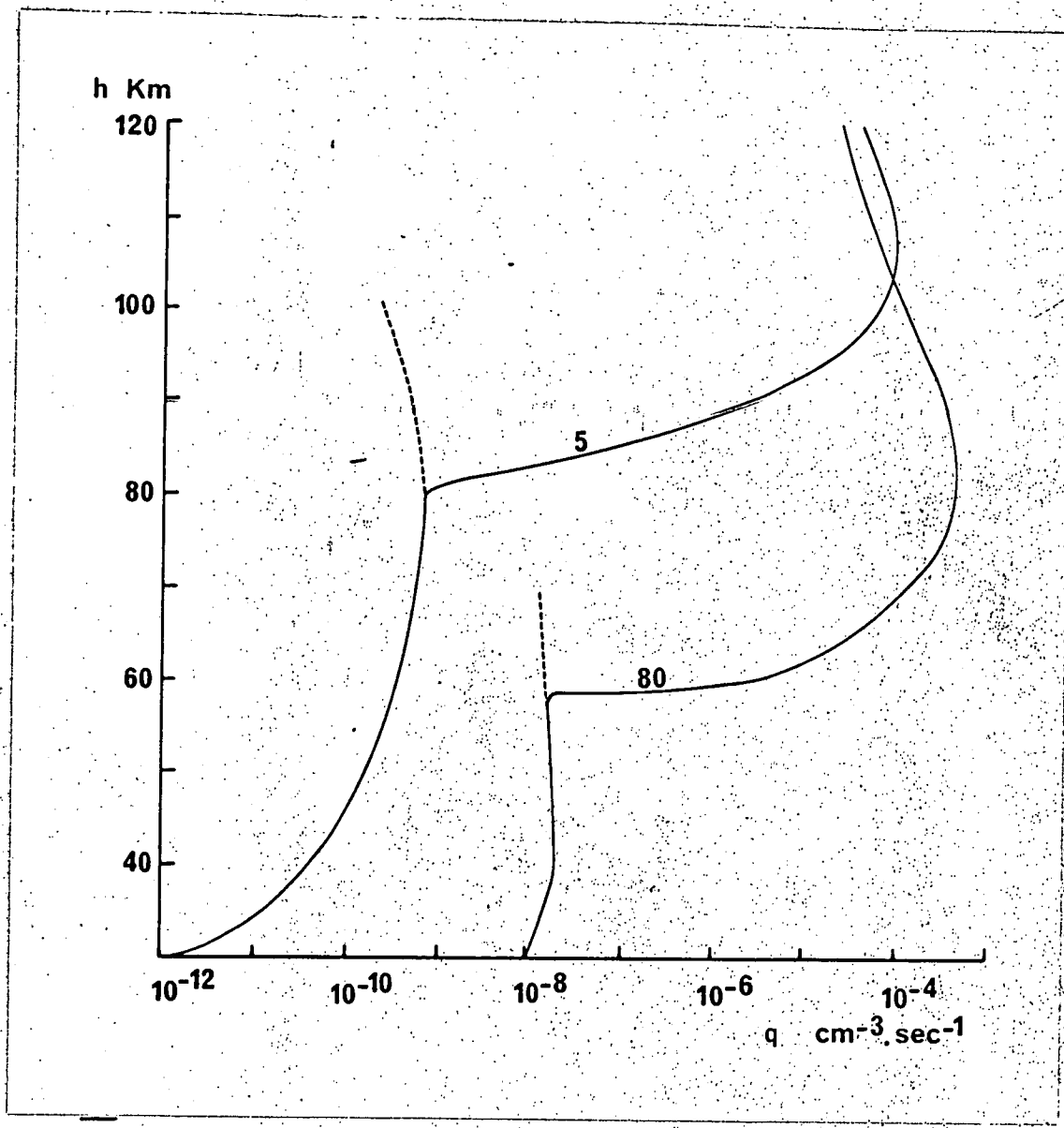

Fig. IV.2

Ion - pair production rates due to both bremmstrahlung and impact ionization resulting from parent flux spectra with e - folding energies of 5 keV. and 80 keV.

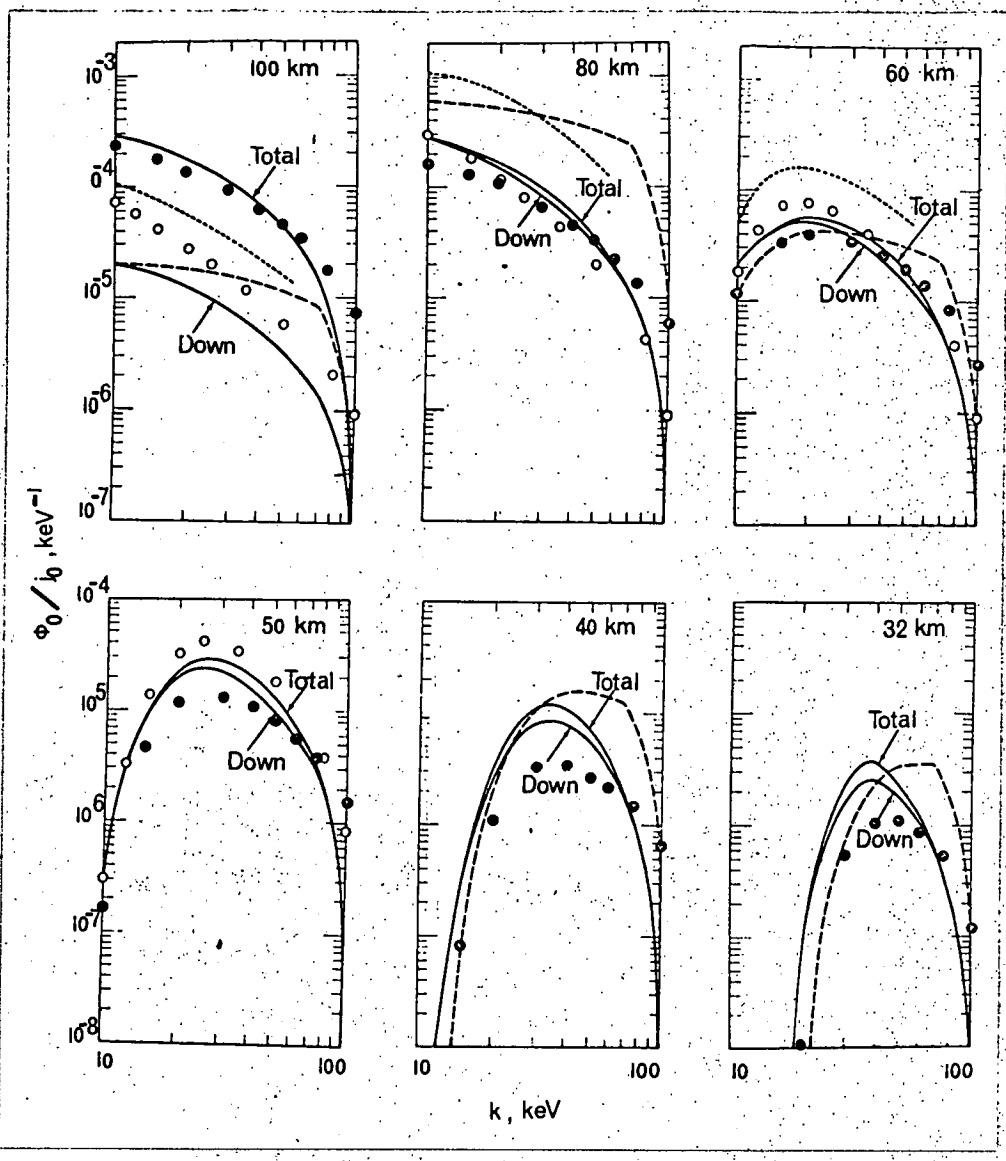

Fig. IV. 3.

Flux of bremmstrahlung photons produced by a mono-energetic electron flux with energy 100 keV (filled circles) superimposed on the results of other workers taken from Berger and Seltzer (1971).

References

Berger, M. J. and S. M. Seltzer (1972). J. Atm.Terr.Phys. 34, 85.

C I R A (1965). COSPAR International Reference Atmosphere. North - Holland, Amsterdam.

Faust, W. R. and M. H. Johnson (1949). Phys.Rev. 75, 467.

Grün, A. E. (1957). Z. Naturf. 12a, 89.

Heitler, W.(1944)."The Quantum Theory of Radiation", Oxford.

Kamiyama, H.(1966). Rep. Ion. Space Res. Japan 20, 374.

Kirkpatrick, P. and L. Weidmann (1945). Phys.Rev.67, 321.

Leipunskii, O. T., B. V. Novozhilov and V. N. Sakharov (.965). "The Propagation of Gamma Quanta in Matter". Pergamon.

Pilkington, G. R. and C. D. Anger (1971). Plan.Space Sci. 19, 1069.

Rees, M. H.(1964a). Plan. Space Sci. 12, 722.

Rees, M. H. (1964b). Plan.Space Sci. 12, 1093.

Sommerfeld, A.(1931). Ann. d. Phys. 11, 257.

Spencer, L. V.(1959). Nat.Bureau of Standards: Monograph 1 U.S.Government Printing Office.

ERRATA

(Inserted following examination 13/8/1973.)

2.3.1

The line before equation (2.5) should read "species and β_{ij} is the production rate of the ith species".

2.3.2

(i) The second diagonal term in the matrix on the left hand side of equation (2.12) should be written

$$-(\delta' + \psi\varsigma)$$

(ii) Before equation (2.13) and after "we find" insert the clause "assuming that ξ is much smaller than θ".

(iii) The second equation from the top of the page following the page on which equation (2.17) appears should read

$$N^+ = \frac{q}{\alpha N^+}\left[1 + \frac{\beta}{\delta'} + \frac{\beta\psi\varsigma}{\delta'\theta} + \frac{\beta\psi\varsigma\xi}{\delta'\theta\gamma_c N^+}\right]$$

2.6

The diagram referred to half way down the page following the page on which equation (2.33) appears should be "Fig. 2.1" not "Fig. 2.2".

3.2.3

The line preceding equation (3.10) should read "At heights where attachment is the dominant process".

4.1

Fig. 4.3(b) is shown overleaf with time scale added.

* * * * * * * * * * * * * *

In addition to the above corrections two whole pages which were missing from the examiners' copies have been inserted.

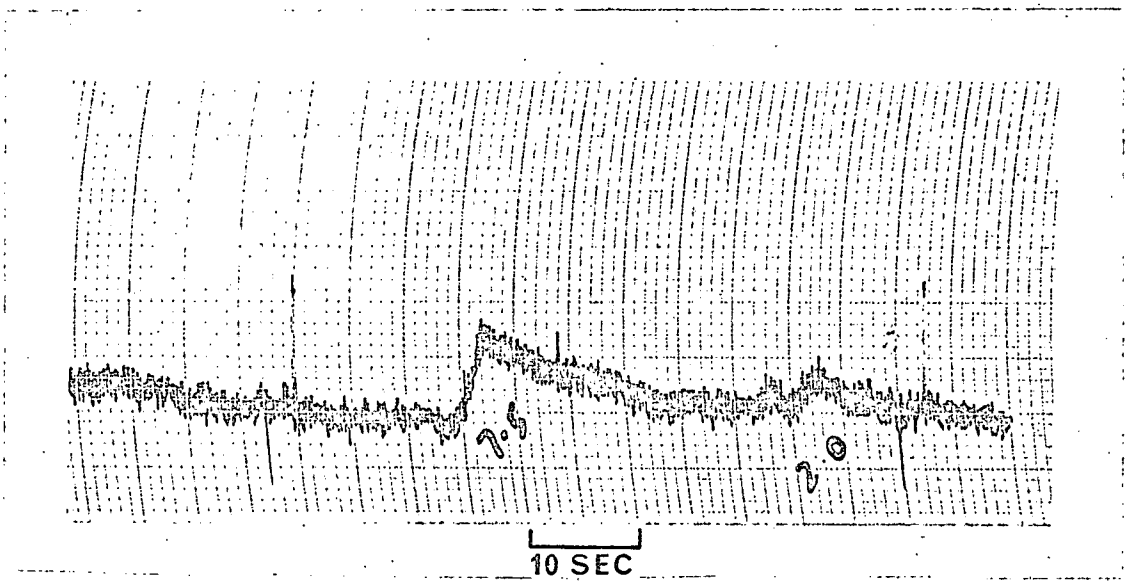

Fig. 4.3

(b) A group of observed c.n.a. pulsations which show very clearly the tendency of smaller pulsations to have faster decay times.

Report on Thesis 'Cosmic Noise Absorption Pulsations' by J.S. Reid

In general, I feel that this thesis represents a worthwhile piece of work, and is worthy of a Ph.D. degree. I have a number of comments, however, that should be brought to the author's attention, and I recommend that he be asked to make appropriate minor revisions.

General Comments:

The only major technical comment relates to the suggestion that the absorption pulsations are an E-region phenomenon. This is not entirely a new idea, and I am enclosing a reprint of a fairly old paper of my own in which I suggested that 'hot' secondary electrons in the E region might contribute appreciably to auroral absorption. This component of the absorption would correlate well with pulsations in luminosity (though probably not with the time-lag observed by the author), and the short decay times of the pulses would represent the cooling time of the electrons rather than their recombination time. I don't really think my mechanism will explain the observations, but it is probably worthy of a mention and a certain amount of discussion, since it has been in the literature for some time.

As far as the presentation is concerned, I think more care could well be taken. I don't expect a thesis to be a literary work of art, but consistent misspellings and careless algebra provide a jarring note that is not really necessary. Throughout the thesis 'dependent' is spelled 'dependant', 'computer' is 'computor', 'detachment' is 'detatchment', 'bremsstrahlung' is bremmstrahlung' (and even 'bremmstrahling' in Appendix 4). These are easily remedied.

Specific Comments:

1.4.2 In equations (1.14) and (1.15), I don't see why the collisional detachment rate should be proportional to [O].

1.5.1 In discussing the NO problem in the D region, more recent work is available than that quoted. The most reliable measurement of NO itself is that of Meira (JGR 76, 202, 1971), while estimates of the ion production rate due to $O_2(^1\Delta_g)$ have been drastically reduced by the results of Huffman et al. (JGR 76, 1028, 1971).

1.6 N_2^+ is very unlikely to exist in any appreciable quantities in the D region, even when particles create most of the ionization. It suffers charge exchange with O_2, producing O_2^+, very efficiently.

2.3.1 I have a minor quibble here, in that I don't like the sudden introduction of equations out of the literature (in this case the Lelevier-Branscomb paper). As far as possible, a thesis ought to be self-contained, and the reader should not suddenly be exposed to a lengthy equation lifted from the middle of a published paper.

In the same section, the β_{ij} terms in the [B] matrix are described as loss rates. Unless I am mistaken, they are actually production rates - the loss terms are the Γ_i's.

2.3.2 The signs of the terms in the matrix in (2.12) seem to be mostly wrong, and in equation (2.14) I get $N_S N_\Lambda = \Psi(\theta + \zeta)$ instead of Ψ/θ, which affects the equations following. I also get a different result for the unnumbered equation at the top of the page after that with (2.12) to (2.17).

2.5.1 There seems to be a section (perhaps only a page) entirely missing from my copy. Section 2.5.1 begins halfway down one page, and the next page begins "Bewersdorff et al."

2.6 There is a reference here to Fig. 2.2, which may refer to Fig. 2.1, since there is no Fig. 2.2.

3.2.3 Following equation (3.10), I don't see why $\gamma N^- N^+$ is expected to be small compared with δN^-. In the case of the terminal negative ions, I would expect the opposite to be true, since they probably have small photodetachment rates, and they do not suffer either associative or collisional detachment.

4.1 Fig. 4.3 has no time-scale, which makes it hard for the reader to verify the statement in the caption.

4.4 In discussing the two-ion idea, some reference should be made to the Norwegians, who have been pushing a similar idea for some time. The key reference is probably Haug and Landmark, JATP 32, 405 (1970).

4.6 Again there is a section missing from my copy, following the page with equation (4.11). The next page in my copy begins "the absorbing region is either thinner or higher. . ."